Institut für Physik und Astronomie

Professur für Statistische Physik und Chaostheorie

Chaotic Diffusion in Nonlinear Hamiltonian Systems

Dissertation
zur Erlangung des akademischen Grades
"'doctor rerum naturalium"'
(Dr. rer. nat.)
in der Wissenschaftsdisziplin "'Theoretische Physik"'

eingereicht an der
Mathematisch-Naturwissenschaftlichen Fakultät
der
Universität Potsdam

von

Mario Mulansky

am

30. August 2012

betreut durch: **Prof. A. Pikovsky**

Published online at the
Institutional Repository of the University of Potsdam:
URL http://opus.kobv.de/ubp/volltexte/2013/6318/
URN urn:nbn:de:kobv:517-opus-63180
http://nbn-resolving.de/urn:nbn:de:kobv:517-opus-63180

Abstract

This work investigates diffusion in nonlinear Hamiltonian systems. The diffusion, more precisely subdiffusion, in such systems is induced by the intrinsic chaotic behavior of trajectories and thus is called "chaotic diffusion". Its properties are studied on the example of one- or two-dimensional lattices of harmonic or nonlinear oscillators with nearest neighbor couplings. The fundamental observation is the spreading of energy for localized initial conditions. Methods of quantifying this spreading behavior are presented, including a new quantity called excitation time. This new quantity allows for a more precise analysis of the spreading than traditional methods. Furthermore, the nonlinear diffusion equation is introduced as a phenomenologic description of the spreading process and a number of predictions on the density dependence of the spreading are drawn from this equation.

Two mathematical techniques for analyzing nonlinear Hamiltonian systems are introduced. The first one is based on a scaling analysis of the Hamiltonian equations and the results are related to similar scaling properties of the NDE. From this relation, exact spreading predictions are deduced. Secondly, the microscopic dynamics at the edge of spreading states are thoroughly analyzed, which again suggests a scaling behavior that can be related to the NDE. Such a microscopic treatment of chaotically spreading states in nonlinear Hamiltonian systems has not been done before and the results present a new technique of connecting microscopic dynamics with macroscopic descriptions like the nonlinear diffusion equation. All theoretical results are supported by heavy numerical simulations, partly obtained on one of Europe's fastest supercomputers located in Bologna, Italy.

In the end, the highly interesting case of harmonic oscillators with random frequencies and nonlinear coupling is studied, which resembles to some extent the famous Discrete Anderson Nonlinear Schrödinger Equation. For this model, a deviation from the widely believed power-law spreading is observed in numerical experiments. Some ideas on a theoretical explanation for this deviation are presented, but a conclusive theory could not be found due to the complicated phase space structure in this case. Nevertheless, it is hoped that the techniques and results presented in this work will help to eventually understand this controversely discussed case as well.

Zusammenfassung

Diese Arbeit beschäftigt sich mit dem Phänomen der Diffusion in nichtlinearen Systemen. Unter Diffusion versteht man normalerweise die zufallsmäßige Bewegung von Partikeln durch den stochastischen Einfluss einer thermodynamisch beschreibbaren Umgebung. Dieser Prozess ist mathematisch beschrieben durch die Diffusionsgleichung. In dieser Arbeit werden jedoch abgeschlossene Systeme ohne Einfluss der Umgebung betrachtet. Dennoch wird eine Art von Diffusion, üblicherweise bezeichnet als Subdiffusion, beobachtet. Die Ursache dafür liegt im chaotischen Verhalten des Systems. Vereinfacht gesagt, erzeugt das Chaos eine intrinsische Pseudo-Zufälligkeit, die zu einem gewissen Grad mit dem Einfluss einer thermodynamischen Umgebung vergleichbar ist und somit auch diffusives Verhalten provoziert.

Zur quantitativen Beschreibung dieses subdiffusiven Prozesses wird eine Verallgemeinerung der Diffusionsgleichung herangezogen, die Nichtlineare Diffusionsgleichung. Desweiteren wird die mikroskopische Dynamik des Systems mit analytischen Methoden untersucht, und Schlussfolgerungen für den makroskopischen Diffusionsprozess abgeleitet. Die Technik der Verbindung von mikroskopischer Dynamik und makroskopischen Beobachtungen, die in dieser Arbeit entwickelt wird und detailliert beschrieben ist, führt zu einem tieferen Verständnis von hochdimensionalen chaotischen Systemen. Die mit mathematischen Mitteln abgeleiteten Ergebnisse sind darüber hinaus durch ausführliche Simulationen verifiziert, welche teilweise auf einem der leistungsfähigsten Supercomputer Europas durchgeführt wurden, dem sp6 in Bologna, Italien.

Desweiteren können die in dieser Arbeit vorgestellten Erkenntnisse und Techniken mit Sicherheit auch in anderen Fällen bei der Untersuchung chaotischer Systeme Anwendung finden.

Inhaltsverzeichnis

Abbildungsverzeichnis

1. Introduction

1.1. Diffusion, Thermalization and Chaos

Diffusion is a fundamental transport phenomenon appearing in physics, biology, chemistry and many other branches of science. In its original formulation it described the migration of particles or molecules in a thermodynamic environment. Its main feature is that diffusion results in mixing or transport without requiring a directed force, opposed to convection, for example. Diffusion is typically formulated for some concentration or density distribution, e.g. a particle density, and its main property is the linear growth with time of the second moment of the concentration/density. This is also encoded in the term itself that comes from the Latin word "diffundere" which means "to spread out". In most applications, as well as in this work, a diffusion process is described in terms of a spatial spreading of some density with time. However, the concept can be used in more abstract environments, e.g. diffusion of energy or probability over any kind of modes that provide a suitable basis. In this abstract sense diffusion might also be considered as a mechanism to describe the equilibration of a system. For example, one can think of diffusion of energy initially trapped in only a few degrees of freedom over the whole system ending in a state well described by a thermal equilibrium. In this work, mainly spatial diffusion of energy will be considered. However, the systems are designed in such a way that the degrees of freedom, or energy modes, coincide with the spatial basis. Hence, the results can also be related to the more abstract situations of spreading over modes and the general process of thermalization due to diffusive behavior.

In 1905, Einstein's work [1] marked a breakthrough in the understanding of diffusion as the dynamical response of particles or molecules to a stochastic forcing induced by the thermodynamic environment. With the emergence of Chaos Theory [2] and by studying the properties of chaotic systems, it became possible to explain diffusive behavior also without employing thermodynamic assumptions. Even more, thermodynamic properties could be, to some extent, derived from microscopic chaotic dynamics [3]. In such situations the system itself, as being chaotic, shows stochastic, quasi-random behavior and thereby can induce diffusion without requiring an external stochasticity. The basic, but very instructive example for this effect is the Standard Map [4] which shows diffusion of energy [5] in the parameter region where chaos governs the motion. This is a very important result as it provides an explanation for thermalization of systems initially out of equilibrium, especially in micro-canonic situations where no interaction with the environment is allowed. Therefore, diffusion in the Standard Map will be discussed in more details in section 1.2. Although being assumed long before and becoming part of physicists intuition, thermalization in closed, classical systems could not be understood until the

emergence of Chaos Theory [3,6]. However, although the overall picture that chaotic behavior leads to thermalization is quite convincing and can even be proven for a number of systems [3], a lot of understanding is still missing in this field. The main purpose of this work is to advance the understanding of high dimensional chaotic systems and to increase the knowledge on the relation between chaotic behavior and diffusive processes. It has to be noted here already that throughout this work the term "diffusion" will be used in a very general meaning including subdiffusive and superdiffusive processes [7], not only the original diffusive behavior as introduced by Fick [8].

One of the first studies investigating chaos as the origin of thermalization were the famous numerical experiments by Fermi, Pasta and Ulam on a nonlinear Hamiltonian system nowadays known as the FPU problem [9, 10]. Fermi, Pasta and Ulam took a, as they thought, very simple toy model to study thermalization properties due to complex dynamics. Their system was a chain of harmonic oscillators with linear and nonlinear couplings. The nonlinearity was expected to induce chaos which then should lead to thermalization. However, this was not observed and the model is now, over 50 years later, still under investigation (see [11] for a review). Despite the nonlinearity, Fermi, Pasta and Ulam found quasi-periodic motion instead of ergodic behavior which was in contradiction to the common understanding that complex, nonlinear, interacting systems should exhibit chaos leading to thermalization. This, among other studies (e.g. coupled map lattices [12, 13]), opened the complex and rich field of chaos in high-dimensional Hamiltonian systems that is also subject of this work. There are several peculiarities in Hamiltonian systems that make the understanding of their chaotic properties exceptionally difficult. This will be shortly summarized in the following using the FPU problem exemplarily.

One of the possible explanations for the absence of ergodicity in the FPU study was later believed to be the existence of KAM-tori, sets of quasi-periodic solutions in weakly perturbed integrable systems. Such tori were first proposed 1954 by Kolomogorov [14], later refined by Moser [15] and rigorously proven 1963 by Arnol'd [16]. Named after these three founders, the KAM theorem proves the existence of quasi-periodic trajectories for weak enough perturbations in Hamiltonian systems. It is a fundamental result on Hamiltonian chaos described in any textbook on chaotic dynamics or nonlinear systems, e.g. [2, 17]. Unfortunately, it gives no estimate on how small the perturbation has to be and in fact it is up to now debated if the parameters chosen in the inital FPU study indeed lie inside such a quasi-periodic tori [18] . Especially the high dimensional phase space in the FPU problem, typically consisting of a chain of hundreds of oscillators, makes it very difficult to find and quantify KAM tori, a situation that will also be faced in this work.

Even before the emergence of the KAM theory, another feature of such systems has been discovered. It was found that there exist localized, nonlinear excitations [19,20], nowadays called breathers [21], solitons or compactons [22]. These structures show quasi-periodic behavior and can either remain at the same position or travel through the chain [23]. In both situations they prevent energy from diffusing into the whole

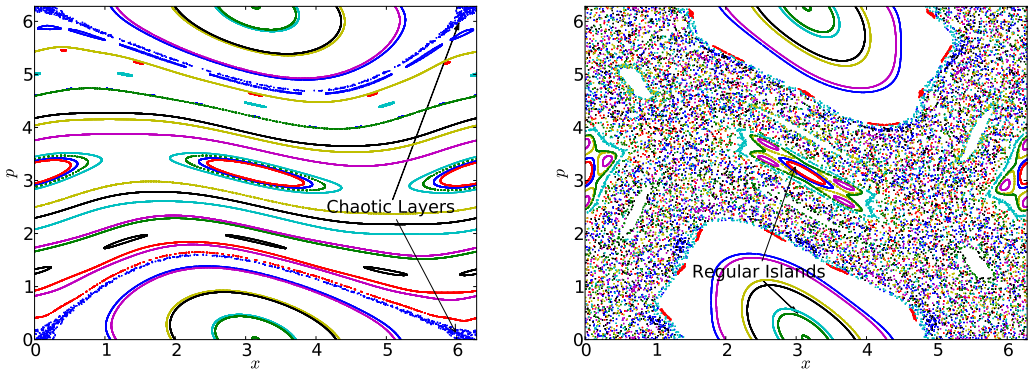

(a) Standard Map with small nonlinearity ($K = 0.6$).

(b) Standard Map with larger nonlinearity ($K = 1.5$).

Figure 1.1.: Phase space of the Standard Map (1.4) for small and larger nonlinearity parameters $K = 0.6, 1.5$. Both plots show the coexistence of regular motion and chaotic parts. For larger nonlinearity, the regular islands get smaller and smaller and a global chaotic region emerges.

system and thus block thermalization. In contrast to KAM tori, such excitations are strictly nonlinear and are not obtained from perturbative methods.

When studying the emergence of chaos in a magnetic trap, Chirikov developed the theory of resonance overlaps that gives a quantitative estimate on the onset of chaos in dependence on the perturbation strength in the system [24]. This can be combined with the KAM theorem by understanding that the phase space of nonlinear Hamiltonian systems can exhibit both regular trajectories with (quasi-)periodic motion and regions with chaotic motion. This is visualized in Fig. 1.1 for the most simple chaotic example: the Standard Map (1.4), explained in more detail in the following section. These graphs show phase space representations of this exemplary model for Hamiltonian chaos and one clearly sees the coexistence of regular and chaotic regions, with chaos getting bigger if the nonlinearity is increased. This possibly very complex phase space structure explains the particular difficulty when dealing with Hamiltonian systems. Indeed, Izrailev and Chirikov found that the chaotic regions might be confined to thin resonance layers if the perturbation is too small [25], as shown in Fig. 1.1a, and thus would not lead to thermalization. Using the resonance overlap criterion, the critical perturbation strength can be estimated above which the resonances start to interact. This interaction of resonances typically creates a global chaotic layer that allows for energy diffusion over the whole phase space hence leading to thermalization. This situation is visualized in Fig. 1.1b, where a trajectory starting inside the chaotic region can access almost the whole phase space except some regular islands that are decreasing further when increasing the nonlinearity. Applied to the FPU problem this was tested successfully by Izrailev [26, 27] who found thermalization by increasing the nonlinearity parameter. Later, these results were refined by considering higher order resonances [28] which explained thermal-

ization for smaller perturbations happening at longer timescales. Very recently and with heavy numerical simulations it was claimed that indeed thermalization happens in this system also for the original small perturbation strength, but on enormous time scales not accessible to Fermi, Pasta and Ulam in the 1950s [29].

Lately, a similar problem arose in a very different system: the nonlinear Anderson model [30]. There, the interplay between disorder and nonlinearity is studied, mostly in the framework of a Discrete Anderson Nonlinear Schrödinger Equation (DANSE). Without nonlinearity, the disorder leads to the celebrated phenomenon of Anderson localization [31–33] stating the "Absence of Diffusion" for initially localized excitations. Again, it was asked if introducing nonlinearity would lead to the possibility of energy diffusion due to the emergence of chaos in this system. This question was addressed very extensively in the past years, numerically [30, 34–51] and analytically [52–56]. It was also picked up experimentally, first investigating Anderson localization disordered system without nonlinearity [57–61], but lately also adding nonlinear interactions [62–65]. Despite the numerous efforts and the numerical agreement on subdiffusive spreading, a clear understanding of the long-term spreading behavior is still lacking [66]. Increasing the understanding of this very actively studied system is one of the main motivations of this work and therefore section 1.3 gives a summary of the known results. However, in this work a simplified, more fundamental situation with possible application to a wider class of Hamiltonian systems will be addressed, but nevertheless some conclusions for the nonlinear Anderson model will be drawn.

The main outcome of this study are the results on the spreading of energy in nonlinear Hamiltonian lattices. The spreading process will be identified as subdiffusive and, at least in some cases, related to chaotic properties of the dynamics. Subdiffusion refers to a process that is similar to diffusion, but much slower. That means, for example, that the second moment for a subdiffusive process follows a power law with an exponent $\alpha < 1$, c.f. (1.9). The systems studied here are one- or two-dimensional lattices of linear or nonlinear oscillators coupled by nonlinear nearest-neighbor interaction. The absence of linear coupling terms excludes the existence of linear traveling waves which makes these models inherently easier to study than, for example, the FPU model. This allows for a much more detailed investigation and leads to a deeper understanding of the fundamental properties of high-dimensional[1] Hamiltonian systems. So while in the FPU model the main question was if the system thermalizes and on what time scale, in this work a more detailed analysis of the route towards equilibration is performed by analyzing the spreading properties of initially localized energy distributions in large systems. To quantify the diffusion process in these systems, the nonlinear diffusion equation (NDE) is introduced as a phenomenological model for the spreading behavior. The application of this macroscopic description

[1] Unfortunately, there will be two notions of dimensionality in this work. When referring to "one- or two-dimensional lattices", the structure of the coupling of oscillators is meant, while when using the expression "high dimensional Hamiltonian" or "high dimensional system" the phase space dimensionality is attributed, a crucial quantity for the properties of chaos. Anyhow, it should be clear from the context which of the two notions of dimension is referred to.

of spreading is accompanied by a detailed study of the microscopic Hamiltonian dynamics in the model leading to a number of analytic predictions on the diffusion properties. The main analytic tools are firstly the identification of scaling properties of the equations of motion. Secondly, a resonance analysis as described by Chirikov [25] will be performed to understand the microscopic dynamics and those results are then connected to the macroscopic spreading. Finally, the whole study is supported by extensive numerical simulations in one- and two-dimensional lattices, partly performed on one of Europe's fastest supercomputers (sp6 at CINECA in Bologna, Italy).

1.2. Chaotic Diffusion

The simplest and most instructive example for a diffusive process is Brownian motion, firstly quantified by the Botanist Robert Brown in 1827 [67, 68]. In one dimension, this can be modeled by a random walk where a particle is assumed to make a jump of length one at every timestep either to the left or to the right with probability one half. Denoting the position of the particle at timestep i by x_i and considering an ensemble of particle trajectories, one obtains for the ensemble average of the squared displacement and for large numbers of steps $i \gg 1$ the diffusion law: $\langle x_i^2 \rangle = 2i$. The mean displacement in this situation tends to zero $\langle x_i \rangle = 0$. This can also be generalized for continuous time leading to the Wiener process:

$$\dot{x}(t) = \xi(t), \tag{1.1}$$

where $\xi(t)$ represents zero mean Gaussian white noise with variance σ^2. Again considering the average over an ensemble of trajectories one finds:

$$\langle x^2(t) \rangle = D \cdot t \qquad \text{with} \qquad D = 2\sigma^2, \tag{1.2}$$

where D is called the diffusion constant and depends on the properties of the random process, here its variance σ^2. While this is based on a random process introduced by the white noise ξ, the behavior of single particles in a thermodynamic environment can be described by exactly the same mechanism as phenomenologically already found by Fick [8]. Later, Einstein derived the relation between the diffusion constant and the temperature T of the environment [1]:

$$D = \mu k_B T, \tag{1.3}$$

where μ denotes the particles mobility and k_B is the Boltzmann factor. This completed the understanding of diffusion in thermodynamic environments.

With the emergence of Chaos Theory, it was later found that diffusion can also be observed in systems that are not subject to any random forcing nor connected to a heat bath. In this case, diffusion is induced by the quasi-randomness of the chaotic system itself and the diffusion constant supposingly depends on the properties of

chaos. In such a situation, the process is denoted as *chaotic diffusion* [69]. The simplest case where this can be studied is the so called Standard Map, introduced by Chirikov [24] and defined as a two dimensional map for an action and an angle coordinate p and φ:

$$\begin{aligned} p_{n+1} &= p_n + K \sin \varphi_n \\ \varphi_{n+1} &= \varphi_n + p_{n+1}. \end{aligned} \tag{1.4}$$

The index n denotes the discrete time and K is the nonlinearity parameter leading to chaos when being large enough. For small values $K \ll 1$, on the other hand, KAM tori prevail and the trajectories are mainly quasi-periodic. For detailed reviews on the properties of the Standard Map see any chaos textbook, e.g. [2] or [17]. Here, only the results on diffusion in the chaotic regime should be emphasized. If K is large enough to ensure the destruction of the last separating KAM tori in the system, $K > K_c \approx 0.972$, one finds diffusion in action space [5, 70]:

$$\langle p^2 \rangle = D \cdot t, \quad \text{with} \quad D \approx \begin{cases} \frac{1}{3}(K - K_c)^3 & \text{for} \quad K_c < K < 4 \\ \frac{1}{2}K^2 & \text{for} \quad K > 4. \end{cases} \tag{1.5}$$

The result for large $K > 4$ can be easily obtained by a random phase approximation assuming uncorrelated phases φ_n and φ_{n+1}. For values K close to the critical strength K_c on the other hand, the phase space is very complicated showing both chaotic regions and islands of stability which makes analytical treatments of the diffusion process very complicated [5]. Moreover, small but still always present correlations give corrections to the relations above, but these details are of minor importance for this work and thus are not further discussed.

Although being the most popular and intensively studied example, the Standard Map is not the only chaotic map that exhibits diffusive behavior. Quite conversely, this is a universal phenomenon in chaotic systems. For example, a whole class of one-dimensional maps has been studied by Klages [69], where a very complex, even fractal, dependence of the diffusion constant on the nonlinearity parameter of the maps is reported. Also, diffusion in coupled lattices has been extensively studied by Kaneoko and Konishi [71]. Despite the possibly very complicated dependence of the diffusion constant on the details of the mappings, these situations have similar fundamental properties:

- Assuming there is one parameter controlling the integrability of the system, from the KAM theorem one expects the existence of a lower bound below which KAM tori prevail and no diffusion is possible due to phase space separation.
- For values above this critical threshold, diffusive behavior is observed with a diffusion constant depending on the system parameters but not on time, hence one always observes normal diffusion in those models.

It should be noted at this point that the Hamiltonian nonlinear oscillator lattices studied later in this work have substantially different properties which will lead to subdiffusive behavior, opposed to the normal diffusion for the mappings presented above.

1.3. Spreading in Nonlinear Anderson Models

First predicted in 1957 by Anderson, the phenomenon of localization in disordered systems is still a subject of intensive studies nowadays. At that time, one was interested in the transport properties of electrons in systems that are not perfectly periodic but exhibit impurities at random places as any material in real life does. Such a situation can be simplified to the fundamental property of having a disordered potential. In his pioneering work titled "Absence of Diffusion in Certain Random Lattices" [31], Anderson describes localized eigenstates in linear systems with disordered on-site potential. One example of such a system is the discrete Schrödinger equation governing the time evolution of some complex valued wavefunction $\psi_n(t)$:

$$i\dot{\psi}_n = V_n\psi_n + \psi_{n-1} + \psi_{n+1}. \tag{1.6}$$

The potential V_n at lattice site n is a random variable, typically chosen uniformly, independent and identically distributed (iid.) from some interval $[-U/2, U/2]$, but fixed in time. The nearest neighbor couplings arise from the discretization of the Laplace operator of the original Schrödinger equation. It is known for such models that in one dimension all eigenfunctions are exponentially localized with a localization length depending on the corresponding energy eigenvalue and the disorder strength U [32]. More details on the properties of linear, disordered systems can be found in the very good review from Lee and Ramakrishnan [72].

The situation gets much more delicate if nonlinearity is added to the system. This allows for interactions between the linear eigenmodes and hence the possibility to destroy Anderson localization by introducing chaotic diffusion. This has been studied very extensively in the framework of the (generalized) Discrete Anderson Nonlinear Schrödinger Equation (gDANSE):

$$i\dot{\psi}_n = V_n\psi_n + \psi_{n-1} + \psi_{n+1} + \beta|\psi_n|^{2\sigma}\psi_n, \tag{1.7}$$

which is the same as above but with an additional nonlinear term $\beta|\psi_n|^{2\sigma}\psi_n$ where β denotes the nonlinear strength and σ the power of nonlinearity. The standard choice is $\sigma = 1$, for which the model is called just DANSE model and that is of considerable physical importance. It describes, for example, Bose-Einstein-Condensates in a random potential in a low-density mean field approach [51, 61, 65]. Moreover, it also appears for light propagation in arrays of optical wave guides using nonlinear optical media [62, 63], where the time t is replaced with the spatial directionalong the wave guides z. This triggered a lot of numerical studies [30, 34–51], mainly aiming at the long-time behavior not yet reachable by experiments, as well as analytic treatments [52–56]. Although other choices $\sigma > 0$ have less physical meaning in terms of experimental observations, they are very important for checking analytical results on the model and verifying theoretical assumption on the relation between nonlinearity, chaos and spreading as shown later in this work.

The understanding of the aymptotic spreading behavior in the DANSE model is one of the main motivations for this work. Thus, a short summary of the vast

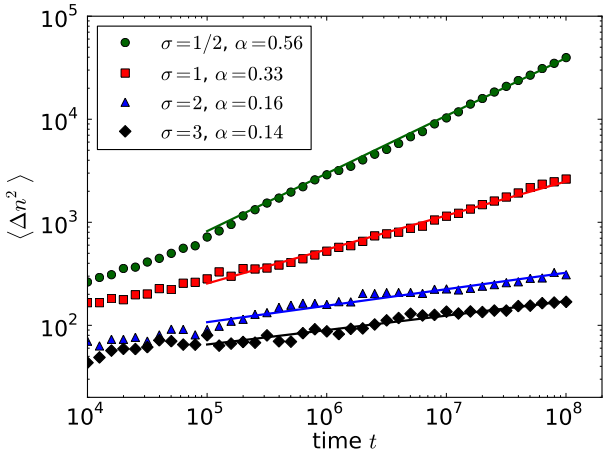

Figure 1.2.: Spreading in the gDANSE model (1.7) for different nonlinearity exponents σ together with power law fits $\Delta n^2 \sim t^\alpha$ (1.9), with the fitting exponents α also shown in the labels. These results were obtained for $\beta = 1$ and $U = 4$ and are part of previous works of the author [44, 73].

numerical results obtained for this problem will be given here. The fundamental observation is a subdiffusive spreading for initially localized distributions in the gDANSE model (1.7). That means one starts with only a few sites initially having positive amplitudes $|\psi_n|^2 > 0$ and observes how other, initially resting sites get excited with time. For the linear case, Anderson localization prevents the excitation of sites far from the starting points. This changes when adding nonlinearity and a slow diffusion, i.e. subdiffusion, of energy into distant parts of the lattice can be observed. This is typically quantified by measuring the second moment of the norm distribution $|\psi_n|^2$ of the wavefunction:

$$\Delta n^2(t) = \sum_n (n - \bar{n}(t))^2 |\psi_n(t)|^2, \qquad \text{with} \qquad \bar{n}(t) = \sum_n n |\psi_n(t)|^2, \tag{1.8}$$

where $\bar{n}(t)$ denotes the spatial center of the distribution. More methods of quantifying the spreading will be described more sophisticatedly in section 2.5. Fig. 1.2 shows the main results obtained in [73], where the spreading of initially localized excitations was studied for different nonlinearity exponents σ. The graphs present averages over disorder realizations and thus describe the average spreading behavior rather than single trajectories. The main observation is a subdiffusive spreading for all considered values of σ:

$$\Delta n^2 \sim t^\alpha, \qquad \text{with} \qquad 0 < \alpha < 1, \tag{1.9}$$

where $\alpha(\sigma)$ is the spreading exponent depending on the power of the nonlinear term. The spreading exponent for the most important case $\sigma = 1$ was found to be $\alpha_1 \approx 1/3$, a value confirmed by many other numerical studies, e.g. [38, 47], but has no convincing theoretical explanation, yet.

To study the spreading mechanism that is induced by the nonlinearity analytically, a transformation to the basis of eigenmodes of the linear system is very helpful. For simplicity, the presentation here will be restricted to the fundamental case $\sigma = 1$, for a similar treatment of the general case see [73]. Denoting the k-th eigenmode represented in the spatial basis with $\varphi_{k,n}$ and the corresponding eigenvalues with ϵ_k, it is known that those eigenmodes are exponentially localized around some center $\bar{n}$ with some localization length ξ_k [32]:

$$|\varphi_{k,n}|^2 \sim \mathrm{e}^{-|n-\bar{n}_k|/\xi_k}. \tag{1.10}$$

The index k in ξ_k indicates the dependence of the localization length on the energy eigenvalue of the mode ϵ_k. Note, that the energy eigenvalues $\{\epsilon_k\}$ depend on the random potential $\{V_n\}$ and are therefore random quantities as well. Introducing the representation in terms of the complex valued eigenmode amplitudes C_k gives:

$$\psi_n(t) = \sum_k \varphi_{k,n} C_k(t). \tag{1.11}$$

Without the nonlinear term, the time evolution of C_k would be a trivial phase rotation. With nonlinearity, however, substituting (1.11) in (1.7) yields:

$$i\dot{C}_k = \epsilon_k C_k + \beta \sum_{p,l,m} V_{k,p,l,m} C_p C_l^* C_m \quad \text{with} \quad V_{k,p,l,m} = \sum_n \varphi_{k,n} \varphi_{p,n}^* \varphi_{l,n} \varphi_{m,n}^*. \tag{1.12}$$

The 4-mode overlaps $V_{k,p,l,m}$ describe the coupling strength between the linear modes due to the nonlinearity. Formally, the local-in-space nonlinearity introduces an all-to-all coupling when viewed in eigenmode space. However, as the eigenmodes are exponentially localized also the overlap $V_{k,p,l,m}$ decreases exponentially with the spatial distance between the modes. Hence, each mode effectively interacts only with those modes that are centered within a distance of roughly the localization length. As the localization length also depends on the disorder strength U, this coupling range can be adjusted by changing U where an increase leads to stronger localization and hence a shorter effective coupling range.

From the structure of the equation one sees that not only the eigenmode frequencies ϵ_k, but also the coupling strengths $V_{k,p,l,m}$ depend on the actual realization of the disordered potential $\{V_n\}$ and hence are random variables. This creates a highly complicated situation with a very complex phase space structure that is hard to treat analytically, also seen from the lack of a convincing spreading theory for this model. Additionally, this model exhibits two conserved quantities: norm and energy [73], opposed to the systems considered later in this work where only the energy is conserved. The qualitative picture, however, that the nonlinear interactions induce chaos in the system which then leads to diffusion of energy seems to be correct, but a quantitative theoretical result on this spreading process is yet to be developed. One approach is presented in [39], where the concept of "chaotic heating" is introduced and the properties of chaos are tried to be modeled by an effective noise theory. This idea was recently also followed by Michaely and Fishman in a

detailed study [48]. In this picture, the excited modes, that is those with non-zero amplitude $|\psi_n|^2 > 0$, show chaotic motion and thus transfer energy to the unexcited modes via the coupling. However, this relies on a number of assumptions, especially on the quantitative role of resonances as a source chaos. Some of those assumptions have been tested in detailed in [74,75], but the picture is still far from complete [66].

In this work a similar, but less complex model will be studied introduced in chapter 2. But before going to this simplification, the essential properties of the DANSE model should be highlighted:

- Hamiltonian structure with norm as additional conserved quantity.
- Absence of linear waves due to Anderson Localization; without nonlinearity no spreading would occur.
- Finite range (exponentially decaying) nonlinear coupling between localized linear modes.
- Neighboring modes have random frequencies ϵ_k and hence are typically not in resonance.

1.4. Scope of this Work

In the following chapters, a class of nonlinear Hamiltonian lattices will be studied that represent a simplification of the DANSE model, but with some similar properties. This allows for a more detailed study of the microscopic dynamics from which theoretical predictions on the exact spreading exponents will be deduced, at least in some cases. The idea is that by considering a simplified system, the microscopic dynamics can be analyzed and spreading can be quantified based directly on dynamical properties. So in this work, no assumptions on the properties of "chaotic heating" or the influence of resonance probabilities will be made, all results are based on the microscopic dynamics of the system. Besides introducing the model and its properties in chapter 2, also a new observable used to quantify spreading will be presented, called excitation time [46]. Then, the properties of the nonlinear diffusion equation and its self-similar solution will be illuminated in chapter 3. This equation serves as a phenomenological model to describe the spreading process and predictions for spreading in Hamiltonian lattices will be made. Chapter 4 contains the main results of the work, including scaling and resonance analysis of the microscopic dynamics in nonlinear Hamiltonian lattices Accordingly, predictions for the spreading properties will be drawn and compared with heavy numerical simulations in one- and two-dimensional lattices. Finally, chapter 5 gives conclusions and also tries to relate these findings back to the original problem of spreading in nonlinear Anderson models.

2. Nonlinear Hamiltonian Lattices

The objects of study in this work are Hamiltonian chains (1D) or lattices (2D), possibly including disorder, of harmonic or nonlinear oscillators with a nonlinear, power-law, nearest neighbour coupling. The one-dimensional oscillator chain will be introduced and described explicitly in the next section. Then, a short preview on the spreading behavior will be given followed by a detailed formulation of how spreading can be quantified in this system. Finally, a generalization to two dimensional lattices of oscillators will be presented.

2.1. One-dimensional Oscillator Chains

The nonlinear Hamiltonian systems studied in most parts of this work are formulated in terms of a Hamilton function $H(\vec{q},\vec{p}) : \mathbb{R}^N \times \mathbb{R}^N \to \mathbb{R}$ for positions $\vec{q} = \{q_k\} \in \mathbb{R}^N$ and momenta $\vec{p} = \{p_k\} \in \mathbb{R}^N$ of oscillators at lattice sites $k = 1 \dots N$:

$$H = \sum_{k=1}^{N} \frac{p_k^2}{2} + U\frac{\omega_k^2}{\kappa} q_k^\kappa + \frac{\tilde{\beta}}{\lambda} \sum_{k=1}^{N-1} (q_{k+1} - q_k)^\lambda \,, \tag{2.1}$$

with parameters κ, λ, U, $\tilde{\beta}$ and $\{\omega_k\}$. The exponents $\kappa \geq 2$ and $\lambda > 2$, $\lambda \geq \kappa$ denote the powers of the on-site potential and the coupling term, respectively. This represents the very general situation of a one-dimensional chain of harmonic ($\kappa = 2$) or nonlinear ($\kappa > 2$) oscillators with a power-law nearest-neighbor coupling. Note that for the sake of simplicity of the presentation, in this work only even powers $\kappa = 2, 4, 6$; $\lambda = 4, 6$ are chosen. A generalization of H to odd or even to non-integer powers is straightforward by writing the local potential as $\sim |q_k|^\kappa$ and the coupling as $\sim |q_{k+1} - q_k|^\lambda$ to ensure positivity of the energy. Many of the later results can be generalized to these cases. Additionally, a local potential strength $U > 0$ and a coupling strength $\tilde{\beta} > 0$ have been included. But as shown in the next section, these generally are not independent parameters of the system and can mostly be set to unity. The tuple $\{\omega_k\}$ are parameters of the local potential, i.e. the oscillator frequencies in the harmonic case $\kappa = 2$, and three situations are considered in this work:

soft disorder: $\omega_k \in [0, 1]$ uniformly random iid., abbreviated "**sd**".

hard disorder: $\omega_k \in [0.5, 1.5]$ uniformly random iid., abbreviated "**hd**".

regular: $\omega_k = 1$, no disorder, abbreviated "**re**".

This system can be viewed as a generalization of the so called Fröhlich-Spencer-Wayne model introduced in [76]. To refer to a specific choice of nonlinearities throughout this work, the expression "κ–λ" will be used. So for example the term 2–4_{sd} refers to the case with harmonic on-site potential $\kappa = 2$, power-4 coupling term $\lambda = 4$, and soft disorder $\omega_k \in [0, 1]$. If not indicated differently, generally the one-dimensional case introduced here is considered. Obviously, the Hamiltonian nature of the model implies that the energy of the system $E = H(\vec{q}(t), \vec{p}(t))$, with $\vec{q}(t)$, $\vec{p}(t)$ being some trajectory, is a conserved quantity $\mathrm{d}E/\mathrm{d}t = 0$.

In this work, the behavior of trajectories $\vec{q}(t), \vec{p}(t)$ obtained from the initial value problem derived from the Hamilton function (2.1) is investigated:

$$\begin{aligned} \dot{q}_k &= \frac{\partial H}{\partial p_k} = p_k \\ \dot{p}_k &= -\frac{\partial H}{\partial q_k} = -\omega_k^2 q_k^{\kappa-1} - \beta \left((q_k - q_{k+1})^{\lambda-1} + (q_k - q_{k-1})^{\lambda-1} \right) \\ q_k(0) &= q_{k,0}, \quad p_k(0) = p_{k,0}. \end{aligned} \tag{2.2}$$

The focus lies on the typical behavior of such trajectories for random potential realizations $\{\omega_k\}$ or random initial conditions rather than a specific result for some carefully chosen potential or initial condition. This typical behavior is extracted by performing Monte-Carlo studies on many potential realizations or initial conditions and then analyzing the averages of these ensembles of trajectories.

More precisely, two different setups will be studied here: In section 2.4, short chains with $N = 8 \ldots 64$ sites are considered and periodic boundary conditions are used $q_{N+1} = q_1$ and $p_{N+1} = p_1$. There, the energy is initially spread over all sites and the properties of chaos of such situations are studied in terms of Lyapunov exponents. The main results on the other hand, presented in chapter 4, deal with localized initial excitations where the energy is distributed over a few sites only. Then the diffusion properties are analyzed in terms of energy spreading. In this situation the number N of oscillators is considered to be large enough such that no boundary effects will occur, hence boundary conditions are irrelevant for those studies.[1]

Before analyzing the properties of this model more deeply in a mathematical way, some general properties should be mentioned, especially in comparison to the DANSE model (1.7). Similarly, the above model does not exhibit linear waves, but rather due to the absence of linear[2] coupling terms than due to Anderson Localization. Therefore, disorder as source of Anderson Localization is not essentially required to block linear waves as they can not exist without linear coupling at all. However, as it will be shown in section 2.3, there might exist *nonlinear* waves in the lattice. As traveling waves complicate the observation of diffusive spreading, their existence should be avoided. This is realized here by introducing local disorder in

[1] Typically, initial excitations will be chosen to lie in the center of the lattice with N being large enough such that the boundary is never reached by the excitation.

[2] $\lambda = 2$ in (2.1) would be a "linear" coupling term as "linearity" refers to the equations of motion not to the Hamilton function itself.

terms of $\{\omega_k\}$ and the two cases hard and soft disorder. So while the disorder in the DANSE model (1.7) is required to block linear waves by the mechanism of Anderson Localization, here disorder is introduced to block possible nonlinear waves, at least in one-dimensional chains. For two-dimensional lattices, however, nonlinear waves seem not to exist even without disorder ($\omega_k = 1$), a situation described later in section 2.6. It should be noted here that the absence of nonlinear waves due to disorder in 1D or in general in 2D systems is not rigorously shown and also not yet studied in much detail. Accordingly, this work mainly relies on the numerical observation that such solutions do not exist or are at least not significant. Further investigations in this matter are definitely required. Another key difference to the DANSE model is the rather simple, nearest neighbor coupling in (2.1), in contrast to the complicated four-mode overlaps with exponentially decaying coupling terms in (1.7) [74, 75]. This creates the possibility to understand the microscopic dynamics and develop theoretical predictions for the spreading exponent which is done in chapter 4. Before, however, some peculiarities of the Hamiltonian system itself have to be explained.

2.2. Scaling Properties

Here, the crucial, independent parameters of the model will be identified and in this course its scaling properties are highlighted. First, consider the Hamiltonian system (2.1) for some fixed powers $\kappa \neq \lambda$ with either hard/soft or no disorder. This case will be called "nonhomogeneous" because of the different nonlinear powers. The Hamiltonian then contains two parameters, U and $\tilde{\beta}$, that govern the strength of local and coupling potential. However, these parameters are not independent and can be set to unity. To show this, a canonical transformation to new positions Q_k, momenta P_k, time t' and Hamilton function H' is performed:

$$\begin{aligned} q_k &= U^b \tilde{\beta}^{-b} Q_k \\ p_k &= U^{\lambda b/2} \tilde{\beta}^{-\kappa b/2} P_k \\ t &= U^{(2-\lambda)b/2} \tilde{\beta}^{(\kappa-2)b/2} t' \\ H &= U^{\lambda b} \tilde{\beta}^{-\kappa b} H', \end{aligned} \tag{2.3}$$

with $b = 1/(\lambda - \kappa)$. This transformation is indeed canonical, as shown in appendix A.1.1. Renaming the variables again: $Q_k \to q_k$, $P_k \to p_k$, $t' \to t$ and $H' \to H$, the Hamiltonian after the transformation reads:

$$H = \sum_{k=1}^{N} \frac{p_k^2}{2} + \frac{\omega_k^2}{\kappa} q_k^\kappa + \frac{1}{\lambda} \sum_{k=1}^{N-1} (q_{k+1} - q_k)^\lambda \,. \tag{2.4}$$

The only remaining parameter, besides the choice of disorder $\{\omega_k\}$, is the total conserved energy E in the system. That means, for example, that changing the nonlinear strength in the original Hamiltonian (2.1) is, by a rescaling of $\{q_k\}$, $\{p_k\}$

and time, equivalent to a change of the total energy of the system connected with a change of the time scale. This is an important observation that will be used heavily in later calculations. However, it should be noted again that this is only true for the *nonhomogeneous* case where $\kappa \neq \lambda$, as immediately seen from the divergence of the transformation parameter b for $\kappa = \lambda$ in (2.3).

For the special case of homogeneous powers, $\kappa = \lambda$, the above canonical transformation is not possible. However, this case is highly interesting as it has the particular property that the energy can be rescaled and is not an independent parameter in the model. To show this, the following variable transformation is performed:

$$\begin{aligned} q_k &= E^{1/\kappa} U^{-1/\kappa} Q_k \\ p_k &= E^{1/2} P_k \\ t &= U^{-1/\kappa} E^{1/\kappa - 1/2} t' \\ H &= E H' \ . \end{aligned} \tag{2.5}$$

This indeed represents a canonical transformation as shown in appendix A.1.2. Again, after renaming the variables back to q_k, p_k, t and H, and with introducing $\beta = \tilde{\beta}/U$, the Hamiltonian is found as:

$$H = \sum_{k=1}^{N} \frac{p_k^2}{2} + \frac{\omega_k^2}{\kappa} q_k^\kappa + \frac{\beta}{\kappa} \sum_{k=1}^{N-1} (q_{k+1} - q_k)^\kappa \ . \tag{2.6}$$

Thus, the only relevant parameter in this model is the relative coupling strength β, while the energy can always be scaled to, e.g. $E = 1$, which also involves a rescaling of time according to (2.5). This is a striking result and will be used later to obtain an exact prediction on the spreading behavior for the homogeneous case.

To summarize, two inherently different cases have been identified here:

1. The nonhomogeneous case $\kappa \neq \lambda$ with the energy as crucial parameter that will be studied in terms of the Hamiltonian (2.4).
2. The homogeneous case $\kappa = \lambda$ where the energy can be scaled out and the relative nonlinear strength β is the crucial parameter, described by the Hamilton function (2.6).

In the nonhomogeneous system, the energy determines the integrability of the system. For very small values $E \to 0$, the oscillators decouple and hence the system is integrable. The general picture of Hamiltonian chaos then is that for fixed N and increasing E, KAM-tori will first prevail and a mixed phase space with regular and chaotic parts will emerge until for some large enough energy, the whole phase space will be chaotic. This will be numerically analyzed in section 2.4.

For the homogeneous model, the integrability is determined by the parameter β, and for $\beta \to 0$ the system is integrable. Increasing β above some threshold also eventually leads to a fully chaotic phase space. Note that the value chosen in this

work $\beta \sim 1$ corresponds to such a situation. Decreasing the energy in this model just slows down the dynamics as seen from the scaling (2.5) and thus also decreases the time scale of chaos but not the phase space structure.

2.3. Phenomenology of Energy Spreading

The main purpose of this work is to understand chaotic diffusion in the nonlinear Hamiltonian systems introduced in the previous sections. The diffusion properties will mainly be studied by analyzing the spreading of initially localized excitations. The fundamental observation is as follows: starting only with a few neighboring oscillators with non-zero amplitude while the others are at rest, more and more oscillators, one after another, become excited with time, due to the nonlinear coupling to an excited neighbor. The level of excitation of an oscillator is measured by its local energy density:

$$w_k = \frac{E_k}{E} = E^{-1}\left(\frac{p_k^2}{2} + \frac{\omega_k^2}{\kappa}q_k^\kappa + \frac{\beta}{2\lambda}[(q_{k+1}-q_k)^\lambda + (q_k - q_{k-1})^\lambda]\right). \tag{2.7}$$

This definition holds for both the homogeneous and the nonhomogeneous case where in the latter $\beta = 1$ should be assumed. The density distribution $\{w_k\}$ fulfills $0 \leq w_k \leq 1$ and $\sum_k w_k = 1$ and hence defines a probability distribution on the lattice.

As mentioned before, this work focuses on the case when this energy transfer from excited to nonexcited oscillators is based on chaotic diffusion. Specifically, this means that the existence of traveling nonlinear waves in the system should be avoided. Such nonlinear waves, also called compactons, are a quite general phenomenon in nonlinear systems [77,78]. They have been studied excessively in a similar nonlinear chain as given by (2.1), but with absence of the local potential $\omega_k = 0$ [22,23]. There, shape and speed of such compactons were found and it was observed that they are stable and emerge out of arbitrary, even random initial conditions. When adding a regular, local potential, i.e. $\omega_k = 1$, those compactons still survive in the sense that one can find traveling waves emerging out of random initial conditions, called "quasi-compactons" here. This is illustrated in Fig. 2.1a, where the time evolution[3] for the 4–6_{re} case is shown ($\omega_k = 1$). The initial conditions were 10 randomly excited sites with a total energy $E = 10$ and one clearly sees the emergence of a quasi-compacton traveling to the right from the initial excitation. Opposed to the case without local potential studied in [22, 23], the quasi-compacton in Fig. 2.1a loses energy as seen from the non-zero energy density at the lattice sites after the compacton passed through. To avoid such quasi-compactons, disorder is introduced as illustrated in Fig. 2.1b. It shows a similar time evolution but for the 4–6_{hd} case, i.e. a disordered local potential $\omega_k \in [0.5, 1.5]$, again with 10 initially excited sites and $E = 10$. There,

[3] Details on the setup of the simulations and the employed numerical methods are given in section 4.1.

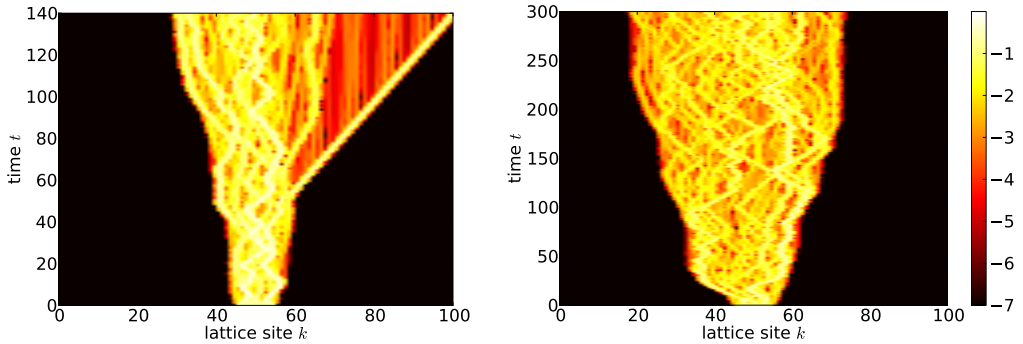

(a) 4–6_{re}, no disorder $\omega_k = 1$.

(b) 4–6_{hd}, hard disorder $\omega_k \in [0.5, 1.5]$.

Figure 2.1.: Time evolution of an initially localized state for the case 4–6 and energy $E = 10$, for both a regular lattice (a), and a lattice with "hard" disorder (b). The color coding corresponds to the logarithm of the local energy density $\log_{10} w_k$. The initial condition was a random excitation on 10 sites. The time evolution is shown up to $T = 140$ for the regular case (a) and $T = 300$ for the disordered potential (b).

no quasi-compactons travel through the system and the spreading is much slower. Also, the dynamics of the excited region seem chaotic and hence it is natural to call the process chaotic diffusion. Of course, Fig. 2.1b shows only an exemplary time evolution and no proof of the absence of quasi-compactons will be presented here. However, no such structures have been observed for any of the numerical studies of this model as soon as disorder was present. Nevertheless, a detailed investigation of such traveling waves and their properties might be an interesting extension of the existing work in this field. It should be noted that only exemplary results for the case 4–6 are shown here. However, these are general observations and can be found for any case of nonlinearly coupled oscillators. Similar results as shown in Fig. 2.1 (and also Fig. 2.2, discussed shortly) have been obtained for other combinations of κ and λ but are omitted here.

Another observation from Fig. 2.1 are the very sharp edges of the excited area (note the logarithmic scale of the color coding). This is seen more clearly in Fig. 2.2 where, for the model 4–6_{sd}, the instantaneous energy densities w_k at different times $t = 10^4,\ 10^6,\ 10^8$ are plotted. The initial condition was a single site excitation with energy $E = 1$ and the main observation are the very sharp edges of the spreading state. Note, that the y-axis is logarithmic and the excitations drop enormously fast in this scale. Hence, the tails of the excitations are decaying clearly faster than exponentially at the excitation border. This is remarkable, but not surprising and rather a general property of systems with purely nonlinear coupling terms. For example, also breathers [79] and compactons [23] in similar models without linear coupling terms were found to have such super-exponential tails. However, this property allows to quite precisely define the excitation area by counting the number of excited sites. This will be used in section 2.5.2 to introduce the notion of excitation times, an important observable to quantify spreading in these systems.

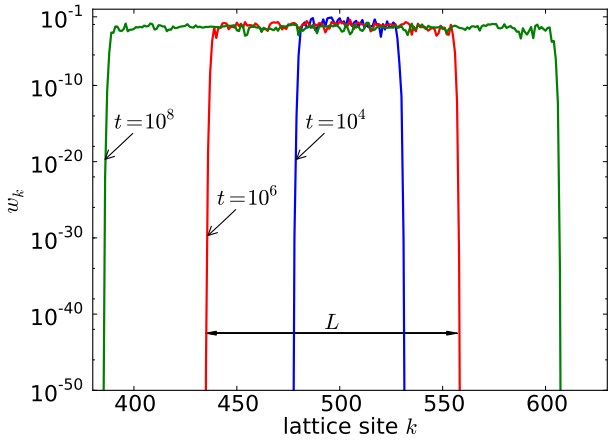

Figure 2.2.: Spreading of an initial single site excitation for the (disordered) case 4–6_{sd} and energy $E = 1.0$. The plot shows local energy density w_k vs. lattice site k for increasing times 10^4, 10^6, 10^8 (inner to outer curves). Note the logarithmic scaling of w_k and the exponential drops in this scale. L denotes the number of excited sites defined in section 2.5.2.

Additionally, Fig. 2.2 already reveals that the spreading takes place on exponential time scales. Increasing the time by two orders of magnitude leads to roughly a doubling of the number of excited sites. This is clearly slower than usual diffusion where the excitation area should have increased roughly by a factor of 10 and therefore this is already an indication for subdiffusive behavior.

2.4. Properties of Chaos

In the previous section, first signatures of spreading were shown. This spreading is claimed to be induced by chaotic behavior of the trajectories. Although it seems quite natural to assume chaoticity in the system due to its complicated, high dimensional phase space, such an assumption needs to be checked carefully. This is especially required as chaos is one of the fundamental ingredients for the understanding of spreading.

A numerical study on the properties of chaos in nonlinear Hamiltonian systems as described by (2.1) has been done by the author et. al in [80] for the case 4–6_{re}. Here, these results are reported together with new outcomes of similar studies on the 2–4 case. These considerations focus on the nonhomogeneous case because only there the energy is the relevant parameter and one obtains interesting results with implications also for the spreading setup.

The idea of [80] was to quantify the fraction of phase space that exhibits chaotic motion by a Monte-Carlo study. Therefore, rather small Hamiltonian chains with $N = 8 \ldots 64$ oscillators with periodic boundary conditions were considered. Such

a setup was studied even before for the DANSE model in [81]. In contrast to the spreading studies performed later, here all oscillators are initially excited and the chaoticity of the trajectory is analyzed. So for some system size N and some fixed energy E, many random initial conditions where chosen and their time evolution up to a time $T = 10^6$ was computed with numerical methods.[4] Simultaneously, the largest Lyapunov exponent λ was obtained as a measure of chaoticity of this trajectory. The Lyapunov exponent is an established way to quantify the strength of chaos along a trajectory by measuring the mean logarithmic growth rate of small perturbations. Positive Lyapunov exponents indicate chaos, while $\lambda = 0$ corresponds to a regular Hamiltonian system, more details can be found in any textbook on this subject, e.g. [2, 17].

Here, a trajectory is identified as being chaotic if $\lambda > 20/T$. In this case the initial condition belonged to the chaotic fraction of the phase space. The positive lower bound for chaotic λ has to be introduced because due to the conserved quantity in Hamiltonian systems, one Lyapunov exponent is always zero and the convergence to this value is typically as $1/T$. The specific choice for the critical value was justified by a statistical analysis of the Lyapunov exponents [80]. Then, the fraction of chaotic initial conditions N_{ch} of the total number of runs N_{tot} was calculated $P_{\mathrm{ch}} = N_{\mathrm{ch}}/N_{\mathrm{tot}}$. This quantity was called *probability of chaos* and can be understood as a measure for how much of the phase space belongs to the chaotic component, while the rest exhibits regular motion. P_{ch} depends on the system size N and the energy E, hence simulations were repeated for many $N = 8 \dots 64$ and energies $E = 10^{-8} \dots 1$. To allow a natural connection of these results with the spreading problem, here the energy density $W = E/N$ will be used as system parameter. For large enough values of the energy density one expects a fully chaotic phase space, hence $P_{\mathrm{ch}} = 1$. This comes from the fact that high energies correspond to strong perturbations which means chaos almost surely for any initial condition. Then for some fixed N and a decreasing energy density W, at some critical value W_c the emergence of KAM-tori will set in. Consequently, a fraction of the initial conditions will lie inside those regular islands (c.f. Fig. 1.1), hence P_{ch} will start to decrease for $W < W_c$.

The important question, however, is the dependence on the system size N, e.g. $W_c(N)$. Generally, one expects that an increase of N allows chaoticity for smaller values of the energy density because the complexity of the system increases. Hence W_c should decrease with increasing N. Here, this influence of N will be revealed numerically by obtaining results on P_{ch} for several values of N and then trying to find a scaling function $f(N)$ such that those curves fall onto each other when plotted for the scaled variables $P_{\mathrm{ch}}(Wf(N))$. The function $f(N)$ has the following meaning: given two system sizes $N_1 < N_2$ with critical densities $W_{c1} > W_{c2}$, then $f(N_1)/f(N_2) = W_{c2}/W_{c1}$. It will turn out that the functions $f(N)$ are particularly easy, i.e. simple power laws $f(N) = N^{\mu}$.

The results of $P_{\mathrm{ch}}(W)$ and its scaling with system size N for the fully nonlinear, nonhomogeneous, regular case 4–6_{re}, as obtained in [80], are are shown in Fig. 2.3a.

[4] For more details on the numerical setup see section 4.1.

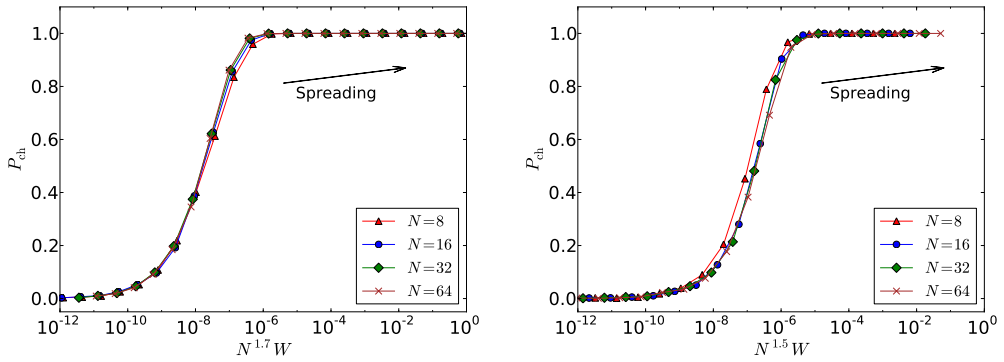

(a) Model 4–6_{re}.

(b) Model 4–6_{hd}.

Figure 2.3.: Probability of chaos $P_{\mathrm{ch}}(W)$ as function of energy density W for different numbers of oscillators N for the regular case 4–6_{re} (a) and the disordered case 4–6_{hd} (b). The x-axis includes the observed scaling with system size N, i.e. $f(N) = N^{1.7}$, $f(N) = N^{1.5}$ respectively. The arrows indicate the direction of spreading states in these plots (see text).

Note, that in [80], a different parametrization has been used with the coupling strength β (denoted γ there) as the only parameter and the energy being fixed to $E = N$. These two parametrization are equivalent and can be compared by identifying $\beta^2 = W$, as seen from the scaling described in section 2.2 in eq. (2.3). Additionally, the disordered case 4–6_{hd} is shown in Fig. 2.3b exhibiting a very similar behavior. In both cases, regular and disordered, one finds the emergence of regular islands at some critical energy density W_c, which is slightly larger for the disordered case as seen in Fig. 2.3b. Morevoer, the scaling with system size is found numerically to follow $N^{1.7}W$ (i.e. $f(N) = N^{1.7}$) for the regular case shown in Fig. 2.3a and $N^{1.5}W$ for the disordered case in Fig. 2.3b. This is seen from the overlap of results for different values $N = 8, 16, 32, 64$ when plotted with this rescaled coordinate.

This scaling has a remarkable consequence for the spreading process. During the spreading, the average energy density $W = E/L$ decreases as the total energy E remains constant, but the number of excited sites L increases. The relation to the spreading can be found from assuming that the phase space of the short chains with length N investigated here also effectively models the phase space around a spreading trajectory currently extended over $L = N$ sites. Then, increasing number of sites can, in this sense, be interpreted as an *effective increase of the dimensionality* of phase space accessed by the trajectory. So assuming $W = E/L$ and $N \sim L$, the scaled variable in Fig. 2.3 increases for spreading states as $N^{1.7}W \sim L^{1.7}W \sim L^{0.7}E$, or $L^{0.5}E$ respectively. That means in the course of spreading the trajectory is driven *away* from the regular parts of the phase space! This is a quite surprising, even counter-intuitive result as one would naturally expect that for small energy densities eventually a KAM-regime will be reached. But this is only true for a fixed system size. For spreading states, however, together with decreasing W, also the

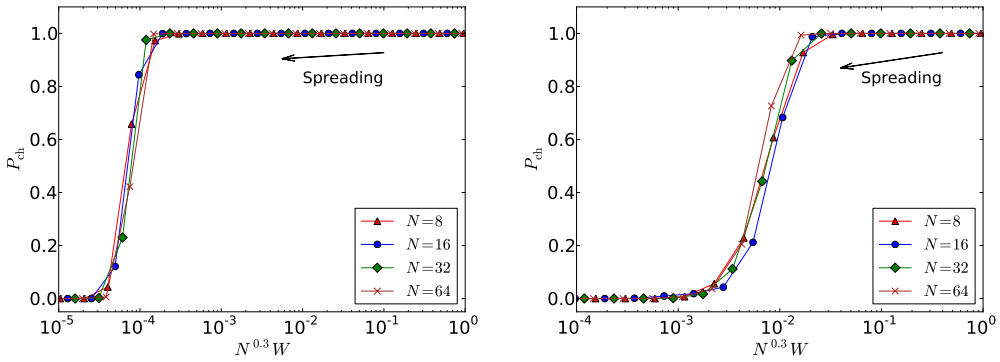

(a) Model 2–4$_{\mathrm{re}}$. **(b)** Model 2–4$_{\mathrm{hd}}$.

Figure 2.4.: Probability of chaos $P_{\mathrm{ch}}(W)$ as function of energy density W for different numbers of oscillators N for the regular case 2–4$_{\mathrm{re}}$ (a) and with disorder 2–4$_{\mathrm{hd}}$ (b). The x-axis includes the observed scaling with system size N, i.e. $f(N) = N^{0.3}$. The arrows indicate the direction of spreading states in these plots (see text).

effective dimensionality is increased and it turns out numerically that the latter effect is stronger ($\sim N^{1.7}$ vs. $\sim 1/N$). Hence, the KAM regime will not be reached for this case. This is true for both regular and disordered potential in the 4–6 model, but with slightly different scaling exponents. However, the comparison of spreading states with the properties of chaos for fixed sized chains is, although physically reasonable, rather speculative at this point requires further justification.

The situation changes fundamentally when linear oscillators are considered, as seen in Fig. 2.4. There, a similar analysis of P_{ch} is obtained for the 2–4 model, again for both the regular case ($\omega_k = 1$, Fig. 2.4a) and a disordered potential ($\omega_k \in [0.5, 1.5]$, Fig. 2.4b). In contrast to the fully nonlinear case before, here the scaled variable is found to be $N^{0.3}W$. This scaling is compatible with recent results on the same model [82]. The focus in this study was rather on the small density behavior than on the onset of regularity studied here, but the scaling at higher densities was reported as $f(N) = N^{0.4\pm0.1}$. Note, that for the regular lattice, Fig. 2.4a, the critical density is about two orders of magnitude smaller than for the disordered case (Fig. 2.4b), but the scaling is the same.

Again, the implications for spreading states will be analyzed by assuming that spreading leads to a decrease of energy density $W \sim E/L$ together with an increase of dimensionality $N \sim L$. In both cases the scaled variable behaves as $N^{0.3}\,W \sim E/L^{0.7}$ and hence the trajectory is driven *towards* the KAM-regime where larger and larger regular islands emerge in phase space. It should be noted that although the trajectory is driven towards the KAM-regime, this does not necessarily mean that spreading must eventually stop. In fact, assuming the trajectory is chaotic in the beginning it must stay inside the chaotic layer and can not become regular, at least as long as the phase space remains finite-dimensional which is assumed in this work. Then, even if at small enough densities the majority of the phase space consists

of islands with regular motion, the chaotic trajectory can travel along tiny chaotic layers, a mechanism called Arnold diffusion [83]. Moreover, the fact that spreading states do eventually enter regimes where regular islands exist does not immediately lead to a clear quantitative statement for the spreading process. When the chaotic layers get smaller and smaller as the regular islands grow (P_{ch} decreases), Arnold diffusion predicts an exponential increase of the time scale [17]. However, Chirikov and Vecheslavov observed the existence of a regime of so-called fast Arnold diffusion (FAD) [84], where the time scale to travel across a web of such thin chaotic layers increases only as a power law. Hence, it is unclear at this point how the change of phase space structure quantitatively influences the dynamics of trajectories in chaotic layers. Nevertheless, the result for 4–6 is very important as it means that there Arnold diffusion should not come into play for spreading states, in contrast to 2–4 where the spreading states potentially reach phase space regions with larger and larger regular islands.

Finally, a short note on the homogeneous case should be made. For $\kappa = \lambda$ the energy is not a free parameter and can be set to, e.g., $E = 1$ as it is shown in section 2.2. Accordingly, also the phase space structure and hence P_{ch} do not depend on the energy density W. Consequently, the course of spreading does not lead to a change of phase space structure – the only way to introduce regular islands is by decreasing the coupling parameter β. Moreover, this scaling of energy even leads to an exact spreading prediction that will be described in section 4.2.

2.5. Measures of Spreading

2.5.1. Second Moment and Participation Number

In this work, spreading is understood as the course of energy transfer from a number of initially excited oscillators into non-excited parts of the lattice. The excitation level of a single oscillator is measured by its local energy density w_k as defined in (2.7). This energy density can be interpreted as probability distribution as it fulfills $0 \leq w_k \leq 1$ and $\sum_k w_k = 1$. Starting from a connected initial condition at lattice sites between some k_0 and k_1, that is choosing q_k and p_k initially such that:

$$w_k \begin{cases} > 0 & \text{for} \quad k_0 < k < k_1 \\ = 0 & \text{else,} \end{cases} \tag{2.8}$$

the excitation will most certainly remain connected in the course of spreading if chaotic diffusion is assumed. That is firstly because due to nearest neighbor coupling the excitation can not jump across a lattice site and leave a hole, and secondly once excited from a chaotic, diffusive process an excited oscillator will most likely never return to zero amplitude. This is also seen in the exemplary trajectories shown in Figs. 2.1b and 2.2 where the excitation area clearly remains connected during the spreading process.

The fundamenal phenomenon studied in this work is the increasing number of excited lattice sites with time, hence a quantification of this excitation area needs to be introduced. Using the fact that the density $\{w_k\}$ represents a probability distribution, the most straight-forward measure is the second moment:

$$\Delta n^2(t) = \sum_k (k - \bar{k}(t))^2 w_k(t), \qquad \text{with} \qquad \bar{k}(t) = \sum_k k w_k(t), \tag{2.9}$$

where $\bar{k}(t)$ is the center of the distribution. The square root of the second moment $\Delta n(t)$ then is a measure for the excitation area at time t. This quantity has been used extensively to study spreading in the DANSE model, e.g. [38, 43, 44]. Another way to estimate the number of excited sites is the so-called participation number:

$$P(t) = \left(\sum_k w_k^2(t) \right)^{-1}, \tag{2.10}$$

also widely used to measure spreading [44,46]. That P indeed is a good estimate for the number excited sites can be seen when considering an excitation where $w_k = 1/L$ on precisely L sites and $w_k = 0$ everywhere else. The participation number then calculates as $P = L$. Note, that the participation number does not require connected excitation areas, it just measures the number of excited sites, not their distribution in the lattice, in contrast to the second moment. Being interested in the average spreading behavior and not single trajectories, one typically measures Δn^2 and P for many trajectories. This is done by changing the disorder realization or taking different, random initial conditions. Finallt, the averages $\langle \Delta n^2 \rangle$, $\langle P \rangle$ over many such trajectories are computed.

2.5.2. Excitation Times

Although the second moment and the participation number are widely used for investigating spreading properties, in this work another, superior method will be employed. This new quantity, firstly introduced by the author et al. in [46], relies on the very sharp edges at the border of the excitations as described previously in section 2.3, and on the connected nature of the excitation area. The basic idea is that due to these super-exponential tails one can simply count the number of excited sites L between those tails, visualized in Fig. 2.2. As the border is very sharp, this gives a very precise estimate of the excitation area. Moreover, it creates the possibility to determine the time ΔT that is required to excite one new oscillator in the system. So suppose having L lattice sites being excited, then $\Delta T(L)$ is the time required to pass from L to $L + 1$ lattice sites and can be understood as a first passage time of getting from L to $L + 1$ sites. We define an oscillator as excited if its local energy density exceeds some critical value $w_B = 10^{-50}$. The actual value of w_B was chosen arbitrarily, but any other choice, e.g. $w_B = 10^{-100}$ would produce similar results, this is precisely a consequence of the sharp edges. Thus, ΔT measures the propagation time for $L \to L + 1$ in dependence of the current

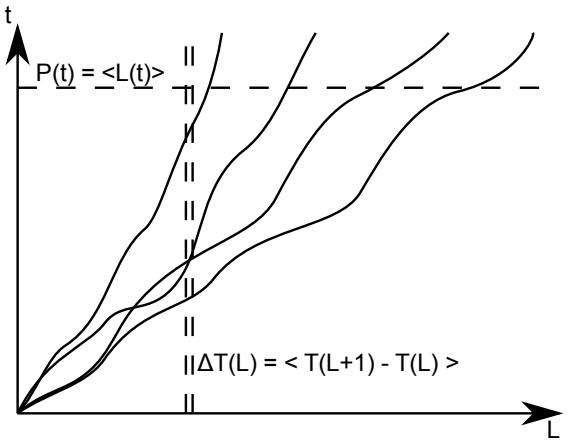

Figure 2.5.: Schematic graph showing the two ways to measure spreading. The solid lines correspond to individual trajectories and the dashed lines indicate the different averaging axes for the two methods. Averaging at fixed L means averaging at fixed energy density, contrary to averaging at fixed time which uses situations with different densities.

excitation area L, which is in some sense "adjoint" to the previous method where the excitation area was determined as a function of time. It can also be understood as the inverse excitation velocity, which is further clarified in section 3.4. Note, that this observable can not be used for spreading states that have exponential tails, like in the DANSE model, because such tails do not allow for a sensible quantification of the excitation area.

Using ΔT to quantify spreading has two important advantages over Δn^2 or P:

1. ΔT contains no explicit time dependence, hence any possible transient behavior occuring before the chaotic diffusion will not influence the values ΔT anymore as soon as the (sub-)diffusive regime is reached. In contrast, the value for $\Delta n^2(t)$ will always include any pre-diffusive behavior.

2. More importantly, using ΔT leads to a more reasonable averaging when considering ensembles of trajectories. This is because for ΔT, the averaging is obtained over situations with the same energy density $W = E/L$. When averaging $\Delta n^2(t)$ of many trajectories for a given time on the other hand, situations with different energy densities are mixed. As it will be shown later as one of the major results, the spreading process is governed mainly by the energy density W, hence the averaging over different densities smears out the results and should be avoided. The two ways of averaging are illustrated in Fig. 2.5.

Note, that for the excitation times a logarithmic averaging will be used: $\langle \log_{10} \Delta T \rangle$, which is essentially the geometric average.

2.5.3. Rényi Entropies

Another, very general method to analyze the shape of a distribution $\{w_k\}$ are the Rényi entropies [85]:

$$I_q = \frac{1}{1-q} \ln \sum_k w_k^q, \tag{2.11}$$

first applied to the spreading states in the DANSE model in [44, 73]. Here, these quantities are used to characterize the spikiness/flatness of the distribution. Consider the entropy I_1, which is just the usual Shannon entropy, and I_2, which is identical to the logarithm of the participation number:

$$I_1 = -\sum w_k \ln w_k \qquad I_2 = -\ln \sum_k w_k^2 = \ln P \; . \tag{2.12}$$

Then the difference

$$S_{\mathrm{str}} = I_1 - I_2, \tag{2.13}$$

called *structural entropy*, provides a measure of the peak structure of the distribution [86]. For a perfectly uniform excitation with $w_k = 1/L$ on L sites and $w_k = 0$ elsewhere, for example, the structural entropy evaluates to $S_{\mathrm{str}} = 0$. Deviations from such an uniform excitation will lead to an increase of S_{str}. For a detailed investigation of the properties of Rényi entropies and the structural entropy and their application to spreading states see [73].

2.6. Generalization to Two Dimensions

Here, the model introduced in section 2.1 will be generalized to two dimensional lattices of oscillators and the different measures of spreading in this case will be described. Essentially, this means introducing a second lattice index and adding another coupling term to the Hamiltonian (2.1). In this work, only quadratic lattices of oscillators will be considered where each oscillator couples to its four nearest neighbors. A generalization to other situations, like triangular or honeycomb lattices is trivial. As the scaling presented for the one-dimensional model in section 2.2 is independent on the lattice structure, it is also valid for 2D lattices and its repetition is omitted here. However, again two situations are present: nonhomogeneous nonlinearities with $\kappa \neq \lambda$, described by the Hamiltonian:

$$H = \sum_{i,k=1}^{N} \frac{p_{i,k}^2}{2} + \frac{\omega_{i,k}^2}{\kappa} q_{i,k}^{\kappa} + \frac{1}{\lambda} \sum_{i,k=1}^{N-1} (q_{i+1,k} - q_{i,k})^{\lambda} + (q_{i,k+1} - q_{i,k})^{\lambda} \; . \tag{2.14}$$

Here, i and k are now two lattice indices referring to the two dimensions of the quadratic grid of oscillators. Again, $\omega_{i,k}$ can either be random (soft $\omega_{i,k} \in [0, 1]$, or hard $\omega_{i,k} \in [0.5, 1.5]$ disorder), or regular $\omega_{i,k} = 1$. As in one dimension, the only parameter is the total energy E of the system. For the homogeneous case $\kappa = \lambda$,

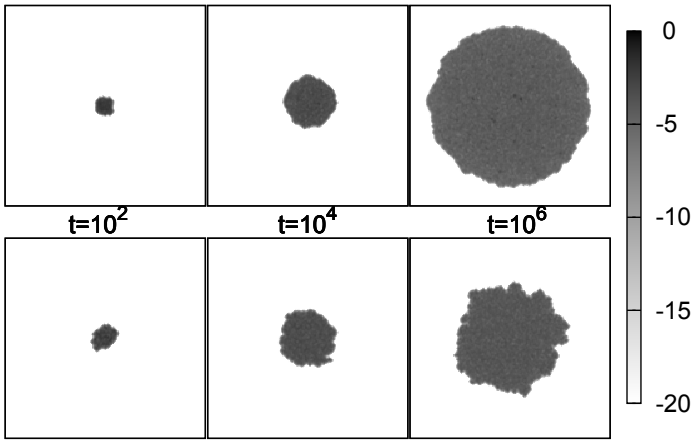

Figure 2.6.: Spreading in the 2D 2–4 model. The upper panels show logarithmic energy density $\log_{10} w_{i,k}$ (grey color coding) for the regular case 2–4$_{\mathrm{re}}$ ($\omega_{i,k} = 1$) with an initial energy $E = 1$, while the lower graphs are for the disordered case 2–4$_{\mathrm{sd}}$ ($\omega_{i,k} \in [0, 1]$) and an inital energy of $E = 10$. The size of the panels correspond to 160x160 lattice sites.

also the scaling shown in section 2.2 can be applied and the resulting Hamiltonian reads:

$$H = \sum_{i,k=1}^{N} \frac{p_{i,k}^2}{2} + \frac{\omega_{i,k}^2}{\kappa} q_{i,k}^{\kappa} + \frac{\beta}{\kappa} \sum_{i,k=1}^{N-1} (q_{i+1,k} - q_{i,k})^{\kappa} + (q_{i,k+1} - q_{i,k})^{\kappa} \,, \tag{2.15}$$

with the relative coupling strength β as the only remaining parameter.

Although the two-dimensional case is not much different when looking at the phase space structure, it has a remarkable advantage over one-dimensional chains: absence of nonlinear waves also for the regular potential $\omega_{i,k} = 1$. Just like in one dimension, the fundamental observable is the energy density, cf. (2.7):

$$\begin{aligned} w_{i,k} &= \frac{E_{i,k}}{E} \\ &= E^{-1}\Big(\frac{p_{i,k}^2}{2} + \frac{\omega_{i,k}^2}{\kappa} q_{i,k}^{\kappa} + \frac{\beta}{2\lambda}[\quad (q_{i+1,k} - q_{i,k})^{\lambda} + (q_{i,k} - q_{i-1,k})^{\lambda} \\ &\qquad\qquad + (q_{i,k+1} - q_{i,k})^{\lambda} + (q_{i,k} - q_{i,k-1})^{\lambda}] \Big) \,, \end{aligned} \tag{2.16}$$

which again can be viewed as probability distribution because $0 \leq w_{i,k} \leq 1$ and $\sum_{i,k} w_{i,k} = 1$. The absence of nonlinear waves is illustrated in Fig. 2.6, where the energy density $w_{i,k}$ is plotted for single trajectories for the two dimensional 2–4 model. The upper row shows the spreading of an initially localized excitation with energy $E = 1$ for the regular case $\omega_{i,k} = 1$. In contrast to one dimension, where quasi-compactons emerged from the excitation as shown, for example, in Fig. 2.1a, in two dimensions no such traveling waves are observed. A complete understanding of quasi-compactons and their existence, especially in two dimensional lattices, is

still missing, but also not subject of this work. Here, rather the numerical fact of the absence of quasi-compactons in 2D will be relied on without further investigation of the issue. However, this absence of nonlinear waves allows for studying the spreading in regular lattices as well. This will turn out to be particularly interesting for the case of linear oscillators $\kappa = 2$. Indeed, already the results shown in Fig. 2.6 indicate that the spreading in the regular lattice (top panels) is much faster than in the disordered case shown in the lower panels. Note, that in the disordered case the energy density was chosen ten times higher than for the regular case, but still the regular case exhibits a higher excitation area at the final time $t = 10^6$. The regular 2D case of harmonic oscillators will be quantified and studied in detail in section 4.3, spreading results for the disordered case are presented in section 4.5.4.

In two dimensions the spreading will be measured in terms of the second moment, which can be defined accordingly to the one dimensional case:

$$\Delta n^2 = \sum_{i,k} \left((i - \bar{i})^2 + (k - \bar{k})^2 \right) w_{i,k}, \tag{2.17}$$

where the mean values $\bar{i}$, $\bar{k}$ are calculated as:

$$\bar{i} = \sum_{i,k} i\, w_{i,k} \qquad \text{and} \qquad \bar{k} = \sum_{i,k} k\, w_{i,k}. \tag{2.18}$$

Similarly, the participation number can be defined as:

$$P = \left(\sum_{i,k} w_{i,k}^2 \right)^{-1}. \tag{2.19}$$

Although the excitations also have very sharp, super-exponential edges in two dimensions and spreading could potentially be analyzed in terms of excitation times as in the one dimensional case, here only results for the second moment will be presented. Studies of the excitation times in two dimensions, however, are also appealing and will be subject of future works. Note, that in two dimensions the second moment Δn^2 directly gives an estimate of the excitation area which is the number of excited sites.

The concept of Rényi entropies can also be applied to two-dimensional probability distributions and one finds:

$$I_q = \frac{1}{1-q} \ln \sum_{i,k} w_{i,k}^q. \tag{2.20}$$

Just like for one-dimensional lattices, the structural entropy S_{str} can be introduced as:

$$S_{\text{str}} = I_1 - I_2. \tag{2.21}$$

3. Nonlinear Diffusion Equation

Previous studies of spreading in the DANSE model revealed subdiffusive behavior where the width of the exciation on average increases as a power law (see section 1.3):

$$\Delta n^2 \sim t^\alpha, \qquad \text{with} \qquad \alpha \approx 1/3. \tag{3.1}$$

This subdiffusive behavior inspired the author et al. to use the nonlinear diffusion equation (NDE) as a phenomenologic macroscopic description of the spreading process, first reported in [44,73]. Although the DANSE model is much more complicated than the Hamiltonian systems introduced before, it has the same basic properties when viewed in its eigenmode basis: harmonic oscillators with random frequencies that are coupled by a fourth order nonlinearity – similar to the models 2–4_{hd} or 2–4_{sd} studied here. Thus, it seems reasonable to also use the nonlinear diffusion equation as a phenomenological description for spreading in the general nonlinear Hamiltonian lattices considered here [46].

3.1. The Nonlinear Diffusion Equation

The nonlinear diffusion equation is a generalization of the usual heat equation and was first introduced to describe transport in porous media [87, 88], but also applies to heat transfer in plasma, for example [89]. It is defined in terms of some space- and time-dependent density $\rho(\vec{r}, t) : \mathbb{R}^d \times [t_0, \infty) \to [0, \infty)$, that will be interpreted as energy density in this work:

$$\frac{\partial \rho(\vec{r}, t)}{\partial t} = \frac{\partial}{\partial \vec{r}} \left(D(\rho(\vec{r}, t)) \frac{\partial \rho(\vec{r}, t)}{\partial \vec{r}} \right), \qquad \text{with} \qquad \int_{-\infty}^{\infty} \rho(\vec{r}, t) \, \mathrm{d}\vec{r} = E \quad \forall\, t. \tag{3.2}$$

The spatial coordinate $\vec{r} \in \mathbb{R}^d$ is generally d-dimensional, but here only $d = 1$ and $d = 2$ will be considered. The time t is defined such that an initial value problem of the NDE starts at t_0. Mathematically, this is not important as one can always transform to a time where $t_0 = 0$. For the comparison with numerical results, however, the notion of t_0 will be useful. The function $D(\rho) : [0, \infty) \to [0, \infty)$ is the generalization of the diffusion constant introducing density dependence which defines the nonlinearity. The second equation represents the conservation law obeyed by solutions of this equation. If $D(\rho) = D_0 = \text{const}$, (3.2) simplifies to the usual, well-known heat equation that describes normal diffusion [90]. By introducing a density dependent diffusion "constant" $D(\rho)$ one creates an inherently different situation which changes both mathematical and physical properties of the equation.

As the NDE will be used to describe spreading induced by simple, power-law nonlinearities, it is appealing to restrict oneself to a special class of diffusion functions: $D(\rho) = D_0\rho^a$. Assuming this dependence, the nonlinear diffusion equation becomes (using $\rho \equiv \rho(\vec{r}, t)$ for simplicity):

$$\frac{\partial \rho}{\partial t} = D_0 \frac{\partial}{\partial \vec{r}} \left(\rho^a \frac{\partial \rho}{\partial \vec{r}} \right) = \frac{D_0}{a+1} \triangle \rho^{a+1}, \qquad \text{with} \qquad \int \rho \, \mathrm{d}\vec{r} = E \, , \tag{3.3}$$

where $\triangle$ is the Laplace operator with respect to $\vec{r}$. This will be the model used to describe the average spreading behavior in nonlinear Hamiltonian lattices. The parameter $a \in \mathbb{R}$, $a > 0$ describes the nonlinearity and will later be related to the nonlinearities κ and λ of the lattice models. This choice of power-law dependence $D \sim \rho^a$ with $a > 0$ is sometimes also called the case of *slow diffusion* (subdiffusion) as it possesses spreading solutions with a spreading rate slower than diffusive. This property is exactly the motivation why the NDE is considered here as a phenomenological model. However, as it will be shown later there are more similarities between the NDE and spreading states in Hamiltonian lattices that further justify the application of the nonlinear diffusion equation.

The NDE (3.3) formally is a *parabolic* nonlinear evolution equation. Strictly speaking, however, this is only true at those points where $D(\rho) > 0$, hence where $\rho > 0$. At points of vanishing diffusion coefficient, i.e. $\rho = 0$, the NDE is said to be *degenerate*. For an introduction and a summary of mathematical results on the NDE (3.3) see, e.g. the book by Vásquez [88] – a comprehensive presentation of theorems and proofs for the general case (3.2) is also given in [91].

It has to be clarified at this point that the introduction of the NDE is purely phenomenological. A derivation of (3.3) from the lattice Hamiltonian, e.g. (2.1), has not been found yet. Although such a derivation might be possible and some results in this direction have been obtained, for example in [92] and [93], a clear and rigorous calculation has not been presented yet. In this work, the validity of the NDE as a description of energy spreading will be checked by comparing its spreading predictions with numerical simulations of the nonlinear lattices. Moreover, some analysis of the microscopic dynamics at the excitation edge will be performed leading to predictions on the relation between the NDE nonlinearity a and the lattice nonlinearities κ and λ. But first, some properties of the nonlinear diffusion equation and its spreading solutions shall be discussed.

3.2. General Properties

As for any nonlinear theory, the solutions of the nonlinear diffusion equation can not be decomposed into a basis of fundamental solutions. So while for the usual heat equation ($a = 0$, $D(\rho) = D_0$) the time evolution of any initial condition can be computed in terms of a convolution of Gauss kernels, such an approach is not possible for the NDE. However, the particular simplicity of the diffusion term $D(\rho) \sim \rho^a$ leads to a number of interesting properties that will be presented in the following.

3.2.1. Existence and Uniqueness

The degenerate nature of the NDE (3.3) leads to considerable difficulties at formulating and proving existence and uniqueness theorems for solutions of the NDE. The main technique to overcome these issues is the introduction of the concept of *weak solutions*, sometimes also called *generalized solutions* [94]. The basic concept is that a weak solution $\rho(\vec{r}, t)$ does not need to fulfill the NDE (3.3) directly, but rather its product with any test function has to obey an integrated version of (3.3). A sophisticated introduction to the theory of weak solutions is by far out of scope of this work and interested readers are referred to more mathematical texts on this subject, e.g. [88, 91, 94]. Nevertheless, the main result of the theory is that, under some conditions of boundedness and smoothness of initial conditions, the existence of a unique weak solution can be shown. Although this is a very important and fundamental mathematical result, here the attention will be drawn to a class of explicit solutions introduced in section 3.3.

3.2.2. Front Propagation

One of the key differences between the normal heat equation and the NDE is that the NDE exhibits a finite front propagation velocity. For the heat equation, any non-zero solution is automatically positive in the whole domain of definition (e.g. Gaussian tails). That means for a connected initial condition that is non-zero in some subdomain and zero everywhere else, the heat equation leads to instantaneous excitation of the whole domain at infinitesimal times. For the NDE, in contrast, such a connected initial condition leads to a propagating front separating the domain with $\rho > 0$ from the rest where $\rho = 0$. It can be shown, even for the general case (3.2), that if the support of the initial datum $\operatorname{supp} \rho(\vec{r}, t = 0)$ is bounded than also $\operatorname{supp} \rho(\vec{r}, t)$ is bounded for all times t. The boundary, however, is generally moving with time – leading to an increase of the support of $\rho(\vec{r}, t)$.

3.2.3. Symmetries

Here, the general NDE (3.2) with $D(\rho)$ is considered as these symmetries do not require the specific power-law form of the diffusion term. As the NDE is homogeneous in space and time, it is invariant under displacements of the coordinate axes [88]. Assuming $\rho(\vec{r}, t)$ is a solution of (3.2), then for every $\vec{r}\,' \in \mathbb{R}^d$ and $t' \in \mathbb{R}$ the function:

$$\tilde{\rho}(\vec{s}, \tau) := \rho(\vec{s} - \vec{r}\,', \tau - t') \tag{3.4}$$

is also a solution of (3.2).

Moreover, the NDE is invariant under spatial rotations, as the Laplace operator $\triangle$ commutes with the operations of the orthogonal group. This is especially important for the two-dimensional case considered later, where rotational invariance motivates

to search for radially symmetric solutions. But also in one dimension this has an important consequence, because it means that if $\rho(x,t)$ is a solution then also $\rho(-x,t)$ is.

3.2.4. Scaling

For the power-law nonlinearity $D(\rho) \sim \rho^a$, the NDE (3.3) additionally exhibits a scaling invariance. Assuming that $\rho(\vec{r},t)$ is a solution of (3.3) and letting $t_0 = 0$ by an appropriate time shift as above, the scaled function:

$$\tilde{\rho}(\vec{r},t) := \alpha\,\rho(\beta\vec{r},\gamma t) \tag{3.5}$$

is again a solution for α, β, $\gamma > 0$ if they fulfill:

$$\alpha^a\beta^2 = \gamma. \tag{3.6}$$

This defines a two-parameter family of transformed solutions [88] and is a very important property of the NDE with power-law nonlinearity. In particular, it allows for finding an interrelation between the energy of a solution and its time scale. Suppose having found a solution with some energy $E > 0$, then by applying the scaling above with $\alpha = 1/E$ and $\beta = 1$ one finds a new solution to the NDE, but with energy $E' = 1$. That means the energy can always be scaled to $E = 1$ by a proper rescaling of density amplitude and time. Or, in other words, for any solution $\rho(\vec{r},t\,;E)$ the energy has to appear in such a way that one can write

$$\rho(\vec{r},t\,;E) = E\tilde{\rho}(\vec{r},tE^a), \tag{3.7}$$

where $\tilde{\rho}$ does not depend on E and $\int\tilde{\rho}\;\mathrm{d}\vec{r} = 1$. Basically, that corresponds to introducing a new time-scale:

$$t' = tE^a. \tag{3.8}$$

The above result allows to compare situations with different energies, hence relate solutions emerging from different initial conditions. However, to obtain more understanding of the properties of a specific solution of the NDE, one can further demand the invariance of the energy $\int\rho\mathrm{d}\vec{r} = E$ under the scaling transformation. This gives another relation between the scaling parameters:

$$\alpha = \beta^d, \tag{3.9}$$

where d denotes the spatial dimensionality, i.e. $\vec{r} \in \mathbb{R}^d$. This, eventually, gives a one-parameter family of scaled solutions and can be expressed in terms of a single scaling parameter, e.g.:

$$\tilde{\rho}(\vec{r},t) := \alpha\,\rho(\alpha^{1/d}\vec{r},\alpha^{a+2/d}t). \tag{3.10}$$

This scaling, for example, relates the spatial profiles of a solution ρ at different times $t_1, t_2 > t_0$. Such a scaling property indicates the existence of so-called self-similar solutions, where the time-dependence can be scaled out using the above relation and one is left with finding the spatial profile. This is subject of the next section.

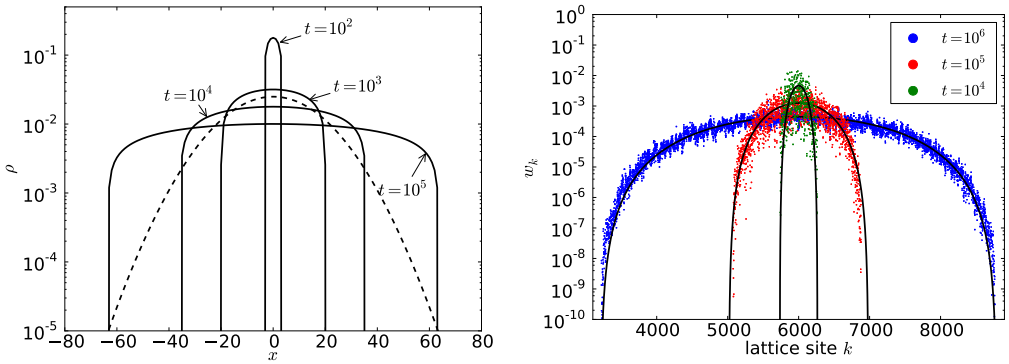

(a) Self-similar solution of the NDE. **(b)** Comparison with spreading states.

Figure 3.1.: The self similar solution $\rho(x,t)$ as given by eq. (3.13) of the one-dimensional NDE, where $x \equiv \vec{r}$ in 1D. In (a) the shape is shown for $a = 2$, $D_0 = 1$ and $E = 1$ at times $t = 10^2, 10^3, 10^4, 10^5$ (inner to outer lines) in logarithmic scale. The dashed line shows a Gaussian profile for comparison. On the right, (b) shows profiles of spreading states in the homogeneous case 4–4_{hd} together with the self-similar solution (black lines) for $a = 1/4$ as predicted by theory (section 4.2).

3.3. Self-Similar Solutions

As said earlier, the nonlinear diffusion equation will be used to give a phenomenological model of the spreading process in Hamiltonian lattices. Therefore, special interest lies in the type of solutions that correspond to spreading of localized initial conditions, opposed to, e.g. traveling wave solutions. Fortunately, such solutions do exist for the NDE and can even be written explicitly. They were first found by Zelkovich and Kompaneetz [95], and shortly after generalized by Barenblatt [96]. Hence, these solutions are sometimes called ZKB- or Barenblatt-solutions. Here, the term self-similar solution will be used as this name already contains the main property of these functions. For convenience, the NDE, as introduced in (3.3), is quickly repeated:

$$\frac{\partial \rho}{\partial t} = D_0 \frac{\partial}{\partial \vec{r}} \left(\rho^a \frac{\partial \rho}{\partial \vec{r}} \right) = \frac{D_0}{a+1} \triangle \rho^{a+1}, \qquad \text{with} \qquad \int \rho \, \mathrm{d}\vec{r} = E \, . \tag{3.11}$$

The self-similar similar solution is a so-called *source solution*, which means that it solves (3.11) with a source term as initial condition:

$$\rho(\vec{r}, t_0) = E \, \delta(\vec{r}), \tag{3.12}$$

where E is the conserved energy and δ is Dirac's delta distribution. For $a > 0$ the self-similar solution for $t > t_0$ is given by [88]:

$$\rho(\vec{r},t) = \begin{cases} (t-t_0)^{-\alpha}\left((\mu E)^{2a\beta} - \frac{a}{2(ad+2)D_0}\frac{|\vec{r}|^2}{(t-t_0)^{2\beta}}\right)^{1/a} & \text{for} \quad |\vec{r}|^2 < R(t)^2 \\ 0 & \text{for} \quad |\vec{r}|^2 > R(t)^2 \end{cases} \tag{3.13}$$

$$\text{with} \quad \alpha = \frac{d}{ad+2} \quad \text{and} \quad \beta = \alpha/d = \frac{1}{ad+2},$$

$$\text{and} \quad R(t)^2 = \frac{2(ad+2)D_0}{a}\left[(\mu E)^a (t-t_0)\right]^{2\beta} . \tag{3.14}$$

The parameter $\mu = \mu(D_0, a, d)$ is some constant of integration depending only on D_0, the nonlinear exponent a and the dimensionality d of the system and is not important for the further considerations. However, a derivation of (3.13) is given in appendix A.2 including an expression for μ. $R(t)$ is the edge of the excitation propagating through space, in one dimension it is just the left and right boundary, while for two dimensions the excitation edge is a circle with radius R. Note, how the scaling requirement (3.7) constitutes nicely in the expression for R^2 (3.14). The time offset t_0 is introduced to account for transient behavior in the later numerical simulations that might not be describable by the NDE.

Fig. 3.1a shows the self similar solution in one dimension in terms of snap-shots of the spatial profiles at times $t = 10^2 \ldots 10^5$ in logarithmic scale. This visualizes nicely the self-similar character of this function as well as the connected support with the edges moving as (3.14). Moreover, the logarithmic scale also emphasizes the property of zero density outside a connected area, especially in contrast to a Gaussian profile that has "only" exponential tails also shown in Fig. 3.1a as a dashed line. Note, that taking the limit $a \to 0$ gives the normal heat equation and also the self-similar solution (3.13) converges towards the Gaussian profile in this limit. A thorough examination of the self-similar solution (3.13) reveals its non-differentiability at the points $|\vec{r}| = R$, hence it is not a true solution of the NDE. However, this problem can be overcome by introducing the concept of "weak solutions" mentioned earlier. Indeed, the self-similar solution solves (3.11) in this sense. However, this mathematical detail can fortunately be neglected for further physical purposes.

The self-similar solution originally has been introduced solely as solution to the source problem $\rho(\vec{r}, t_0) = E\delta(\vec{r})$. However, in 1971 Peletier found a remarkable property [97], making those solutions an even more important subject of study. There, it was shown that quite arbitrary initial conditions converge towards a suitable chosen self-similar solution. That means it does not only solve the, rather special, source problem but also serves as a prototypical solution for a whole class of initial conditions as their long time behavior follows the self-similar solution [98,99]. As this work focuses especially on the asymptotic spreading behavior, the properties of these self-similar solutions appear to be the right quantities to investigate. This

is further motivated by comparing the spatial profile of a spreading state with the self-similar solution in Fig. 3.1b. There, the energy density w_k of an initial single site excitation in a lattice of type 4–4_{hd} at time $t = 10^4$, 10^5 and 10^6 is shown. Additionally, the self-similar solution (3.13) with a nonlinearity parameter $a = 1/4$ is plotted. This value of a can be derived exactly from scaling arguments as will be seen later in section 4.2. The remarkable agreement of the self-similar solution with the spatial profiles of the spreading states encourages to apply the nonlinear diffusion equation to nonlinear Hamiltonian lattices.

Following the ideas introduced for the lattice models, an excitation area A can be defined as the area where $\rho > 0$:

$$A(t) \sim R(t)^d \sim (E^a(t - t_0))^\alpha, \tag{3.15}$$

where only the behavior with energy and time is considered. As $0 < \alpha < d/2$ for $a > 0$, this corresponds to subdiffusive behavior with exponent $\alpha(a, d)$. Using the definition of α (3.13) one finds $a\alpha = 1 - 2\alpha/d$ and the spreading can be written in a form that emphasizes the energy scaling:

$$\frac{A(t)}{E} \sim \left(\frac{t - t_0}{E^{2/d}}\right)^\alpha. \tag{3.16}$$

This quantifies spreading of the self-similar solution and will later be compared to spreading results of the Hamiltonian lattices. Unfortunately, this still includes the transient time t_0 that is generally unknown and must be fitted. However, by considering the inverse spreading velocity, a quantity with no dependence on t_0 can be obtained as follows [46]. First, eq. (3.15) is solved for $t - t_0$:

$$t - t_0 \sim A^{1/\alpha} E^{-a} \tag{3.17}$$

and then one immediately finds for the inverse spreading velocity $\mathrm{d}t/\mathrm{d}A$, using $1/\alpha - 1 = a + (2 - d)/d$:

$$\frac{1}{A^{(2-d)/d}} \frac{\mathrm{d}t}{\mathrm{d}A} \sim \left(\frac{A}{E}\right)^a. \tag{3.18}$$

3.4. NDE Predictions for Spreading in Lattices

In section 2.5 the methods of quantifying spreading in Hamiltonian lattices were introduced and in the previous section the spreading behavior of the nonlinear diffusion equation was analyzed. Here, these results are combined and the implications from self-similar solutions for the spreading observables introduced in 2.5 will be discussed in detail. As numerical results are obtained for one- and two-dimensional systems, these two cases will be analyzed explicitely.

3.4.1. Spreading in One Dimension

For one-dimensional systems, $d = 1$, the excitation area A of the self similar solution can be compared with the excitation length L, namely the number of excited sites, of spreading states in Hamiltonian lattices: $L \sim A$. Furthermore, the participation number as well as the square root of the second moment are expected to exhibit the same time dependence as the excitation length. Hence one finds:

$$P(t) \sim \sqrt{\Delta n^2(t)} \sim L(t) \sim A(t) \sim R(t). \tag{3.19}$$

Although this relation is quite intuitive, it can even be obtained from an exact calculation by defining, e.g. $P = E^2/\int \rho^2 \mathrm{d}\vec{r}$ and using the self-similar solution for ρ. This is shown, also for Δn^2, in appendix A.3. Then, from the result for the behavior of the excitation area of the self-similar solution (3.16), the following prediction is obtained for spreading states in one-dimensional Hamiltonian lattices:

$$\frac{P(t)}{E} \sim \frac{\sqrt{\Delta n^2(t)}}{E} \sim \left(\frac{t - t_0}{E^2}\right)^{\alpha_1} \qquad \text{with} \qquad \alpha_1 = \frac{1}{a+2}. \tag{3.20}$$

Furthermore, in section 2.5.2 the concept of excitation times as the time ΔT to excite a new lattice site is introduced. This can be compared with the inverse spreading velocity defined in (3.18) $\mathrm{d}t/\mathrm{d}A \sim \Delta T/\Delta L$, where ΔL corresponds to the increase by exactly one lattice site, hence $\Delta L = 1$. Therefore, the self-similar solution predicts for the excitation times:

$$\frac{\Delta T(L)}{L} \sim \left(\frac{L}{E}\right)^a. \tag{3.21}$$

These relations, (3.20) and (3.21), are the two predictions that will be tested numerically in one-dimensional systems in order to verify the applicability of the nonlinear diffusion equation. Specifically, they include a prediction on the energy scaling that basically already follows from the scaling property of the nonlinear diffusion equation (3.7) and is not limited to the self-similar solution. This energy scaling can be tested nicely by running the simulations for different energies, which will be presented in chapter 4.

Finally, it is quite natural to expect a constant structural entropy if spreading states follow the self-similar solution:

$$S_{\mathrm{str}} = \mathrm{const.} \tag{3.22}$$

This is because due to self-similarity, the peak structure and hence the structural entropy of spreading states should not change. However, this can also be found from an explicit calculation for the self-similar solution as shown in appendix A.3.

3.4.2. Spreading in Two Dimensions

For two dimensional lattices, $d = 2$, the results are very similar. There, spreading states in Hamiltonian lattices exhibit a two-dimensional excitation area similar to

the excitation length for the one-dimensional case. As the participation number and the second moment defined in section 2.6 follow the behavior of the excitation area, one finds the relation between these quantities and the excitation area A of the self-similar solution to be:

$$P(t) \sim \Delta n^2(t) \sim A(t) \sim R^2(t). \tag{3.23}$$

Again, a rigorous calculation of this relation by explicit integration of the self-similar solution can be found in appendix A.3.

From the spreading results (3.16) of the NDE one then finds for spreading states in two-dimensional lattices:

$$\frac{P(t)}{E} \sim \frac{\Delta n^2(t)}{E} \sim \left(\frac{t - t_0}{E}\right)^{\alpha_2} \qquad \text{with} \qquad \alpha_2 = \frac{1}{a+1}. \tag{3.24}$$

This will be the main relation to be checked for two-dimensional lattices. For completeness, also the prediction for the excitation times is given, although it will not be used later:

$$\Delta T(A) \sim \left(\frac{A}{E}\right)^a, \tag{3.25}$$

where A here denotes the number of excited lattice sites in the two-dimensional lattice. Just as above, the self-similarity of the NDE solution corresponds to a constant structural entropy and thus also for the 2D case one expects:

$$S_{\text{str}} = \text{const.} \tag{3.26}$$

Again, this can be shown by an explicit calculation, given in appendix A.3.

4. Energy Diffusion in Nonlinear Lattices

This chapter contains the main results of this work: a detailed analysis of the properties of chaotic diffusion in nonlinear Hamiltonian lattices in the meaning of energy spreading of initially localized excitations. Several combinations of the nonlinear exponents $\kappa \geq 2$ and $\lambda > 2$ will be investigated, with and without disorder and for one- and two-dimensional lattices. The main idea is to compare predictions from the NDE, especially on the scaling of energy, with numerical results of spreading states in nonlinear Hamiltonian lattices. Moreover, a relation between the nonlinearity a of the NDE and the nonlinear exponents κ, λ of the lattices is tried to be derived and compared to numerical observations. For this analytical treatment, two different techniques are used. Firstly, the energy scaling properties of the Hamiltonian system are analyzed and compared with the scaling properties of the NDE and hence a relation between the lattice nonlinearity and the nonlinear parameter of the NDE a is obtained. However, this is only possible for the homogeneous case with equal nonlinear powers $\kappa = \lambda$ because only in this case an energy scaling relation can be used. For the other cases $\kappa \neq \lambda$, the microscopic dynamic at the edge of the excitation area is investigated, where a non-excited oscillator is driven by its excited neighbor. The dynamical properties of this situation are studied in detail using resonant perturbation theory, and as result exact predictions for the subdiffusive spreading are obtained. Note, that this approach is fundamentally different from previous attempts, where instead of trying to understand the microscopic dynamics, the chaotic behavior of excited oscillators is interpreted as an effective noise and its properties are studied in a statistical, hence macroscopic sense [48].

The results will be presented in the order of "increasing complexity" of the dynamical behavior starting from the homogeneous case $\kappa = \lambda$, followed by a study on regular lattices. Then the fully nonlinear case is investigated and finally the most difficult situation of disordered harmonic oscillators and nonlinear coupling is addressed.

4.1. Numerical Methods

Before getting to the actual results, some notes on the numerical methods used in this work should be made. The Hamiltonian system of study was introduced in section 2. Numerically, this model is treated in terms of an initial value problem of the corresponding system of ordinary differential equations for functions $q_k(t) : [0, \infty) \to \mathbb{R}$,

$p_k(t) : [0, \infty) \to \mathbb{R}$ as defined in 2.2:

$$\begin{aligned} \dot{q}_k &= \frac{\partial H}{\partial p_k} = p_k, \\ \dot{p}_k &= -\frac{\partial H}{\partial q_k} = -\omega_k^2 q_k^{\kappa-1} - \beta \left((q_k - q_{k+1})^{\lambda-1} + (q_k - q_{k-1})^{\lambda-1} \right), \\ q_k(0) &= q_{k,0}, \quad p_k(0) = p_{k,0}. \end{aligned} \tag{4.1}$$

The equations for two dimensions are similar and can easily be obtained from the corresponding Hamiltonians (2.14) or (2.15). The boundary conditions are not important, as explained later. (4.1) defines a system of ordinary differential equations and given some initial condition $q_{k,0}$, $p_{k,0}$, a trajectory can be obtained by numerical integration. This gives, obviously, only an approximation of an actual trajectory as the numerical routines can not provide exact results. For more details on numerical integration of ODEs see any of the vast amount of textbooks on this subject, e.g. [100–102].

To account for the Hamiltonian structure of the problem, in this work a *symplectic* integration routine is used [103]. Symplectic routines ensure the conservation of phase space volume, a property of Hamiltonian systems. Physically, this can be understood from the fact that a symplectic routine does not provide a trajectory of the original Hamiltonian system, defined by the Hamilton function H, but of a slightly disturbed Hamilton function $H + \Delta H$. This is a crucial difference to non-symplectic routines, where the approximate trajectory generally does not belong to any Hamilton function. Practically, this means that by using a symplectic routine it is ensured that no dissipation is introduced by the numerical treatment, a quite remarkable advantage over simple, non-symplectic methods.

Specifically, in this work a 4-th order symplectic Runge-Kutta-Nystrom [104] method is used for integrating the equations of motion, in both one and two dimensions. The time step of the method was set to $\Delta t = 0.1$, unless indicated otherwise. This ensured energy conservation with an accuracy $\Delta E \lesssim 10^{-3}$. However, some of the results were tested with smaller time steps and no qualitative difference was observed. After averaging, no dependence on the time step of the reported results was observed. The very sharp, super-exponential tails of the spreading states allow for using an adaptive lattice during the numerical integration. E.g. for the one-dimensional case and an initial condition consisting of L_0 excited sites, as mostly chosen here, the lattice is initially implemented as having $N = L_0 + 10$ sites with five zero amplitude sites at the left and right boundary. With time, as the excitation starts to spread, new sites get excited. The simulation was written in such a way that with each newly excited site also the lattice increases such that always a boundary of five zero-amplitude sites remain to the left and right. This heavily increases the efficiency of the numerical scheme as the simulation of "empty sites" is mostly avoided. Furthermore, no boundary conditions need to be worried about as the excitation is ensured to never reach the boundary at all. A similar technique is used for the two-dimensional case where the lattice is quadratic and the boundary is a strip of width five around the excitation area.

The observables to quantify spreading in this work are the excitation times ΔT and the second moment Δn^2, introduced in section 2.5. The results presented here are obtained from a Monte-Carlo study of many trajectories, either for different realizations of disorder for systems where disorder is present, or for many random initial conditions in the case of regular lattices. For each of these numerical trajectories, the macroscopic variable ΔT, or Δn^2 respectively, are calculated and then an averaging over such an ensemble of results is performed. For the excitation times, the averaging is obtain for the logarithmic quantity, hence $\langle \log_{10} \Delta T \rangle$ is calculated, while the second moment is averaged directly $\langle \Delta n^2 \rangle$. The size of ensembles over which the averaging is performed varies greatly from only $M = 10$ for some 2D results up to $M = 1000$ for some of the one-dimensional studies. It has been checked, however, that the method of averaging, logarithmic or direct, does not influence the fundamental outcomes of this work (scaling and spreading exponents).

All simulations were implemented in C++ and for the numerical scheme the `odeint` library was used [105, 106]. Most of the one-dimensional results were obtained on usual x86 CPUs, with many runs done on the ZEIK-Cluster of the University of Potsdam, but some also on CUDA GPUs. The 2D results, on the other hand, were computationally much more challenging, thus for those the CINECA sp6 supercomputer in Bologna was employed within the Project HPC-EUROPA2 (Project number 228398).

4.2. Homogeneous Nonlinearities

The first situation that will be studied is that of homogeneous nonlinearities, i.e. $\kappa = \lambda$ because there the analysis of the spreading process is particularly simple. The Hamiltonian in one dimension reads (cf. (2.6)):

$$H = \sum_{k=1}^{N} \frac{p_k^2}{2} + \frac{\omega_k^2}{\kappa} q_k^\kappa + \frac{\beta}{\kappa} \sum_{k=1}^{N-1} (q_{k+1} - q_k)^\kappa \ . \tag{4.2}$$

For a fixed nonlinear power κ, the coupling strength β is the only relevant parameter when considering averaged results over disorder realizations $\{\omega_k\}$.

4.2.1. Scaling-Implied Spreading Prediction

In section 2.2 the scaling property for the homogeneous case $\kappa = \lambda$ was found (2.5). Specifically, this implies that when rescaling the energy from some value E to unity $E' = 1$, the time scale changes as $t' \sim E^{1/2-1/\kappa}$. Remarkably, the nonlinear diffusion equation exhibits a similar property when transforming from arbitrary energies to the case $E' = 1$: $t' \sim E^a$ (3.8). If one assumes that the NDE is the correct description for spreading in this homogeneous situation, these two scalings have to be equivalent

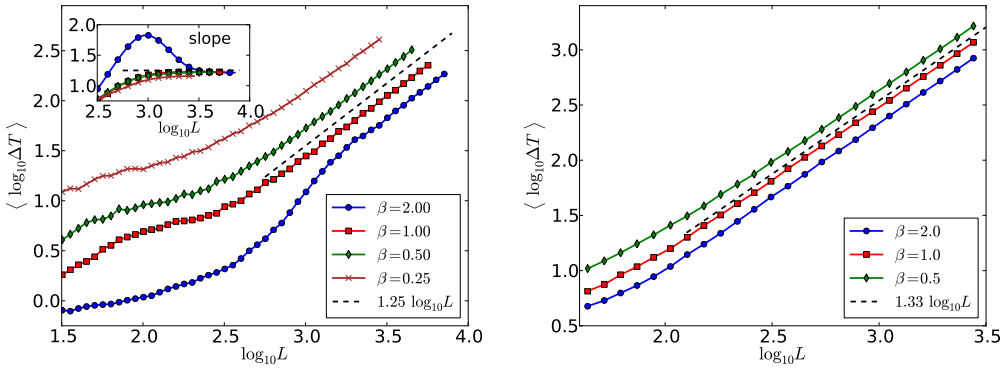

(a) Model 4–4$_{\mathrm{sd}}$ in 1D. **(b)** Model 6–6$_{\mathrm{sd}}$ in 1D.

Figure 4.1.: Excitation times ΔT for one-dimensional lattices with homogeneous nonlinearities, $\kappa = \lambda = 4$ (a) and $\kappa = \lambda = 6$ (b) for soft disorder ($\omega_k \in [0, 1]$). The black dashed lines show the predicted asymptotic behavior (4.4): $\Delta T \sim L^{a+1}$ with $a = (\kappa - 2)/(2\kappa)$. The inset in (a) shows the slopes of the curves and their convergence towards $a + 1 \approx 5/4$.

and one finds an exact relation between the nonlinear parameter of the NDE a and the nonlinear power of the lattice Hamiltonian κ:

$$a = \frac{\kappa - 2}{2\kappa}. \tag{4.3}$$

Note that both scalings are independent of the dimensionality and thus this relation holds for any dimension d. It gives a nice, exact prediction on the spreading process that can be checked numerically.

4.2.2. Numerical Results in 1D

To verify the application of the NDE as an adequate description of the spreading process, first a study of excitation times ΔT for the one-dimensional models 4–4$_{\mathrm{sd}}$ and 6–6$_{\mathrm{sd}}$ was performed. In both cases the potential was chosen as "soft disorder": $\omega_k \in [0, 1]$ and several values for the nonlinear strength were used $\beta = 1/4 \ldots 2$, all large enough to ensure chaoticity in the system. The prediction of the NDE for the excitation times was calculated in section 3.4 as $\Delta T \sim L^{a+1}$ (c.f. (3.21)). Using the scaling result above (4.3), the following exact prediction is found:

$$\Delta T \sim L^{5/4} \quad \text{for 4–4,} \qquad \text{and} \qquad \Delta T \sim L^{4/3} \quad \text{for 6–6.} \tag{4.4}$$

Fig. 4.1 shows that the spreading states indeed nicely converge towards this power-law behavior with exponent 5/4, 4/3 respectively. In Fig. 4.1a, results for initial single site excitations are shown and one finds good convergence towards the exponent $a + 1 = 5/4$ as is emphasized in the inset where the instantaneous exponent

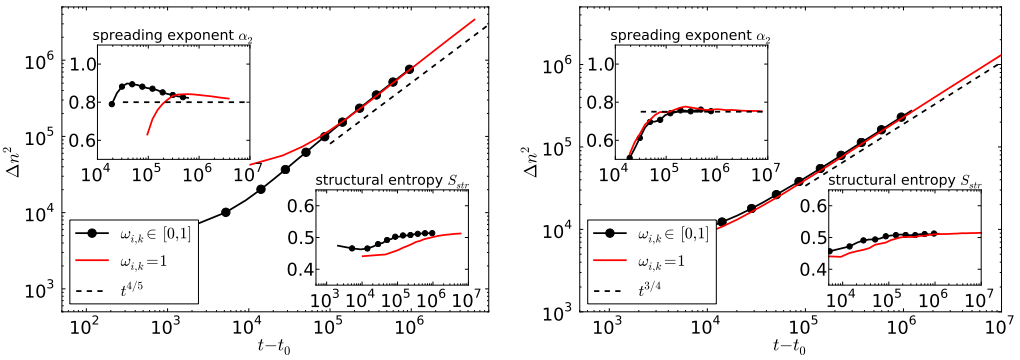

(a) Model 4–4 in two dimensions. **(b)** Model 6–6 in two dimensions.

Figure 4.2.: Second moment $\Delta n^2(t)$ for the 2D models 4–4 (a) and 6–6 (b) with regular potential ($\omega_{i,k} = 1$) and soft disorder ($\omega_{i,k} \in [0, 1]$). The insets show the numerical spreading exponents α_2 obtained from finite differences and the structural entropy $S_{\mathrm{str}}(t)$.

obtained from finite differences in the log-log representation is plotted. The averaging $\langle \log_{10} \Delta T \rangle$ was done over $M = 100$ realizations of disorder and logarithmic bins in L.

A similar procedure was performed for the case $\kappa = \lambda = 6$ and the results are plotted in Fig. 4.1b. In contrast to above, here the initial condition was a uniform excitation of $L_0 = 10$ lattice sites, which is presumably the reason for the much faster convergence against the power-law prediction.

This quite convincing correspondence of the NDE prediction with numerical results provides a first justification of the validity of the NDE as a phenomenological description of spreading in nonlinear lattices.

4.2.3. Numerical Results in 2D

In a second approach, simulations in two-dimensional lattices were performed and compared with the nonlinear diffusion equation. There, the scaling result (4.3) is also valid, but the NDE prediction will be checked in terms of the second moment Δn^2 rather than excitation times. For the self-similar solution, the second moment was found to follow the power law $\Delta n^2 \sim t^{\alpha_2}$, with $\alpha_2 = 1/(a + 1)$ (c.f. eq. (3.24)). Assuming the validity of the NDE and again using the scaling result (4.3), the second moment should, asymptotically, follow the power law:

$$\Delta n^2 \sim (t - t_0)^{4/5} \quad \text{for 4–4,} \qquad \text{and} \qquad \Delta n^2 \sim (t - t_0)^{3/4} \quad \text{for 6–6.} \tag{4.5}$$

This was quite accurately confirmed in numerical simulations as shown in Fig. 4.2. Remember that for 2D also in the regular case no traveling waves exist and hence

one can safely study spreading as manifestation of chaotic diffusion also for the non-random potential $\omega_{i,k} = 1$. In Fig. 4.2a results for the models 4–4_{re} (red) and 4–4_{sd} (black circles) are presented, while Fig. 4.2b shows results for 6–6_{re} (red) and 6–6_{sd} (black circles). The curves in these plots correspond to the second moment $\Delta n^2(t)$ of single trajectories for a random 5x5 site excitation. To account for the transient, non-subdiffusive behavior, the parameter t_0 was included and adjusted by eye to a value of $t_0 \approx 10^3 \ldots 10^4$. Opposed to the one-dimensional case, here the excitation eventually spreads over more than 10^6 lattice sites, which means a reasonable self-averaging and thus no further averaging over disorder realizations or random initial conditions seems required. This has been checked by exemplary additional runs with different initial conditions that produced perfectly overlapping curves. It is remarkable that asymptotically, there is even no difference between the regular case $\omega_{i,k} = 1$ and disordered potentials $\omega_{i,k} \in [0, 1]$. The convergence of the spreading exponents towards the predicted value $\alpha_2 = 4/5$, $\alpha_2 = 3/4$ respectively, is emphasized in the upper insets where the instantaneous (logarithmic) slope of the numerical results is shown. These results are again a convincing indication for the applicability of the NDE. Furthermore, an analysis of the structural entropy, shown in the lower insets in Fig. 4.2 reveals the convergence of S_{str} towards some constant value, another sign of the NDE.

By assuming the validity of the NDE an exact prediction for the power-law behavior could be obtained based on comparing the scaling behavior of the NDE with that of homogeneous nonlinear Hamiltonian lattices. This prediction was then to a convincing accuracy confirmed by numerical simulations for one and two dimensional systems and different values of the lattice nonlinearities $\kappa = 4, 6$, and for both disordered and regular potentials. In all cases the predicted spreading exponent was numerically verified and one is encouraged to try to apply the NDE also to the more complicated situation of nonhomogeneous lattices, were no such scaling argument can be employed.

Note, that here no assumption on chaoticity of the spreading trajectories is required as the spreading prediction is obtained solely from a scaling analysis. However, for the choice of the coupling parameter $\beta \sim 1$, the system surely is chaotic, and stays chaotic for any energy density as a consequence of scaling.

4.3. Resonant Lattices

After having understood the homogeneous nonlinearity, now the simplest nonhomogeneous case will be subject of study. Namely, the situation of harmonic oscillators, $\kappa = 2$, with a regular potential, i.e. equal frequencies $\omega_k = 1$, coupled by a nonlinear term with $\lambda = 4$ or $\lambda = 6$ is considered. The Hamilton function for this case in one dimension reads:

$$H = \sum_{k=1}^{N} \frac{p_k^2}{2} + \frac{q_k^2}{2} + \frac{1}{\lambda} \sum_{k=1}^{N-1} (q_k - q_{k+1})^{\lambda}. \tag{4.6}$$

This will be called the "resonant case", because all oscillators have the same frequency, hence are in resonance. A careful analysis of this situation will reveal remarkable properties that again allow to find a prediction for the power-law spreading. This is done in the next section and will be followed by numerical results confirming these arguments.

4.3.1. Dynamics at the Excitation Edge

To understand the spreading process in such a fully resonant Hamiltonian (4.6) the dynamics at the excitation border are studied, i.e. the dynamics of the first non-excited oscillator exactly at the edge of the excitation. In this case, all oscillators have the same frequency $\omega_k = 1$ and hence are in resonance, even for arbitrarily small local excitations $q_k \sim \epsilon \ll 1$ as will be seen later. To find an estimate for the spreading exponent, the spreading state is assumed to have some excitation length L and an uniform energy density $W = E/L$. This is a severe simplification of the spreading process and can not be rigorously justified at the moment. However, the numerical results presented later validate these assumptions. For this situation, an estimate of the time scale at which a new oscillator will be excited in dependence on the energy density W will be calculated. Therefore, the focus is laid on the oscillator at the edge of the excitation area that is not yet excited, but subject to forcing from its neighbor which is assumed to have a local energy W. Also, first only the specific case $\lambda = 4$ is treated, followed by the generalization to arbitrary $\lambda > 2$. In this simplified picture there are two oscillators, denoted by q_d, p_d for the excited, driving oscillator and q , p for the oscillator initially at rest. The Hamiltonian describing such a situation reads:

$$H_2 = \frac{p_d^2}{2} + \frac{q_d^2}{2} + \frac{p^2}{2} + \frac{q^2}{2} + \frac{1}{4}(q - q_d)^4 \tag{4.7}$$

As the driving oscillator is assumed to have an energy density W, its motion is further approximated by a periodic function with amplitude $\epsilon \sim \sqrt{W}$ and frequency Ω:

$$q_d(t) \approx \epsilon \cos(\Omega t) \qquad \text{with} \qquad \Omega \approx 1 + \frac{3}{8}\epsilon^2. \tag{4.8}$$

The nonlinear correction of the frequency $\sim \epsilon^2$ is due to the term q_d^4 appearing after an expansion of the coupling, as seen below. Substituting this periodic solution for q_d into the Hamiltonian (4.7) one arrives at a Hamiltonian for a single oscillator subject to periodic forcing:

$$H = \frac{p^2}{2} + \frac{q^2}{2} + \frac{1}{4}(q - \epsilon \cos \Omega t)^4 \tag{4.9}$$

This highly simplified system can now be analyzed thoroughly using resonant perturbation theory [25]. Therefore, the Hamiltonian is split into an integrable part $H_0(q, p)$ and a perturbation $H_1(q, p, t)$ with:

$$H_0 = \frac{p^2}{2} + \frac{q^2}{2} + \frac{q^4}{4}. \tag{4.10}$$

For small amplitudes $a_0 \ll 1$ the solution for H_0 in lowest order a_0 writes [107]:

$$q(t) \approx a_0 \cos(\omega t) \qquad \text{with} \qquad \omega \approx 1 + \frac{3}{8} a_0^2. \tag{4.11}$$

Note, that this nonlinear frequency shift $\sim a_0^2$ is the reason why the periodic forcing was assumed to have $\Omega = 1 + 3\epsilon^2/8$ because this forcing comes from a similar nonlinear oscillator with amplitude ϵ.

Writing H_0 in the action/angle variables I, θ with $q = \sqrt{2I}\cos(\theta)$, $p = \sqrt{2I}\sin(\theta)$ one finds:

$$H_0 = I + \gamma I^2, \qquad \text{hence} \qquad \omega(I) = \frac{\partial H_0(I)}{\partial I} = 1 + 2\gamma I, \tag{4.12}$$

with some prefactor γ whose value is not important for the result. The perturbation then writes:

$$\begin{aligned} H_1 &= -q^3 \epsilon \cos(\Omega t) + \frac{3}{2} q^2 \epsilon^2 \cos^2(\Omega t) - q\epsilon^3 \cos^3(\Omega t) \\ &= -(2I)^{3/2} \epsilon \cos^3\theta \cos(\Omega t) + 3I\epsilon^2 \cos^2\theta \cos^2(\Omega t) \\ &\quad - (2I)^{1/2} \epsilon^3 \cos\theta \cos^3(\Omega t). \end{aligned} \tag{4.13}$$

Now from the fact that here the regular, "fully resonant" case is considered, the driving frequency Ω and the frequency of the oscillator at rest ω are known to be equal, up to quadratic corrections, c.f. (4.8):

$$\Omega - \omega \sim \epsilon^2. \tag{4.14}$$

This encourages to further analyze the main 1:1 resonance, i.e. where $\omega \approx \Omega$. Therefore, the perturbation (4.13) is written in action-angle variables and only the resonant terms $\sim \cos(\theta - \Omega t)$ are kept while the others disappear after averaging over one period of the perturbation frequency Ω:

$$\begin{aligned} \langle H_1 \rangle = &-\frac{3}{2\sqrt{2}} I^{3/2} \epsilon \cos(\theta - \Omega t) + \frac{3}{4} I\epsilon^2 \left(1 - \frac{1}{2}\cos(2\theta - 2\Omega t)\right) \\ &-\frac{3}{4\sqrt{2}} I^{1/2} \epsilon^3 \cos(\theta - \Omega t). \end{aligned} \tag{4.15}$$

Details of this calculation are shown in appendix A.4. The complete Hamiltonian thus is:

$$\begin{aligned} H = I + \gamma I^2 &-\frac{3}{2\sqrt{2}} I^{3/2} \epsilon \cos(\theta - \Omega t) + \frac{3}{4} I\epsilon^2 \left(1 - \frac{1}{2}\cos(2\theta - 2\Omega t)\right) \\ &-\frac{3}{4\sqrt{2}} I^{1/2} \epsilon^3 \cos(\theta - \Omega t). \end{aligned} \tag{4.16}$$

By applying a canonical transformation to new variables J and ψ induced by the generating function:

$$F(I, \psi, t) = -I\,(\psi + \Omega t), \qquad \text{where} \qquad \Omega = 1 + \frac{3}{8}\epsilon^2, \tag{4.17}$$

one finds, with $J = -\partial F/\partial\psi = I$:

$$H = -\frac{3}{8}J\epsilon^2 + \gamma J^2 - \frac{3}{2\sqrt{2}}J^{3/2}\epsilon\cos\psi + \frac{3}{4}J\epsilon^2\left(1 - \frac{1}{2}\cos 2\psi\right) - \frac{3}{4\sqrt{2}}J^{1/2}\epsilon^3\cos\psi. \tag{4.18}$$

Quite remarkably, by another canonical rescaling of variables the small parameter ϵ disappears as seen by setting:

$$J \to \tilde{J} = J/\epsilon^2, \qquad t \to \tau = \epsilon^2 t \qquad \text{and} \qquad H \to \tilde{H} = H/\epsilon^4. \tag{4.19}$$

The Hamiltonian in those new variables is:

$$\tilde{H} = -\frac{3}{8}\tilde{J} + \gamma\tilde{J}^2 - \frac{3}{2\sqrt{2}}\left(\tilde{J}^{3/2} + \frac{1}{2}\tilde{J}^{1/2}\right)\cos\psi + \frac{3}{4}\tilde{J}(1 - \frac{1}{2}\cos 2\psi). \tag{4.20}$$

This is the universal, ϵ–independent resonance Hamiltonian for the forced oscillator (4.9). Thus, it is found that the small parameter ϵ in such a situation scales out of the dynamics and only influences the time scale. Going back to two coupled oscillators with one being at rest while the other one has a local energy W, eq. (4.19) means the second oscillator should get excited at a time scale $\sim \epsilon^2 \sim W$. This is verified numerically in Fig. 4.3a, where the energy $E = (p^2 + q^2)/2$ of the initially resting oscillator is analyzed using the scaled variables suggested by (4.19): E/W vs $t\,W$. $W = p_d^2/2 + q_d^2/2$ is the initial energy of the driving oscillator and the curves for different values $W = 0.1 \ldots 0.001$ perfectly coincide, supporting the validity of the above calculation. Note that the curves in Fig. 4.3a represent the envelopes of the energy to neglect the fast oscillations with frequency $\omega \approx 1$.

A similar calculation can be done for the general case with arbitrary even integers $\lambda > 2$, where the Hamilton function of the forced oscillator is:

$$H = \frac{p^2}{2} + \frac{q^2}{2} + \frac{1}{\lambda}(q - \epsilon\cos\Omega t)^\lambda. \tag{4.21}$$

The nonlinearity induces a frequency shift $\Omega = 1 + \gamma\epsilon^{\lambda-2}$, with some constant γ. After introducing action-angle variables, the integrable part of the Hamiltonian can be chosen as:

$$H_0 = I. \tag{4.22}$$

The perturbation in those variables is:

$$H_1 = \frac{1}{\lambda}(\sqrt{2I}\cos\theta - \epsilon\cos\Omega t)^\lambda = \frac{\epsilon^\lambda}{\lambda}(\sqrt{2I/\epsilon^2}\cos\theta - \cos\Omega t)^\lambda \tag{4.23}$$

Analyzing the main resonance $\theta \approx \Omega t$ by averaging over all fast oscillations one gets:

$$\langle H_1\rangle = \epsilon^\lambda G(\sqrt{2I/\epsilon^2}\cos(\theta - \Omega t), \sqrt{2I/\epsilon^2}\sin(\theta - \Omega t)), \tag{4.24}$$

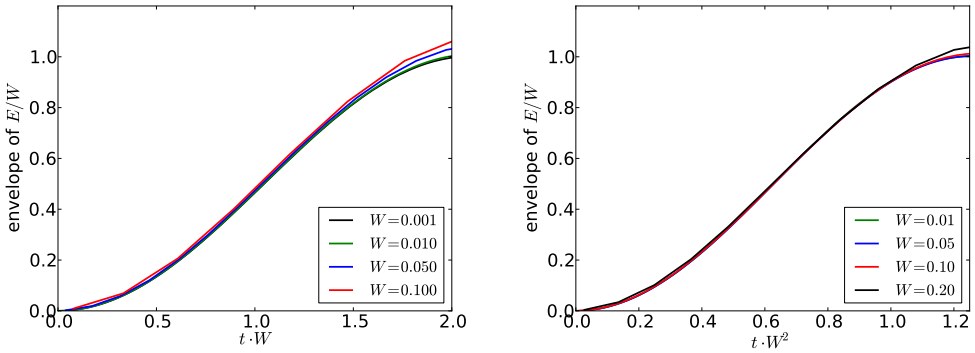

(a) Resonance scaling for $\lambda = 4$ **(b)** Resonance scaling for $\lambda = 6$

Figure 4.3.: Nonlinear resonance for the model (4.7) for different energies W and $\lambda = 4$ (a) and $\lambda = 6$ (b). The graphs show the envelope of E/W omiting fast oscillations to increase visibility. E here is the energy of the oscillator originally at rest. Results plotted in scaled variables derived from resonance theory E/W vs. $t\,W$ for $\lambda = 4$ and E/W vs. $t\,W^2$ for $\lambda = 6$.

where $G(x, y)$ denotes the averaging, which is not explicitly performed here:

$$G(x, y) = \frac{2\pi}{\lambda} \int_0^{2\pi} (x \cos\varphi - y \sin\varphi - \cos\varphi)^\lambda \mathrm{d}\varphi. \tag{4.25}$$

Note, how the trigonometric identiy $\cos\theta = \cos(\theta - \Omega t + \Omega t) = \cos(\theta - \Omega t)\cos(\Omega t) - \sin(\theta - \Omega t)\sin(\Omega t)$ was used in this last step. Again, a canonical transformation can be applied that is induced by the generating function:

$$F(I, \psi, t) = -I(\psi + \Omega t), \qquad \text{where} \qquad \Omega \sim 1 + \epsilon^{\lambda-2}, \tag{4.26}$$

which gives the Hamiltonian:

$$H = -\epsilon^{\lambda-2} J + \epsilon^\lambda G(\sqrt{J/\epsilon^2}\cos(\psi), \sqrt{J/\epsilon^2}\sin(\psi)). \tag{4.27}$$

Just like before, the small parameter ϵ can be scaled out of the equations, but now the scaling reads:

$$J \to \tilde{J} = J/\epsilon^2, \qquad t \to \tau = \epsilon^{\lambda-2} t \qquad \text{and} \qquad H \to \tilde{H} = H/\epsilon^\lambda, \tag{4.28}$$

which eventually gives the ϵ-independent resonance Hamiltonian for any λ:

$$\tilde{H} = -\tilde{J} + G\left(\sqrt{\tilde{J}}\cos(\psi), \sqrt{\tilde{J}}\sin(\psi)\right). \tag{4.29}$$

This scaling, again, is verified by a numerical analysis of the energy of an oscillator initially at rest driven by another oscillator with energy W. For $\lambda = 6$, (4.28) suggests rescaling with energy W when using the time scale $t\,W^2$. Fig. 4.3b shows the results in these scaled variables and one again finds perfect overlap of the curves

for different energies $W = 0.01 \ldots 0.1$. Note, that this calculation can be easily generalized to $\lambda \in \mathbb{R}$, $\lambda > 2$.

As the aim was to find a prediction for energy spreading in large systems, now a conclusion from the above analysis of microscopic dynamics back to the situation of spreading states will be drawn. The idea is that in a situation of L excited sites with an energy density $W = E/L$, the excitation of a new oscillator at site $L+1$ can be modeled as being induced by the forcing of its excited neighbor. Hence, the scaling found previously is applied. The calculation above then shows that a situation with arbitrary energy $E \sim \epsilon^2$ can be scaled to $E' = 1$ by changing the time $t \to t'$ as:

$$t' = E^{\lambda/2-1} t. \tag{4.30}$$

Hence, the analysis of the microscopic dynamics done above results in a scaling relation between the energy of the system and its characteristic time scale. Such a relation was found for the homogeneous case before where it was a simple consequence of the Hamilton function itself. In contrast, here the resonant structure of the oscillators induces this time-energy-scaling and it is obvious that such a result can not be found for disordered lattices, where ω_k are random and hence are generally not in resonance for small ϵ. Again, the scaling result (4.30) can be compared with the similar property of the NDE (3.8): $t' \sim E^a$, and one finds:

$$a = \frac{\lambda - 2}{2}. \tag{4.31}$$

Thus, a careful investigation of the microscopic dynamics at the excitation edge leads to a scaling prediction which, again assuming validity of the NDE, provides an exact result for the spreading behavior that can be checked numerically.

The above calculation does not contain any notion of chaoticity, merely the typical time-scale of two resonantly interacting oscillators is analyzed. From this result one can not deduce chaotic diffusion, the additional assumption made above to arrive at the spreading prediction was to describe the state with an uniform excitation with energy density $W = E/L$, and apply the nonlinear diffusion equation. Hence the statement is rather that if the system equilibrates to a roughly uniform shape while spreading and is describable by the nonlinear diffusion equation, the spreading should asymptotically follow the above prediction.

4.3.2. Numerical Results in 2D

To verify the assumptions and conclusions for resonant oscillators presented above, a numerical study of spreading in regular lattices 2–4_{re} and 2–6_{re} was performed. As one-dimensional regular lattices exhibit quasi-compactons that interfere with chaotic diffusion, here results for two-dimensional lattices are reported where no such quasi-compactons are observed (see section 2.6). The main observable in two-dimensional studies is the second moment $\Delta n^2(t)$, and both the energy scaling of the spreading

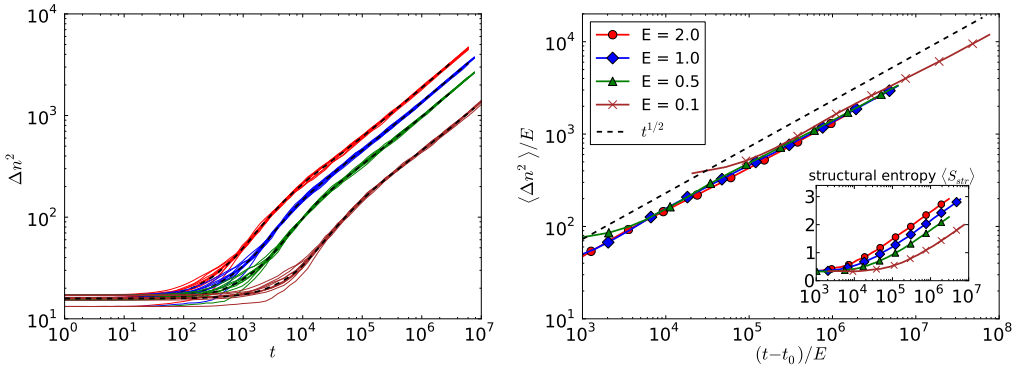

(a) Spreading in the 2D model 2–4_{re} **(b)** The same data, averaged and scaled

Figure 4.4.: Spreading results for the two-dimensional inhomogeneous case 2–4_{re} with regular potential ($\omega_{i,k} = 1$) for different energies. Graph (a) shows the plain results for $M = 10$ initial conditions with the averages as dashed black lines. In (b), only the averages are shown with the scaling suggested by the NDE: $\langle \Delta n^2 \rangle / E$ vs t/E. The dashed line represents the analytical spreading law (4.32) and the inset shows the behavior of the averaged structural entropy $\langle S_{\mathrm{str}}(t) \rangle$.

as well as the exact prediction on the exponent will be checked. From the scaling result above (4.31) one has $a = (\lambda - 2)/2$. On the other hand, the properties of the self-similar solution in two dimensions (3.24) predict a spreading exponent $\alpha_2 = 1/(a+1)$. Thus, the following results for the behavior of the second moment are obtained:

$$\begin{aligned} \frac{\Delta n^2(t)}{E} &\sim \left(\frac{t-t_0}{E}\right)^{1/2} \qquad \text{for 2–4,} \\ \frac{\Delta n^2(t)}{E} &\sim \left(\frac{t-t_0}{E}\right)^{1/3} \qquad \text{for 2–6.} \end{aligned} \tag{4.32}$$

These predictions were tested by numerical integrations of random initial excitations on 5x5 sites in a quadratic 2D lattice, starting with the case 2–4_{re}, i.e. $\lambda = 4$. These simulations were repeated for several energies $E = 0.1 \ldots 5$, and for each value of the energy the results were averaged over $M = 10$ random initial conditions giving the average $\langle\, \Delta n^2 \,\rangle$. The results are presented in Fig. 4.4. Fig. 4.4a shows the plain results $\Delta n^2(t)$, thus $M = 10$ curves for each energy E. One sees that the individual curves are hardly fluctuating and thus increasing the number of realizations M seems not required. In Fig. 4.4b only the averages are plotted and the transient, non-subdiffusive behavior is omitted by introducing t_0, adjusted by eye and ranging from $t_0 = 10^3$ for $E = 2$ to $t_0 = 10^4$ for $E = 0.1$. Furthermore, the scaling prediction of the NDE is applied by plotting the scaled variables $\Delta n^2/E$ vs t/E. As one sees from the almost perfect overlap of the curves for different energies, the NDE scaling prediction is verified quite accurately by these numerical results. Moreover, the spreading exponent also nicely coincides with the prediction (4.32) as seen from the dashed lines in Fig. 4.4b. Hence, for the case 2–4_{re}, numerical results confirm the spreading predictions obtained above.

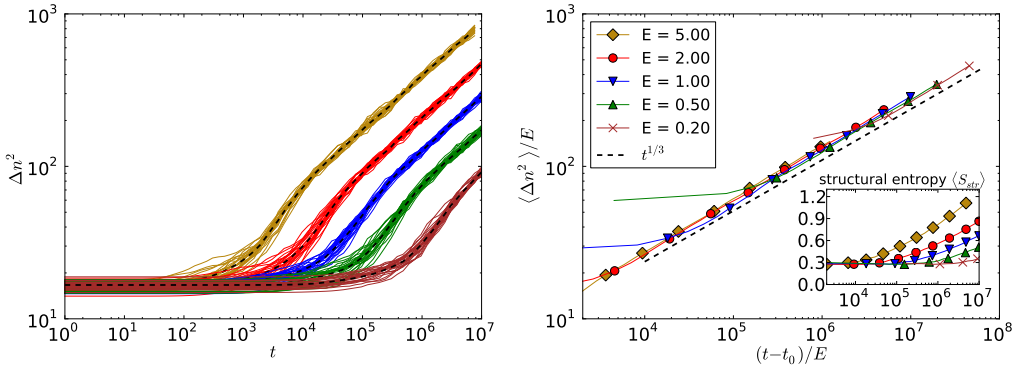

(a) Spreading in the 2D model 2–6_{re} **(b)** Spreading in the 2D model 2–6_{re}

Figure 4.5.: Spreading results in two dimensions as in Fig. 4.4 but for the case 2–6_{re}. (a) shows the plain results for $M = 24$ initial conditions with the averages as dashed black lines. In (b), the scaling suggested by the NDE: $\langle \Delta n^2 \rangle / E$ vs t/E is applied and the dashed line represent the analytical spreading law (4.32). The inset shows the behavior of the averaged structural entropy $\langle S_{\mathrm{str}}(t) \rangle$.

A similar study has been done for the case 2–6_{re} and the results are shown in Fig. 4.5. Here, the averaging was done over $M = 24$ realizations as the data exhibited slightly more fluctuations. Fig. 4.5a again shows the plain data with averages as dashed black lines, while in Fig. 4.5b the offset t_0 is introduced to account for the transient behavior and the data are plotted in scaled variables. As before, the scaling prediction is verified quite convincingly and also the predicted spreading law is found. Hence, the numerical results confirm that one can indeed understand the spreading process for the resonant case by studying the dynamics only of the edge oscillators and relate these result with the nonlinear diffusion equation.

Both cases exhibit long transient behavior, with increasing transient time for decreasing energy. As in this work the main interest is the asymptotic behavior, the transients are simply cut off by using t_0. However, their origin and properties are not understood and may be an interesting subject of study on their own.

The structural entropy S_{str} shown in the insets in Figs. 4.4b and 4.4b, however, exhibits a non-constant behavior, which is in contradiction to the self-similar solution. Indeed, a logarithmic increase of S_{str} is observed for all energies during the spreading, which is a clear indication that the spreading state is not truly self-similar in time. A possible explanation for such behavior is the existence of some long-living breather states in this system that trap some of the energy and decay much slower than the spreading process, if at all. As the measure of the excitation area Δn^2 is mainly governed by the excitation boundary, it is insensitive to such non-decaying breathers which might explain why still the predicted scaling is found.

To summarize, numerical results for the resonant case, i.e. $\kappa = 2$ and regular potential $\omega_{i,k} = 1$, obtained in two dimensions do confirm the energy scaling predicted by the nonlinear diffusion equation. Furthermore, a calculation for the dynamical be-

havior of the oscillator at the excitation edge led to a prediction for the nonlinearity parameter $a = (\lambda - 2)/\lambda$ of the NDE in dependence on the lattice nonlinearity λ. This result was also confirmed to convincing accuracy by the numerical simulations. Thus, also in this case the NDE proved to be a fruitful tool for understanding the properties of spreading in nonlinear lattices. However, the results on the structural entropy indicate deviations from a self-similar spreading and it remains an open question to fully understand the origin of this observation.

4.4. Fully Nonlinear Lattices

After dealing with resonant harmonic oscillators, in this section the nonhomogeneous, fully nonlinear case will be studied, where $\kappa > 2$ and $\lambda > \kappa$. For simplicity, the calculations presented in this work are obtained for the specific case $\kappa = 4$, $\lambda = 6$, but most of the results can be generalized based on the ideas presented here. Namely, an oscillator chain of the following form is investigated:

$$H = \sum_{k=1}^{N} \frac{p_k^2}{2} + \frac{\omega_k^2}{4} q_k^4 + \frac{1}{6} \sum_{k=1}^{N-1} (q_k - q_{k+1})^6. \tag{4.33}$$

Again, note that the only parameter is the conserved total energy that governs the relative strength between the local and coupling term in (4.33), as described in chapter 2.

4.4.1. Dynamics at the Excitation Edge

For the resonant case studied in the last section, an analysis of the dynamics of the oscillators at the excitation edges turned out to be very successful, hence the same idea will be applied here as well. That means, a simplified model describing edge oscillators is tried to be obtained for which a characteristic time scale can be deduced leading to an estimate of the energy dependence of excitation times. The analysis of these simplified models is done using standard resonance theory, very comprehensively introduced in [25], but also found in any textbook on chaos or nonlinear dynamics, e.g. [2, 17].

Two-Oscillator Description

The most simple case is considered first where the edge of the excitation area is modeled by two oscillators for the regular case ($\omega_k = 1$):

$$H = \frac{p_1^2 + p_2^2}{2} + \frac{q_1^4 + q_2^4}{4} + \frac{\beta}{6}(q_1 - q_2)^6. \tag{4.34}$$

Note, that in this section the calculations are done for the case where β is used as independent parameter while the energy density is fixed $W = 1$. However, this can

easily be related to the original system (2.4) by identifying $\beta = \sqrt{W}$, as described in section 2.2. Thus, special interest lies in the case of small $\beta \ll 1$ as this mimics the asymptotic spreading behavior when W gets small. The reason for this choice of parametrization here is that it simplifies the perturbative calculation presented below.

As the Hamiltonian (4.34) is supposed to model the excitation edge, the amplitude of the first oscillator is assumed to be $a_1 \approx 1$ while the second one is at rest $a_2 \approx 0$. Introducing action-angle variables $I_{1,2}$ and $\theta_{1,2} = \Omega_{1,2}t$ of the uncoupled Hamiltonian and splitting the system into an integrable part and a perturbation, one finds [25]:

$$H_0 = (AI_1)^{4/3} + (AI_2)^{4/3}, \quad \text{with} \quad A = \frac{3\gamma}{2\sqrt{2}}, \quad \gamma = \frac{\pi}{2K(1/\sqrt{2})} \approx 0.8472. \tag{4.35}$$

$$H_1 = \frac{\beta}{6}(a_1 \cos\theta_1 - a_2 \cos\theta_2)^6, \qquad a_{1,2} = (3\gamma I_{1,2})^{1/3}, \tag{4.36}$$

where $a_{1,2}$ denote the oscillator amplitudes and $K(x)$ is the full elliptic integral of the first kind. The nonlinear frequency of the angle variable calculates as:

$$\Omega_{1,2} = \partial H/\partial I_{1,2} = A^{4/3} I_{1,2}^{1/3} = \gamma a_{1,2}. \tag{4.37}$$

At this point it is already seen that the two oscillators are typically not in resonance, as $\Omega_1 \sim a_1 \sim 1$, while $\Omega_2 \sim a_2 \sim 0$. Such a non-resonant perturbation typically does not induce chaos. Hence, one expects intuitively that below some β_c, KAM tori will prevail and any small amplitude $a_2 \approx 0$ will remain small for all times. This implies that for some critical energy density $W_c = \beta_c^2$ spreading should stop because new oscillators at the excitation would not get excited.

To get a rough estimate for β_c the resonance overlap criterion [17,25] is applied. Due to Chirikov's arguments, a global chaotic region in phase space emerges if different resonances induced by the periodic perturbation overlap. Applying this criterion, the main 1:1 resonance, i.e. $\Omega_1 = \Omega_2$, of this system is analyzed and the critical value β_c is calculated as the point when this resonance overlaps with the 1:3 resonance. The structure of the perturbation is such that no 1:2 resonance exists in the coupling terms and hence the 1:3 resonance indeed is the second most important one and should be used to apply the resonance overlap criterion. This is interpreted as the rough estimate for the onset of global chaos that allows diffusion from small $a_2 \approx 0$ to large $a_2 \approx 1$ amplitudes. Expanding H_1, one finds:

$$\begin{aligned} H_1 = \frac{\beta}{6}(&a_1^6 \cos^6\theta_1 - 6\, a_1^5 a_2 \cos^5\theta_1 \cos\theta_2 + 15\, a_1^4 a_2^2 \cos^4\theta_1 \cos^2\theta_2 \\ &- 20\, a_1^3 a_2^3 \cos^3\theta_1 \cos^3\theta_2 + 15\, a_1^2 a_2^4 \cos^2\theta_1 \cos^4\theta_2 \\ &- 6\, a_1 a_2^5 \cos\theta_1 \cos^5\theta_2 + a_2^6 \cos^6\theta_2). \end{aligned} \tag{4.38}$$

Using trigonometric identities like $\cos^5\theta_1 = 5/8\cos\theta_1 + 5/16\cos 3\theta_1 + 1/16\cos 5\theta_1$ and $\cos\theta_1\cos\theta_2 = 1/2\cos(\theta_1 - \theta_2) + 1/2\cos(\theta_1 + \theta_2)$, and averaging over any fast

oscillation but the main 1:1 resonance $\sim \cos(\theta_1 - \theta_2)$, the averaged perturbation is obtained:

$$\langle H_1 \rangle = -\frac{\beta}{6}\left(\frac{15}{8}a_1^5 a_2 + \frac{45}{8}a_1^3 a_2^3 + \frac{15}{8}a_1 a_2^5\right)\cos(\theta_1 - \theta_2) \tag{4.39}$$

$$=: \beta\, V(a_1, a_2)\cos(\theta_1 - \theta_2). \tag{4.40}$$

The detailed calculation is omitted as it cuts down to repeated application of trigonometric identities and an averaging similar to the presentation in appendix A.4. The Hamiltonian $H_0 + \langle H_1 \rangle$ describes the main resonance in the system. For further analysis, a transformation to resonance variables J, J_2, ψ, ψ_2 is performed:

$$J = \frac{1}{2}(I_1 - I_2), \qquad J_2 = \frac{1}{2}(I_1 + I_2) - I_r = 0$$
$$\psi = \theta_1 - \theta_2, \qquad \psi_2 = \theta_1 + \theta_2.$$

The resonance actions are $I_{1,r} = I_{2,r} = I_r$ and are equal for the 1:1 resonance. Their value can be calculated from $1 = H_0 = 2(AI_r)^{4/3}$ as $I_r = 2^{-3/4}/A$. After expanding H around the resonance action $I_{1,2} = I_r \pm J$ up to second order one arrives at the resonance Hamiltonian:

$$H_r = \frac{J^2}{2M} - \beta\, V(a_r, a_r)\cos(\psi), \tag{4.41}$$

with

$$a_r = (3\gamma I_r)^{1/3} = 2^{1/4}, \quad V(a_r, a_r) = \frac{75}{48}a_r^6, \quad M^{-1} = \frac{2\gamma^2}{a_r^2}. \tag{4.42}$$

This describes a resonance with half-width:

$$\Delta J = 2\sqrt{\beta M V} = 2\frac{a_r^3}{\gamma}\sqrt{\frac{75}{96}\,\beta} \;\approx\; 3.5 \cdot \sqrt{\beta}. \tag{4.43}$$

As a very rough estimate for the critical value β_c below which the existence of KAM tori that prevent energy diffusion from I_1 to I_2 is expected, the value for β at which this 1:1 resonance overlaps with the 1:3 resonance is calculated. The values for the 1:3 resonance are denoted with primes. The resonance actions $I'_{1,2;r}$ of the 1:3 resonance can be obtained from $\Omega'_{1,r} = 3\Omega'_{2,r}$ and $1 = H_0 = (AI'_{1,r})^{4/3} + (AI'_{2,r})^{4/3}$ using the fact that $\Omega_{1,2} = \partial H_0/\partial I_{1,2}$:

$$I'_{1,r} = \frac{1}{A}(1 + 3^{-4})^{-3/4} \approx \frac{1}{A}, \qquad I'_{2,r} = \frac{1}{3^3}I'_{1,r} \approx \frac{1}{27A}. \tag{4.44}$$

The width of this 1:3 resonance is neglected as being small and thus β_c is calculated as the value for β at which the main 1:1 resonance reaches the point $I'_{2,r}$.

$$\begin{aligned} I_r - \Delta J &= I'_{2,r} \\ 2^{-3/4}/A - 3.5\sqrt{\beta_c} &= \frac{1}{27A} \\ \longrightarrow \beta_c &= \left(\frac{27 \cdot 2^{-3/4} - 1}{3.5 \cdot 27A}\right)^2 \approx 0.03. \end{aligned} \tag{4.45}$$

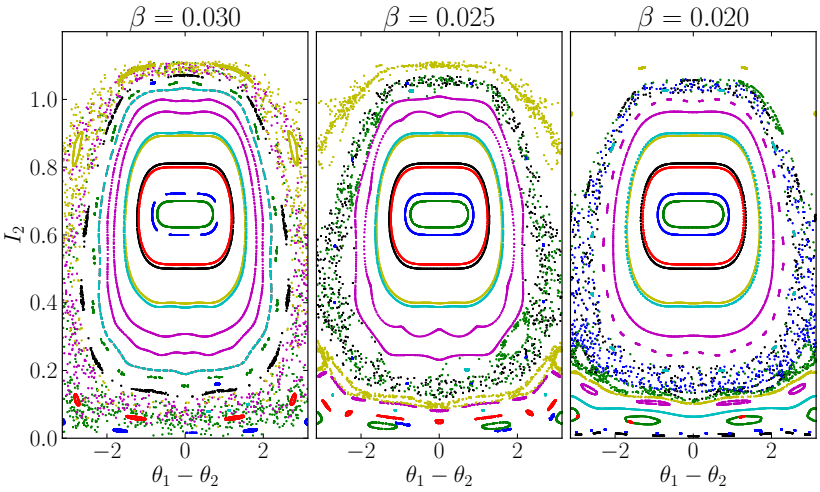

Figure 4.6.: Phase space portraits of the Hamiltonian (4.34) for different values of β close to the predicted critical value $\beta_c \approx 0.03$. Points in these graphs are intersections of trajectories with the plane $\theta_1 + \theta_2 = \pi$.

This result is checked numerically by obtaining a phase space portrait of the original Hamiltonian (4.34) in Fig. 4.6 for different values of β around the predicted critical value $\beta_c \approx 0.03$. Note, that the trajectories in the four dimensional phase space are confined to the three dimensional energy surface and points in Fig. 4.6 represent intersections of trajectories with the plane $\theta_1 + \theta_2 = \pi$ resulting in a two dimensional plot, called Poincaré section. For $\beta = 0.03$ a global chaotic region is found, which means that in this case even small amplitudes of the second oscillator $I_2 \approx 0$ can reach values $I_2 \approx 1$ by traveling along the chaotic component. When decreasing β, however, the chaotic component separates and invariant tori appear that prevent small initial conditions I_2 to reach values $I_2 \approx 1$. This observation confirms the estimations above and the first expectation is indeed true that for $\beta < \beta_c$ any small initial condition $I_2 \approx 0$ will remain small for all times.

Going back to the spreading problem this would mean that as soon as the critical energy density $W_c = \beta_c^2 \approx 10^{-3}$ is reached, the spreading should stop. This is because from the above arguments, the oscillator at the edge of the excitation can not be excited up to the level of the others due to the existence of KAM tori as described above. However, claiming the absence of spreading in chains of oscillators from the above observation is not correct, as numerical results clearly indicate spreading as shown in section 4.4.2. Rather, one has to conclude that using just two oscillators to model the edge of the excitation is too simple and not sufficient to describe the spreading problem. Indeed, increasing the dimensionality by increasing the number of oscillators from two to three or more one might find that even though KAM tori may exist at small densities $W < W_c$ they do not necessarily lead to separation of the phase space and still allow for a considerable increase of small amplitudes, hence spreading. This idea will be followed in the next section.

Many-Oscillator Description

As the simple case of two coupled oscillators does not lead to spreading, now higher-dimensional situations are considered starting with $N = 3$ oscillators. Again this is supposed to describe the excitation edge, thus it is assumed that initially the first two oscillators are excited with an energy density $W \sim 1$, while the third one is at rest. The fundamental question again is whether it is possible that the third oscillator gets excited to the same energy density even in the limit of small coupling $\beta \ll 1$. As above, a transformation to action-angle variables is obtained and only the main 1:1 resonance is studied. By averaging over fast oscillations, a simplified Hamiltonian can be obtained describing the two main resonaces between oscillator one and two and between two and three:

$$H = (AI_1)^{4/3} + (AI_2)^{4/3} + (AI_3)^{4/3} + \beta\, V_1 \cos(\theta_1 - \theta_2) + \beta\, V_2 \cos(\theta_2 - \theta_3). \quad (4.46)$$

The coupling parameters $V_1(I_1, I_2)$, $V_2(I_2, I_3)$ depend on the resonance actions similar as above (4.42). As initially $I_1 \approx I_2 \approx I_r$, the system is always inside the main resonance of the first two oscillators. This resonance can be analyzed in the same way as before. For small β one finds that the system is described again by a pendulum Hamiltonian (4.41) for $J = (I_1 - I_2)/2$ while $I_3 = \text{const}$ is a constant of motion [25]. Hence, the initial condition $I_3 \approx 0$ will always remain small provided β is small enough such that the resonance description is valid. Essentially, this is the same result as for two oscillators, only the critical value β_c below which I_3 will not grow should be different, presumably smaller.

As for three oscillators the phase space has six dimensions and the trajectories lie on a five-dimensional sub-manifold, the simultaneous intersections of trajectories with three surfaces are required to obtain a two-dimensional phase space plot like Fig. 4.6. Unfortunately, it is very difficult, if not impossible, to find three surfaces through which all trajectories travel frequently. Thus, an as conclusive numerical verification as for $N = 2$ can not be obtained for $N = 3$. However, later a numerical study will be presented that tests the above predictions and is shown in Fig. 4.7.

But before that, the next case of $N = 4$ oscillators should be investigated. The resonance Hamiltonian then writes:

$$H = H_0(\vec{I}) + \sum_{n=1}^{N-1} \beta\, V_n \cos(\vec{m}_n \cdot \vec{\theta}), \quad (4.47)$$

where $\vec{I} = (I_k)$ and $\vec{\theta} = (\theta_k)$ with $k = 1 \ldots 4$ are 4-dimensional vectors of action- and angle-coordinates and $\vec{m}_n$ with $n = 1 \ldots 3$ are integer vectors describing the three main 1:1 resonances, more precisely:

$$H_0(\vec{I}) = \sum_{n=1}^{N} (AI_n)^{4/3}, \quad \vec{m}_1 = \begin{pmatrix} 1 \\ -1 \\ 0 \\ 0 \end{pmatrix}, \quad \vec{m}_2 = \begin{pmatrix} 0 \\ 1 \\ -1 \\ 0 \end{pmatrix}, \quad \vec{m}_3 = \begin{pmatrix} 0 \\ 0 \\ 1 \\ -1 \end{pmatrix}, \quad (4.48)$$

The initial conditions are again chosen as $I_1 \approx I_2 \approx I_3$, while the fourth oscillator is at rest $I_4 \approx 0$. This initial condition lies on the intersection of the resonance planes defined by $\vec{m}_1$ and $\vec{m}_2$. This is a fundamentally different case than before as the system behavior is not described by a single resonance but rather by two resonances, even for arbitrary small β. This means the system typically exhibits a complicated chaotic behavior for any small β, because for the oscillator I_2, the resonances from the couplings to the left and right always overlap and thereby give rise to chaos. The double-resonance Hamiltonian for the resonance variables $J_1 = (I_1 - I_2)/2$, $J_2 = (I_2 - I_3)/2$ and $\psi_1 = \theta_1 - \theta_2$, $\psi_2 = \theta_2 - \theta_3$ up to second order in J writes as [25]:

$$H_r \approx \underbrace{\frac{J_1^2}{2M_{11}} + \frac{J_2^2}{2M_{22}} + \frac{J_1 J_2}{2M_{12}}}_{H_{\text{kin}}} + \beta\, V_1 \cos\psi_1 + \beta\, V_2 \cos\psi_2, \tag{4.49}$$

with

$$M_{11} = \vec{m}_1 \cdot \frac{\partial\vec{\omega}}{\partial\vec{I}} \cdot \vec{m}_1, \quad M_{22} = \vec{m}_2 \cdot \frac{\partial\vec{\omega}}{\partial\vec{I}} \cdot \vec{m}_2, \quad M_{12} = M_{21} = \vec{m}_1 \cdot \frac{\partial\vec{\omega}}{\partial\vec{I}} \cdot \vec{m}_2. \tag{4.50}$$

Although the trajectories might be chaotic, the existence of an effective quadratic kinetic energy H_{kin} bounds the motion to remain inside this double resonance of width $\sim \sqrt{\beta}$ [25]. This is, of course, only true for small enough perturbations β where the above expansion is valid. For larger β resonance overlaps are expected and chaotic trajectories might leave the double resonance along the chaotic layer. Nonetheless, in the limit of small enough β one, as for $N = 3$, finds that small initial values $I_4 \approx 0$ will remain small for all time as the trajectories remain inside the double resonance where I_4 is a constant of motion. Hence, even taking four oscillators to model the excitation edge is not enough to describe spreading. As above, this is also numerically verified in a later study, shown in Fig. 4.7.

Thus, the number of oscillators is now increased to $N = 5$. The Hamiltonian is the same as (4.47) but now exhibiting four 1:1 resonances described by the resonance conditions:

$$\vec{m}_1 = \begin{pmatrix} 1 \\ -1 \\ 0 \\ 0 \\ 0 \end{pmatrix}, \quad \vec{m}_2 = \begin{pmatrix} 0 \\ 1 \\ -1 \\ 0 \\ 0 \end{pmatrix}, \quad \vec{m}_3 = \begin{pmatrix} 0 \\ 0 \\ 1 \\ -1 \\ 0 \end{pmatrix}, \quad \vec{m}_4 = \begin{pmatrix} 0 \\ 0 \\ 0 \\ 1 \\ -1 \end{pmatrix}. \tag{4.51}$$

The initial condition is now $I_1 \approx I_2 \approx I_3 \approx I_4 \approx I_r$ while I_5 models the non-excited edge oscillator being at rest: $I_5 = 0$. This initial condition hence lies at the triple resonance at the intersection of the resonance planes defined by $\vec{m}_1$, $\vec{m}_2$ and $\vec{m}_3$. Because of the triple resonance, the motion will always be chaotic even for arbitrarily small β, just like for the double resonance before. As above, a calculation on the size of this chaotic region in the limit of small β will be performed. So to analyze

this resonance, the following variables are introduced:

$$\begin{aligned} &J_1 = (I_1 - I_2)/2, \qquad J_2 = (I_2 - I_3)/2, \qquad J_3 = (I_3 - I_4)/2, \\ &I_r = (I_1 + I_2)/2 = (I_2 + I_3)/2 = (I_3 + I_4)/2. \end{aligned} \tag{4.52}$$

To obtain the resonance Hamiltonian, H_0 is written in terms of these new variables:

$$\begin{aligned} H_0(\vec{I}) &= \sum_{n=1}^{N} (AI_n)^{4/3} \\ &= A^{4/3} \left[(I_r - J_1)^{4/3} + (I_r + J_1)^{4/3} + (I_r - J_3)^{4/3} + (I_r + J_3)^{4/3} \right]. \end{aligned} \tag{4.53}$$

The resonance Hamiltonian follows from an expansion of the above for small J_i up to second order. However, the important outcome is already seen in (4.53). Remarkably, the triplet resonance structure leads to the fact that the resonance Hamiltonian becomes independent of J_2. Consequently, the effective kinetic energy in the resonance Hamiltonian is also independent of J_2 and therefore the motion in J_2 is not bounded, even for arbitrary small β. This can be understood also geometrically from the fact that $\vec{m}_1 \perp \vec{m}_3$, which means that the motion of the resonance $\vec{m}_1$ goes along the resonance plane of $\vec{m}_3$ and hence never leaves the chaotic region induced by the double resonance created by $\vec{m}_1$ and $\vec{m}_3$, a situation already described by Chirikov [25]. While in the previous case with four oscillators, the resonance structure forced both resonance actions J_1 and J_2 to remain small, now only $|J_1| \lesssim \sqrt{\beta}$ and $|J_3| \lesssim \sqrt{\beta}$ are bounded while J_2 can grow indefinitely inside the resonance. Although large changes of J_2 means that one leaves the $\vec{m}_2$ resonance, one still would be inside the chaotic region induced by the double resonance of $\vec{m}_1$ and $\vec{m}_3$. Thus, there is a direction in phase space in which the chaotic layer emerging from this triplet resonance is not bounded. For the original actions I_n to remain inside this chaotic region one finds:

$$2|J_1| = |I_1 - I_2| \lesssim \sqrt{\beta} \quad \text{and} \quad 2|J_3| = |I_3 - I_4| \lesssim \sqrt{\beta}. \tag{4.54}$$

Particularly, this means that the chaotic resonance region spawns down to small values of I_4 and thus overlaps with the resonance $\vec{m}_4$ even for an initial value of $I_5 = 0$. This is true for any small perturbation β and leads to the conclusion that the triple resonance always overlaps with the resonance $\vec{m}_4$. The existence of such overlaps with the triplet resonance even for arbitrary small β imply that the chaotic region expands further, also including the point $I_5 = 0$. Hence, the resonance description is not applicable at all and one expects to find a global chaotic region connecting small values $I_5 \approx 0$ with macroscopic excitations $I_5 \approx 1$ even for small perturbations β. That means, no critical β_c should exist, a crucial difference to the findings above with $N < 5$.

Note, that this result does not imply that the motion in such systems with five or more oscillators is always chaotic even for arbitrarily small perturbations $\beta \ll 1$. Rather, here a special initial condition was chosen where four oscillators are already

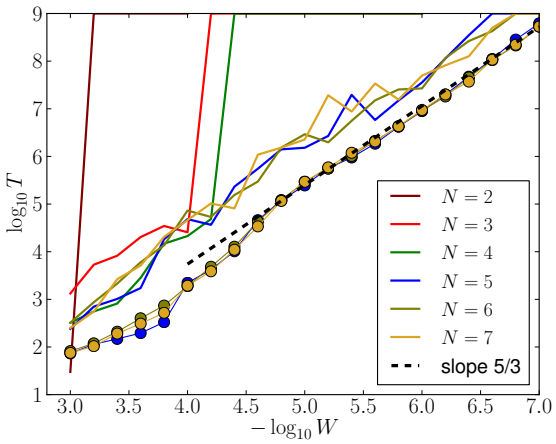

Figure 4.7.: Excitation time T of the edge oscillator as function of the energy density W of excited oscillators for different numbers N of oscillators. Simulations were done for 100 random initial conditions and solid lines represent the maximum $\max\{\log_{10} T\}$ while circles correspond to averages $\langle \log_{10} T \rangle$.

in a triplet resonance and it was merely argued that the chaotic region emerging from this resonance should also include the resting oscillator. Thereby, this initially resting oscillator can become excited by diffusing along the chaotic layer.

As mentioned above, this can not be checked in terms of phase space diagrams due to the high dimensionality. However, a different way of confirming these predictions was found. The idea is that if, for small β, the motion of the excited oscillators is confined in some region, no considerable increase of the energy of the edge oscillator initially at rest should be observed. The emergence of an extended chaotic region, on the other hand, as predicted for $N \geq 5$ would lead to a macroscopic excitation of the resting oscillator even for small β. To check this numerically, systems with $N = 2 \ldots 7$ oscillators are initialized such that the first $N - 1$ oscillators have an energy density W, hence a total energy of $W(N - 1)$, while the last oscillator is at rest. The initial conditions are random with the condition that individual energies w_i obey $W - W^2 < w_i < W + W^2$ for the first $N - 1$ oscillators. To make this study comparable with later spreading results, it is done for the set of variables where $\beta = 1$ and the energy is the crucial quantity. Again, the relation to the above calculations can be drawn by using $\beta = \sqrt{W}$. As observable, the time T is measured until the local energy of the last oscillator reaches some border value, the exact value of the border is rather arbitrary, here chosen as $0.1 \cdot W$. This is done for decreasing energy densities $W = 10^{-3} \ldots 10^{-7}$ and 100 random intial conditions for each density. Fig. 4.7 shows the *maximum time* $\max\{\log_{10} T\}$ of these 100 runs for different numbers of oscillators as solid lines. The simulations where done up to a total time $T_{\max} = 10^9$ and if the border is not reached within this time, T is considered as divergent. For $N = 2$, this time diverges immediately for $W < 10^{-3}$, which corresponds nicely to the above results as from $\beta_c \approx 0.03$ one

finds $W_c = \beta_c^2 \approx 10^{-3}$. For $N = 3$ and $N = 4$ also divergence of T is found, as expected from the above arguments. The critical value there is $W_c \approx 10^{-4}$, hence $\beta_c \approx 10^{-2}$. For $N = 5$, one clearly sees an increase of T with decreasing density W, but in contrast to $N < 5$, there is no divergence down to densities as small as $W = 10^{-7}$. This is a numerical verification of the above arguments showing that for $N = 5$ indeed the a global chaotic region exists that allows energy transfer to the resting oscillator even for arbitrary small perturbations β. Additionally, Fig. 4.7 shows the mean value $\langle \log_{10} T \rangle$ averaged over the random initial conditions (circles). One finds that asymptotically, the times seem to exhibit a power law dependence with exponent 5/3:

$$T \sim W^{-5/3}. \tag{4.55}$$

The value of the exponent is a purely numerical result at this point. An analytic derivation appears to be rather difficult and has not yet been found. However, this exponent will be compared to numerical findings on spreading states in large lattices in the next section.

Summarizing the above considerations, it was found that using five oscillators to model the excitation edge results in a resonance structure that connects the initial state $I_5 = 0$ with the desired point at $I_5 \approx W$ by a chaotic layer emerging from the triplet resonance and the overlapping $\vec{m}_4$ resonance. This provides a geometric argument for the possibility of macroscopic excitation of I_5. However, the time scale at which this excitation happens could not be deduced from these findings. A numerical study verified these arguments and suggested a power-law dependence of the excitation time on the energy density (perturbation strength), given in eq. (4.55).

These results are obtained only for the regular case without random potential. But the general ideas also hold when introducing local disorder, because the local disorder does only change the unperturbed Hamiltonian $H_0 = \sum \omega_k^2 (AI_k)^{4/3}$, but the resonance picture is still applicable. This is true because the fully nonlinear oscillator allows to tune its frequency from zero to infinity by adjusting its amplitude appropriately. Hence, one still finds single, double and triple resonances for $N = 3, 4, 5$ oscillators if the initial amplitudes of the oscillators are chosen in the right way. Thus, the above arguments are applicable in the same way and one would find the same results when investigating oscillators with some random parameters. The situation is completely different for oscillators with a harmonic local potential and random frequencies. There, the nonlinear frequency can not be tuned in such a way and for small perturbation strengths one typically does not find 1:1 resonances.

4.4.2. Numerical Results in 1D

After having developed a theory for the dynamics of the edge oscillators for the fully nonlinear case with $\kappa = 4$, $\lambda = 6$, now the original spreading problem for this case will be attacked numerically. As before, the goal on one the hand is to verify the scaling prediction from the NDE, and on the other hand to apply the results of the

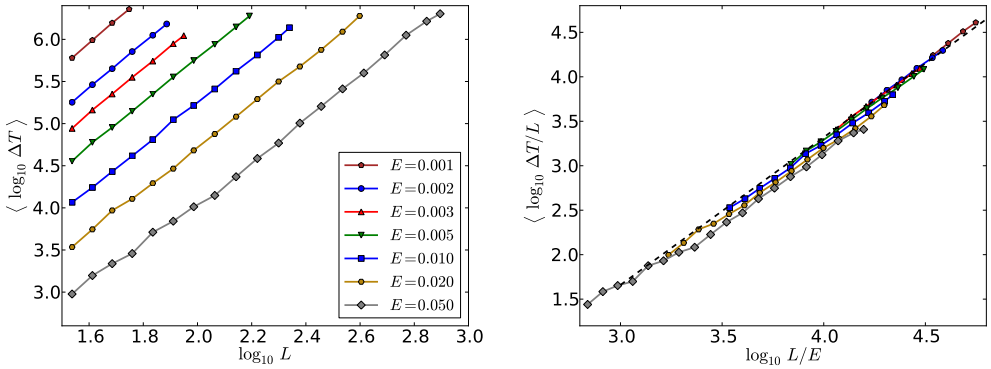

(a) Excitation times for 4–6_{hd} (1D). **(b)** The same data but in rescaled variables.

Figure 4.8.: Excitation times $\Delta T(L)$ for the one-dimensional case 4–6_{hd}, i.e. $\omega_k \in [0.5, 1.5]$, with energies $E = 0.001 \ldots 0.05$. Left plot shows results in original variables, while on the right the scaling prediction of the NDE is applied by plotting $\Delta T/L$ vs $1/W$ where $W = E/L$. The dashed black line shows the behavior $\Delta T/L \sim W^{-5/3}$.

excitation edge dynamics to properties of spreading states. The numerical results are obtained for the one-dimensional 4–6_{hd} model, hence with a disordered local potential $\omega_k \in [0.5, 1.5]$ to avoid the existence of traveling quasi-compactons.

In a first study, again the excitation times $\Delta T(L)$ are investigated for different initial energies $E = 0.001 \ldots 0.05$. The results are obtained by averaging over $M = 10^3$ disorder realizations where for each realization the initial condition was a uniform excitation of 10 lattice sites. The results are shown in Fig. 4.8. While Fig. 4.8a shows the plain results, in Fig. 4.8b the same data is plotted but in rescaled coordinates as suggested by the NDE (3.21): $\Delta T/L$ vs. L/E. As a first observation one finds that the scaling works quite well as seen from the overlap of curves in the scaled plot Fig. 4.8b. However, the scaled data still show a recognizable trend as curves for smaller energies are shifted upwards. This means the scaling of the nonlinear diffusion equation is not perfectly fulfilled and there might be some other process involved that requires further investigation. Nevertheless, the power law behavior of the spreading times are again a justification of the applicability of the nonlinear diffusion equation. Secondly, from the study of the dynamics at the excitation edge presented before in section 4.4.1, the following prediction of the excitation times in dependence of the energy density was found: $T \sim W^{-5/3}$ (4.55). As there the excitation length L was kept fix while decreasing the energy density, this result directly translates to the following prediction for the excitation times ΔT of spreading states, using $W = E/L$:

$$\frac{\Delta T}{L} \sim \left(\frac{L}{E}\right)^{5/3}. \tag{4.56}$$

This prediction is plotted in Fig. 4.8b as a dashed black line and one sees that the numerical data quite perfectly follow this prediction. Thus it seems that again the

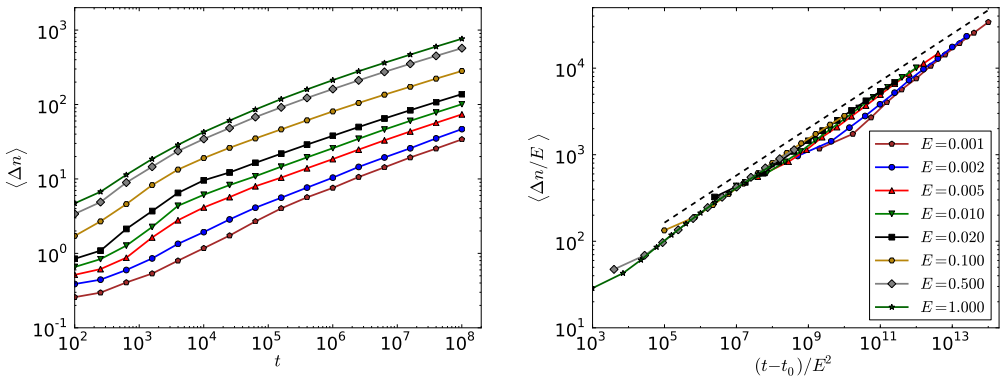

(a) Second moment for 4–6_{hd} (1D). **(b)** Same data in rescaled variables.

Figure 4.9.: Square root of the second moment $\Delta n(t)$ for spreading states in the one-dimensional 4–6_{hd} model for different energies $E = 10^{-3} \ldots 1$. In (a), the plain results are presented, while (b) shows the same data but in rescaled variables $\Delta n/E$ vs. $(t - t_0)/E^2$. The dashed line represents the behavior $\Delta n \sim t^{3/11}$ given in (4.57).

NDE provides a good description of the spreading behavior. Moreover the analysis of the dynamics of the excitation edge gives the correct power law prediction.

Additionally, a numerical study on the second moment $\Delta n^2(t)$ of spreading states was done. There, the nonlinear diffusion equation suggests the scaled variables (3.16): $\Delta n/E$ vs. $(t-t_0)/E^2$. By comparing eq. (4.56) with (3.21) on identifies the nonlinear exponent of the NDE to be $a = 5/3$, hence the spreading exponent in one dimension calculates as $\alpha_1 = 1/(a+2) = 3/11$. Putting everything together, the square root of the second moment Δn should exhibit the following behavior:

$$\frac{\Delta n}{E} \sim \left(\frac{t - t_0}{E^2} \right)^{3/11} . \tag{4.57}$$

This is checked in a numerical study where the second moment Δn^2 is measured for single site initial excitations for different energies $E = 10^{-3} \ldots 1$. For each energy the results are averaged over $M = 48$ realizations of disorder and the plain results are plotted in Fig. 4.9a. For each energy, some transient behavior has to be neglected by fitting t_0 which gave values $t_0 \approx 10^3$. However, this does not influence the asymptotic observation. Fig. 4.9b shows the same data in rescaled coordinates and using t_0, again nicely verifying the scaling prediction. Moreover, the prediction on the spreading exponent again is plotted as a dashed line and like for the excitation times before, the numerical results very accurately follow this prediction.

Hence, both ways of measuring spreading, excitation time ΔT and second moment Δn^2, give compatible results and both support the validity of the nonlinear diffusion equation by following its scaling prediction in a large range of tested energies $E = 10^{-3} \ldots 1$. Additionally, the prediction on the nonlinear exponent $a \approx 5/3$

found numerically from an analysis of the microscopic dynamics was verified convincingly up to enormous values of rescaled time $t/E^2 = 10^{14}$ by this numerical study of spreading states.

Note, that here the excitation of zero-amplitude oscillators heavily relies on chaoticity of the trajectory and hence the term "chaotic diffusion" is perfectly suited to describe this situation. Without a chaotic region connecting zero-amplitude states with the higher amplitudes of initially resting oscillators, no energy spreading would take place. By virtue of the nonlinear diffusion equation, the properties of chaos could be translated to a diffusion prediction that was perfectly matched in numerical simulations. Such a quantitative result had not been found before and is thus one of the major outcomes of this work.

4.5. Disordered Lattices of Harmonic Oscillators

Finally, the most complicated situation will be studied, harmonic oscillators with random frequencies and nonlinear coupling. The Hamilton function in one dimension for this case writes as (c.f. (2.4)):

$$H = \sum_{k=1}^{N} \frac{p_k^2}{2} + \omega_k^2 \frac{q_k^2}{2} + \frac{1}{\lambda} \sum_{k=1}^{N-1} (q_k - q_{k+1})^\lambda, \tag{4.58}$$

where ω_k are the random frequencies and chosen iid. as $\omega_k \in [0, 1]$ (soft disorder) or $\omega_k \in [0.5, 1.5]$ (hard disorder). Two values of the coupling nonlinearity will be studied: $\lambda = 4$ and $\lambda = 6$ for both one- and two-dimensional lattices.

This case is more difficult to understand then those presented before and a full theory is still lacking, unfortunately. The reason is that due to the random frequencies, the oscillators are typically not in resonance. For the regular case studied in section 4.3 it was found that all oscillators are always in resonance, even for arbitrary small amplitudes. But this was due to the equal frequencies, $\omega_k = 1$, a property explicitly violated here. For fully nonlinear oscillators it was found in section 4.4 that although the non-excited oscillator is not in resonance with those with finite amplitudes, they form a multi-resonance that overlaps with the small-amplitude resonance of the edge-oscillator. This creates the possibility for an oscillator at rest to reach an excited state by diffusion along a chaotic region in phase space. But this relied on the fact that one can find four oscillators in a 1:1 resonance, which in the case of disorder is only possible if the oscillator frequency can be tuned considerably by amplitude modulations. As that is not the case for harmonic disordered oscillators, the techniques used in the previous chapters can not be applied directly.

4.5.1. High Density Estimation

For large energy densities $W \sim 1$, the nonlinear perturbation introduced by the coupling might be big enough to overcome the frequency detuning introduced by

disorder. Then, the situation would be similar to the fully resonant case studied in section 4.3, because although the frequencies may differ, the energy density and hence the perturbation is strong enough to bring all oscillators in resonance. Here, exemplarily only the case $\lambda = 4$ should be analyzed. There, the frequency $\tilde{\omega}_k$ of one harmonic oscillator with amplitude a_0, including the nonlinear shift due to the coupling in lowest order, calculates as $\tilde{\omega}_k \approx \omega_k + 3a_0^2/(8\omega_k)$ (c.f. (4.11)). Furthermore, the local energy density of this oscillator depends on the amplitude as follows: $w_k = \omega_k^2 a_0^2/2$. A global resonance is found in a chain of such oscillators if the nonlinear frequency shift of an excited oscillator $\sim 3a_0^2/8\omega_k$ is typically greater than the frequency detuning to its non-excited neighbor $\Delta\omega_1 = |\omega_1 - \omega_2|$, that is the zero-amplitude oscillator is in resonance with its neighbor that has a local energy $W = w_k$. By taking averages one arrives at the following relation for the critical amplitude a_c and hence the critical energy density W_c below which it becomes unlikely to find such a global resonance:

$$\overline{\Delta\omega_k} = \frac{3a_c^2}{8}\overline{\omega_k} = \frac{3}{4\,\overline{\omega_k^3}}W_c, \tag{4.59}$$

where $\overline{x}$ denotes the average over an ensemble of random iid. frequencies. A straight forward calculation gives $\overline{\Delta\omega_k} = 1/3$ and thus one finds, in the case $\lambda = 4$, for W_c for soft ($\omega_k \in [0, 1]$) and hard ($\omega_k \in [0.5, 1.5]$) disorder:

$$\begin{aligned} W_{c,\mathrm{sd}} &\approx 1/18 \approx 10^{-1.25} \\ W_{c,\mathrm{hd}} &\approx 4/9 \approx 10^{-0.35}, \end{aligned} \tag{4.60}$$

where the powers of 10 are given for comparison with later numerical findings. For energy densities around these values, the oscillators are typically in a global resonance and from the results of section 4.3 one expects spreading with the nonlinearity parameter of the NDE $a \approx 1$.

Without a detailed calculation on the critical density, it should just be noted that for $\lambda = 6$ at high energy densities $W \sim 1$, the resonance results from section 4.3 predict spreading with the nonlinearity parameter $a \approx 2$.

4.5.2. Dynamics at the Excitation Edge

If the density W is too small to create a full 1:1 resonance in the system, spreading is still possible because the trajectory can move along thin chaotic layers created by high-order resonances [28]. Such high-order resonances are induced by the quartic coupling, which leads to terms $\sim \cos(\theta_1 - 3\theta_2)$ where $\theta_{1,2}$ are the angle variables of the two coupled oscillators. This, for example, induces a 1:3 resonance between those oscillators. Furthermore, the solution of a single harmonic oscillator with quartic perturbation obtained from:

$$H = \frac{p^2}{2} + \omega_0^2\frac{q^2}{2} + \frac{q^4}{4} \tag{4.61}$$

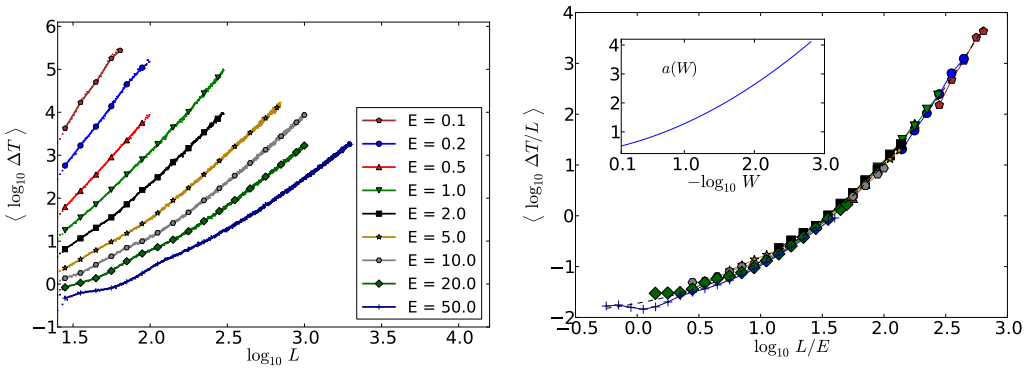

(a) Excitation times for 2–4_{sd} in 1D.

(b) The same data in scaled variables.

Figure 4.10.: Excitation times $\Delta T(L)$ for an one-dimensional lattice of harmonic oscillators and coupling nonlinearity $\lambda = 4$ and soft disorder $\omega_k \in [0, 1]$. In (a) the direct results $\Delta T(L)$ are plotted while for (b) the scaling from the NDE has been applied. Each color/symbol belongs to an averaged value over disorder realization for a fixed energy E. The inset in (b) shows the dependence of the nonlinearity index $a(W)$ on the density W, obtained via polynomial fitting of the scaled data (dashed line).

also includes high frequency terms, e.g.:

$$q(t) = a_0 \cos(\omega_0 + \omega_1) + \frac{a^3}{32\omega_0^2}(\cos 3\omega_0 t - \cos \omega_0 t) + \dots \tag{4.62}$$

with $\omega_1 = 3a_0^2/8\omega_0$ as above. Hence, a whole cascade of high-order resonances are possible for two harmonic oscillators with a nonlinear coupling. However, a full analysis of this resonance structure with the aim to obtain similar results as before is rather difficult, firstly because of the complicated resonance structure itself and secondly because additionally, an ensemble average over the random frequencies must be obtained. So at this point, the only at least to some extent definite result is that one might expect a behavior similar to the full resonant case for large energy densities. But as the density decreases, the main resonance is not accessible anymore because the nonlinear frequency shifts are getting too small. The implications for spreading states remain unclear at this point and here numerical results are employed to obtain further insight on this problem, discussed in the next sections.

4.5.3. Numerical Results in 1D

At first, the one-dimensional chain is considered, starting with the case where the nonlinear coupling exponent is set to $\lambda = 4$. As before for one-dimensional systems, the excitation times $\Delta T(L)$ are measured for different initial energies. Results are (logarithmically) averaged over $M = 1000$ realizations of disorder while the initial condition was always a uniform distribution over $L_0 = 10$ sites. Fig. 4.10 shows

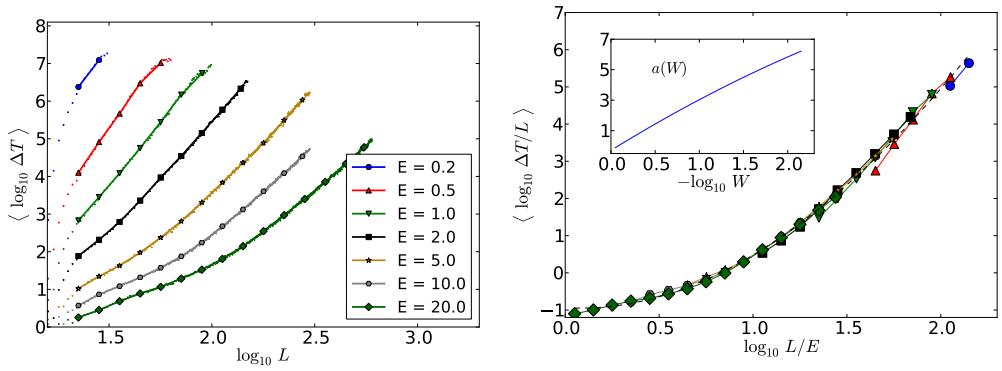

(a) Excitation Times for 2–4_{hd} in 1D.

(b) The same data in scaled variables.

Figure 4.11.: The same as Fig. 4.10 but for "hard disorder", i.e. $\omega_k \in [0.5, 1.5]$. Again, the inset in (b) shows the numerically obtained nonlinear exponent $a(W)$.

results for soft disorder, i.e. $\omega_k \in [0, 1]$. Again the data are plotted in usual variables as well as following the scaling prediction from the NDE (3.20): $\Delta T/L$ vs. L/E. One finds perfect energy scaling and hence good verification of the scaling property of the nonlinear diffusion equation. However, it is also clearly seen that the curves do not follow a straight power-law, but rather bend upwards, which means an increasing density dependent NDE parameter $a(W)$, where the density $W = E/L$. To account for such a density dependence, the following quantity is defined:

$$a(W) = -\frac{\mathrm{d}\log_{10}\Delta T/L}{\mathrm{d}\log_{10} W}. \tag{4.63}$$

This is illustrated in the inset of Fig. 4.10b, where a numerical estimate of this quantity is shown obtained from fitting the data points in log-log scale by a polynomial and then taking the derivative. Although the scaling works perfectly, the exponent changes from roughly $a \approx 1$ at high densities up to $a \approx 4$ at the lowest densities $W \approx 10^{-3}$ reached in this study. At this point, no signature of saturation of $a(W)$ can be identified, but nevertheless, no definite answer on the true asymptotic behavior can be given.

Similar results were found for 2–4_{hd}, i.e. random frequencies $\omega_k \in [0.5, 1.5]$. Fig. 4.11 again shows the numerical outcome in both normal and scaled variables. As before, the scaling works perfectly as the curves for different energies nicely overlap onto a single curve. But again the result is not a straight line, but rather bends upwards which as above indicates a density dependent exponent $a(W)$. As shown in the inset of Fig. 4.11b, the values $a(W)$ now increase even faster than before, reaching almost $a \approx 7$ for the final density of $W \approx 10^{-2}$. However, as before the true asymptotic behavior can not be concluded from these results.

It was also checked whether this density dependent spreading exponent can be found when looking at the direct spreading measure rather then excitation times. Fig. 4.12

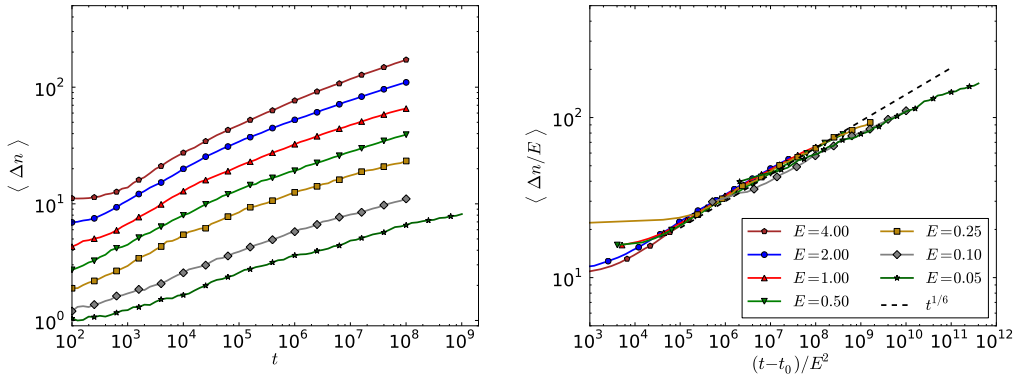

(a) Second Moment for 2–4_{sd} (1D). **(b)** The same data in scaled variables.

Figure 4.12.: Result for the second moment $\Delta n^2(t)$ for the model 2–4_{sd}, hence the same as in Fig. 4.10. (a) shows the plain numerical results and (b) the scaling prediction of the NDE. Results are averaged over $M = 100$ disorder realizations.

shows results for the second moment exemplarily for the model 2–4_{sd}. Hence this should be compared with the data in Fig. 4.10. One finds that the scaling prediction of the NDE, suggesting to use $\Delta n/E$ and $(t-t_0)/E^2$ as scaled variables to account for energy dependence, works again reasonably well, shown in Fig. 4.12b. The density dependence of the nonlinearity exponent $a(W)$ should manifest in this result as a density dependent spreading exponent $\alpha_1(W) = 1/(a(W) + 2)$. An indication of this is also seen in Fig. 4.12b, as the data points rather follow a curve bending downwards than a straight line, especially when compared to the exemplary power law $\Delta n \sim t^{1/6}$ plotted as dashed line. However, the results are much less clear and a quantification of the spreading exponent is much harder than it was from measuring $\Delta T(L)$ before. This is exactly due to the fact that when calculating disorder averages $\langle \Delta n \rangle$, one averages over different values of Δn, hence situations with different densities, as explained in section 2.5. Thereby, the density dependence $a(W)$ gets, to some extent, averaged away and thus is very hard to be extracted from results like Fig. 4.12. So only by introducing the new spreading quantification $\Delta T(L)$ it was possible to obtain a clear quantitavie result on the density dependent spreading exponent, as the measures used before are not suitable for this kind of detailed analysis.

Furthermore, simulations for the case with coupling nonlinear power $\lambda = 6$ were performed. Fig. 4.13a shows the results for soft disorder 2–6_{sd}, $\omega_k \in [0, 1]$ and Fig. 4.13b for hard disorder 2–6_{hd}, $\omega_k \in [0.5, 1.5]$. Both graphs are already plotted in scaled variables $\Delta T/L$ vs. L/E and once again the scaling prediction from the NDE is verified perfectly, indicated by the collapse of curves for different energies. However, as for quartic couplings, again the numerical results suggest an energy dependent nonlinearity $a(W)$, which as above is further visualized by showing numerical derivatives (4.63) in the insets.

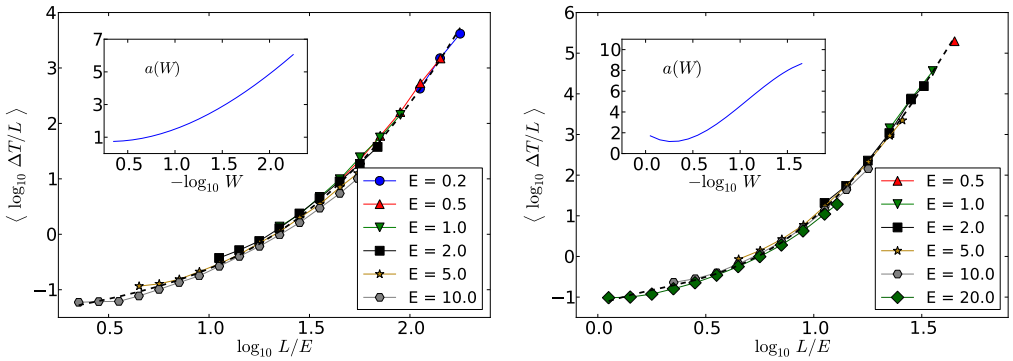

(a) Excitation times for 2–6$_{\mathrm{sd}}$ (1D). **(b)** Excitation times for 2–6$_{\mathrm{hd}}$ (1D).

Figure 4.13.: Scaled excitation times $\Delta T(L)$ for the one-dimensional case 2–6$_{\mathrm{sd}}$ ($\omega_k \in [0,1]$) and 2–6$_{\mathrm{hd}}$ ($\omega_k \in [0.5, 1.5]$). The insets show the density dependencies $a(W)$ obtained from polynomial fits.

This density dependent exponent $a(W)$ is a fundamental difference to the other cases presented before, as there the spreading always appeared to follow a pure power law with a constant exponent. The reason for this behavior is not yet understood, but a qualitative picture might indeed be that by needing to employ higher and higher resonances as the density decreases, the chaotic layers on which spreading states can travel get smaller and smaller which could induce such a slower-than-power-law behavior. Note that for the 4–6 models, it was shown that the trajectory can always follow the main 1:1 resonance which leads to a pure power law behavior. For harmonic oscillators, this is surely not true and it seems quite reasonable that this leads a to behavior with increasing nonlinear exponent a. This is also, in a qualitative sense, supported by the findings on the properties of chaos shown in the beginning in Fig. 2.4b. There, it was shown that chaos in random harmonic chains depends on the chain-length and density in such a way that spreading states at some point enter a KAM regime where the chaotic region of phase space gets smaller and smaller. In contrast, for example, to the fully nonlinear case where spreading states are moving away from the KAM region as presented in Fig. 2.3.

In conclusion, for one-dimensional random harmonic lattices and coupling nonlinearities $\lambda = 4, 6$, the NDE scaling prediction is fulfilled very accurately by spreading states as found from an extensive numerical study. However, in all cases the spreading exponent showed a clear density dependence $a(W)$ and due to the lack of a conclusive theoretical description for this complicated situation, no reliable prediction for the asymptotic behavior can be made at this point. The possibilities are that $a(W)$ might saturate at some point giving again asymptotic subdiffusive behavior, or $a(W)$ diverges which would lead to a stop of the spreading process, or $a(W)$ might keep growing which would mean a sub-subdiffusive process. Additional results on the second moment showed that studies based on this quantity might be misleading as the density dependence is surpressed by averaging.

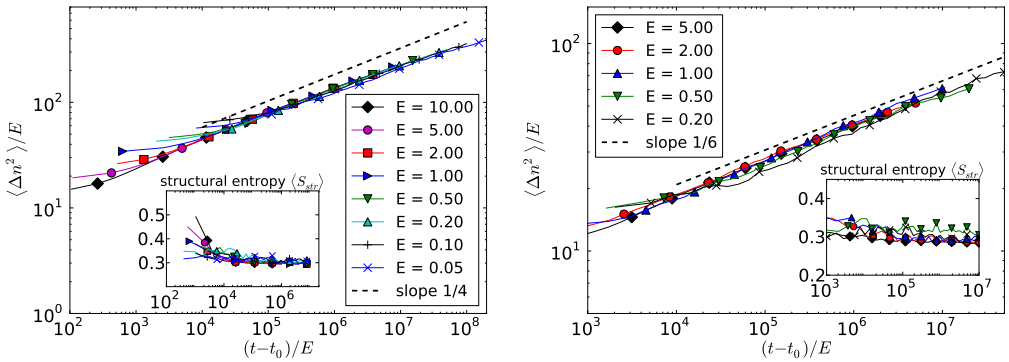

(a) Spreading for 2–4_{sd} in 2D.

(b) Spreading for 2–6_{sd} in 2D.

Figure 4.14.: Spreading results for the two-dimensional harmonic lattice with nonlinear coupling exponent $\lambda = 4$ (a) and $\lambda = 6$ (b) with "soft disorder" ($\omega_{i,k} \in [0, 1]$ iid.). The results are averaged over random potential realizations and plotted using the NDE scaling prediction $\langle \Delta n^2 \rangle / E$ vs t/E. The insets show the behavior of the structural entropy $\langle S_{\mathrm{str}} \rangle(t)$.

4.5.4. Numerical Results in 2D

Finally, also two-dimensional lattices of harmonic oscillators with random frequencies are investigated. For the 2D case, spreading is measured in terms of the second moment, defined in section 2.6, where also the Hamiltonian is presented. The nonlinear diffusion equation predicts the following scaling behavior of the energy (3.24):

$$\frac{\Delta n^2(t)}{E} \sim \left(\frac{t - t_0}{E} \right)^{\alpha_2}, \qquad \text{with} \qquad \alpha_2 = \frac{1}{a+1}. \tag{4.64}$$

This is checked numerically by analyzing the behavior of the second moment of initial 5x5 uniform excitations in a quadratic lattice. This was done for several values of the initial energy and the results are averaged over $M = 32$ realizations of disorder for each energy. In a first study, the model 2–4_{sd} is considered and the results are shown in Fig. 4.14a. Fig. 4.14b shows the data obtain for the case 2–6_{sd}. For both models, the scaling is nicely verified by the numerical results as seen from the collapse of curves for different energies. Moreover, the structural entropy saturates in all cases further supporting the self-similarity of the spreading states. The spreading exponent α_2 is roughly identified as $\alpha_2 \approx 1/4$ for 2–4, while for 2–6 one finds $\alpha_2 \approx 1/6$. Note that in the resonant case studied in section 4.3, these exponents where calculated as $\alpha_2 = 1/2$ and $\alpha_2 = 1/3$ respectively. Hence spreading is much slower in the presence of disorder.

Furthermore, these result do not exhibit a clear deviation from the power law behavior that was found in one dimension before. A careful observation of the result for 2–4 in Fig. 4.14a does reveal some signature of a density dependent nonlinear parameter $a(W)$ as the curve seems to bend downwards, but this is effect is hardly

visible and not observed for 2–6 at all. As the above arguments for a density dependent exponent are not limited to one dimension, such a behavior should also be observed here. There are two reasons why this is not the case. Firstly, the second moment used as observable is not a very good tool to identify such a behavior, because the density dependence might get averaged out as explained previously and is visible when comparing the results of Fig. 4.10b and Fig. 4.12b. Moreover, instead of having just one excited neighbor as before, in two dimensions the edge oscillator at rest typically has two, maybe even three, excited neighbors. As it is enough to have a resonance with one of those neighbors, this reduces the average detuning: $\overline{\Delta\omega} = \overline{\min(\Delta\omega_1, \Delta\omega_2)}$, which allows for smaller energy densities until higher order resonances need to be considered. This essentially stretches the curves $a(W)$ and together with the averaging issue this could be the explanation why in 2D no such clear density dependence of the spreading exponent is observed.

In conclusion, again the scaling prediction has been very successfully verified by the numerical results. Also the structural entropy supports the validity of the nonlinear diffusion equation for spreading in two-dimensional random harmonic lattices. It should be said that as only results for the second moment are obtained, a conclusive answer to the density dependence could not be obtained. A study on the excitation times for this case is appealing and will be subject of later works. However, the true asymptotic behavior thus also remains unrevealed here.

5. Summary and Conclusions

5.1. Summary

In this work, the problem of diffusion induced by chaotic behavior in nonlinear Hamiltonian systems was discussed. The model, rather academically, were chains or lattices of harmonic or nonlinear oscillators with a nonlinear nearest neighbor coupling. A thorough analysis of these models revealed two classes of scaling that turned out very helpful. The diffusion was measured in terms of energy spreading of initially localized excitations and several observables to quantify this spreading were introduced. Specifically, the connected nature and the super-exponential tails of the spreading states in such models allowed for defining a new quantity called excitation time ΔT. This quantity was shown to have severe advantages over existing methods and served as the most important measure of spreading in one-dimensional chains, while for the two-dimensional studies results were quantified in terms of the well-known and often used second moment Δn^2.

As a macroscopic description for the spreading process, the nonlinear diffusion equation (NDE) was presented and its properties were analyzed in detail. From this, a number of predictions for the spreading states have been found, mainly on the expected role of the energy as the only free parameter in both the oscillator model and the nonlinear diffusion equation. Although it is up to now not possible to give a rigorous derivation of the NDE starting from the microscopic dynamics of the oscillators, these predictions provide a convincing set of tests that have been checked numerically in this work.

The choice of such a relatively simple model of nonlinear oscillators with nearest neighbor coupling was motivated by the hope of being able to gain deeper insight on the properties of chaotic diffusion by mathematical treatments. Indeed, for a special case of nonlinearities, called the "homogeneous case", an exact prediction for the energy diffusion based on scaling properties was found and numerically verified in section 4.2. This encouraged the application of the nonlinear diffusion equation also for more complicated situations where such a simple scaling argument is not readily found.

In section 4.3 the special case of a harmonic lattice of fully resonant oscillators was analyzed. There, the spreading problem was reduced to the simple consideration of two coupled oscillators mimicking the edge of the excitation. This simplification turned out to be very effective. By making use of the fact that all oscillators are in resonance, again an exact prediction on the spreading behavior for this case could be deduced. The argumentation was based on the scaling properties found from

analyzing the resonance dynamics and then by assuming the validity of the NDE, the spreading prediction was found. This was also verified numerically, but here a two-dimensional lattice had to be used to avoid the influence of quasi-compactons that are observed in one-dimensional, fully resonant chains. Despite the nice correspondence of the numerical results with the analytic prediction on the spreading exponent, the peak structure of the spreading states was found to deviate from a self-similar behavior that is suggested by the nonlinear diffusion equation. The reason for this might be the existence of persisting breather states that are initially excited and decay very slowly, but this effect was not further examined here.

After that, the fully nonlinear case was investigated in section 4.4. Motivated by the previous results, again it was tried to derive the spreading properties from the dynamics of the oscillators at the edge of the excitation. It was found that considering just two oscillators to model the excitation edge is not enough as this leads to a critical density below which no spreading would be observed. By geometric arguments about the resonance structure, it was found that with five (or more) oscillators, the chaos induced by resonance overlaps at the excitation edge is such that even for arbitrarily small densities spreading can take place. A numerical study revealed a power-law dependence of chaotic excitation times on the energy density in this simplified model which, by using the nonlinear diffusion equation, was translated to a spreading prediction in large oscillator chains. This prediction was then compared to the spreading exponent obtained from numerical simulations and a perfect correspondence was found. Thus, again by starting at the microscopic dynamics, an exact prediction for the macroscopic spreading behavior was extracted and numerically verified. Furthermore, the scaling prediction of the energy from the nonlinear diffusion equation for the spreading states was checked as well in this case. The results were not as perfect as in other cases but still quite convincing. However, the slight deviation from the predicted scaling might indicate that the chaotic diffusion in this case is not perfectly described by the NDE and a further analysis of this observation will be subject of later works.

Finally, the most complicated case of lattices of harmonic oscillators with random frequencies and nonlinear coupling was studied. There, no conclusive theory on the spreading behavior was found as the resonance structure of this situation is considerably more complicated. By some heuristic arguments and supported from previous results on the properties of chaos for such lattices, some ideas for explaining the non-power-law spreading were presented. However, the major outcome for this case are the extensive numerical results for one- and two-dimensional lattices presented in section 4.5. In all numerical studies done for this case of harmonic oscillators, a perfect verification of the scaling prediction of the NDE was observed. This, again, showed the usability of the nonlinear diffusion equation as a macroscopic description of spreading in such nonlinear Hamiltonian lattices. However, the numerical results indicated a density dependence of the nonlinear exponent of the NDE, that was originally assumed to be a constant. Some arguments were given trying to relate this observation to the complicated resonance structure in the system, but a convincing calculation was not found for this case.

Model	Analytic Result	Equation	Numerical Result	Figure
1D 4–4_{sd}	$a = 1/4$, $\alpha_1 = 4/9$	(4.3), (4.4)	$\Delta T \sim L^{a+1} \sim L^{5/4}$	4.1a
1D 6–6_{sd}	$a = 1/3$, $\alpha_1 = 3/7$		$\Delta T \sim L^{a+1} \sim L^{4/3}$	4.1b
2D 4–4_{re}	$a = 1/4$, $\alpha_2 = 4/5$	(4.3), (4.5)	$\Delta n^2 \sim t^{\alpha_2} \sim t^{4/5}$	4.2a
2D 4–4_{sd}	$a = 1/4$, $\alpha_2 = 4/5$		$\Delta n^2 \sim t^{\alpha_2} \sim t^{4/5}$	4.2a
2D 6–6_{re}	$a = 1/3$, $\alpha_2 = 4/5$		$\Delta n^2 \sim t^{\alpha_2} \sim t^{3/4}$	4.2b
2D 6–6_{sd}	$a = 1/3$, $\alpha_2 = 4/5$		$\Delta n^2 \sim t^{\alpha_2} \sim t^{3/4}$	4.2b
1D 2–4_{re}	$a = 1$, $\alpha_1 = 1/3$	(4.31), (4.31)	– (quasi-compactons)	
1D 2–6_{re}	$a = 2$, $\alpha_1 = 1/4$		– (quasi-compactons)	
2D 2–4_{re}	$a = 1$, $\alpha_2 = 1/2$		$\Delta n^2/E \sim (t/E)^{1/2}$	4.4
2D 2–6_{re}	$a = 2$, $\alpha_2 = 1/3$		$\Delta n^2/E \sim (t/E)^{1/3}$	4.5
1D 4–6_{hd}	Semi-Analytic Result	(4.55)	$\Delta T/L \sim (L/E)^{5/3}$	4.8
	$a = 5/3$, $\alpha_1 = 3/11$	(4.56),(4.57)	$\Delta n/E \sim (t/E^2)^{3/11}$	4.9
	Numerical Observation			
1D 2–4_{sd}	$a(W) \approx 1 \ldots 4$		$\Delta T/L \sim (L/E)^{a(W)}$	4.10
1D 2–4_{hd}	$a(W) \approx 1 \ldots 7$		$\Delta T/L \sim (L/E)^{a(W)}$	4.11
1D 2–6_{sd}	$a(W) \approx 1 \ldots 6$		$\Delta T/L \sim (L/E)^{a(W)}$	4.13a
1D 2–6_{hd}	$a(W) \approx 2 \ldots 8$		$\Delta T/L \sim (L/E)^{a(W)}$	4.13b
2D 2–4_{sd}	$\alpha_2 \approx 1/4$		$\Delta n^2/E \sim (t/E)^{1/4}$	4.14a
2D 2–6_{sd}	$\alpha_2 \approx 1/6$		$\Delta n^2/E \sim (t/E)^{1/6}$	4.14b

Table 5.1.: Overview of the analytic and numerical results found in this work. The abbreviations for the models refer to the nonlinear powers and the choice of random (hd or sd) or regular (re) local potential, as explained in section 2.1. a denotes the nonlinear exponent of the NDE (3.3) and $\alpha_{1,2}$ are the corresponding spreading exponents for 1D (3.20) and 2D (3.24). ΔT is the excitation time as described in section 2.5.2 while Δn^2 denotes the second moment. For the semi-analytic result the resonance analysis was performed analytically using geometric arguments, while the actual value relied on a numerical study. For the density dependent result $a(W)$, no theoretical description could be found.

Overall, in this work it was found that the nonlinear diffusion equation is a very useful tool to describe spreading in nonlinear Hamiltonian systems. With only some small deviations in a few cases, the scaling prediction of the NDE has been numerically verified for the harmonic or nonlinear oscillators studied in this work. Secondly, the technique of analyzing the microscopic dynamics of the oscillators at the edge of the excitation turned out to be very fruitful leading to several predictions on the spreading behavior that were also nicely verified by numerical simulations. Table 5.1 provides an overview of the studied cases and the analytic and numerical results presented in this work. Unfortunately, the highly interesting case of harmonic oscillators with random frequencies is also the most difficult. However, it is hoped that the techniques, findings and results presented here might eventually also lead to a full understanding of the observed diffusion in this model.

5.2. Comparison with Spreading Results in Nonlinear Anderson Models

One of the motivations for this work was to find a theoretical explanation for the observed subdiffusive behavior that has been found in disordered nonlinear systems with linear coupling terms. The most prominent example of such a system is the DANSE model, where also subdiffusive spreading of initially localized states is observed, as described in section 1.3. Moreover, another model has gained considerable attention lately, e.g [38]: the disordered Klein-Gordon model (K-G). Like the DANSE model it has local disorder, local nonlinearity and a linear nearest-neighbor coupling. But in contrast to the former, the Klein-Gordon model has only one conserved quantity, while in the DANSE model both energy and norm are conserved. However, both models consist of harmonic oscillators with random frequencies and quartic coupling terms, when transformed into the basis of linear, localized eigenmodes. Thus, they are similar to the 2–4 cases studied here, but with a more complicated nonlinear coupling of localized linear modes that includes not only nearest neighbors. In several works, mostly dealing with one-dimensional lattices, the observation of two spreading regimes was reported [43, 108]. Recently, such a behavior was also found in two-dimensional Klein-Gordon lattices [109]. For rather large energy densities, numerical results indicated an exponent of the nonlinear diffusion equation of $a \approx 2$ and the situation was called "strong chaos". While for small densities, numerical data suggested $a \approx 4$, denoted by "weak chaos".

Here, also an increase of this nonlinearity exponent for the case of harmonic oscillators with random frequencies and nonlinear coupling was found, as reported in section 4.5. However, the numerical results presented here do not suggest the existence of a crossover, nor the convergence of a towards a constant for small densities. Rather, $a(W)$ seems to monotonically increase for decreasing densities W. The reason for this discrepancy might be due to the fact that in the DANSE or Klein-Gordon model, spreading states always have exponential tails, induced from the exponential tails of the linear modes. Therefore, the technique of measuring excitation times that lead to the very precise findings of $a(W)$ can not be applied there because of the absence of sufficiently sharp excitation edges. In those situations one has to rely on measuring the second moment to quantify spreading, but as explained in section 2.5, this has the clear disadvantage that with averaging over disorder realization, one also averages over different energy densities. Consequently, $a(W)$ is effectively averaged over densities as well and it is very difficult to extract the true behavior of $a(W)$. This problem is illustrated in section 4.5.3, where results for $\Delta T(L)$ and $\Delta n(t)$ are shown in Figures 4.10 and 4.12. While for ΔT the results very clearly indicated a density dependent exponent $a(W)$, the results for Δn were much less obvious, though still supporting this claim.

Moreover, by interacting not only with nearest, but with several neighbors, the density dependence $a(W)$ should become less dramatic. This is because to become excited, it is sufficient for a linear mode at the edge to exhibit a resonance overlap with one of its interacting neighbors. Hence, the effective average frequency distance

of interacting modes decreases and smaller densities can be reached before higher order resonances have to be employed. For typical choices of disorder, i.e. disorder strength $U = 4$, the localization volume V of the linear eigenmodes was found to be roughly $V \approx 330/U^2 \approx 20$ [108]. That means the nonlinearity couples effectively 20 modes, instead of just two nearest neighbor oscillators as in this work. It seems quite reasonable that this leads to a stretching of the density dependence found in this work. Accordingly one is required to go to much smaller energy densities to find this dependence. A first indication of this effect might be the results for two dimensions presented in section 4.5.4. In two dimensions, the number of interacting neighbors of a non-excited mode is increased to two, and already the density dependence is very hard to detect when using the second moment as the spreading measure as it is seen in Fig. 4.14a. Nevertheless, a definitive statement on the role of the coupling length requires a more detailed study that is left for future works. It may well be that the density dependence is indeed due to the nearest neighbor coupling and by allowing more interactions, one again finds power-law behavior due to some effects not yet understood. But from the considerations of microscopic dynamics performed here, no reason for such a claim was found. This remains an open problem and definitely asks for clarification in subsequent studies.

Another discrepancy between the results obtained here and those presented for the DANSE- and Klein-Gordon model is the prediction of the spreading behavior for large densities. In [38], this regime was introduced as "strong chaos" as there the density is large enough to typically ensure resonance overlaps of 1:1 resonances and hence allow for spreading along this main chaotic layer. A simple calculation gave the prediction $a = 2$ for this case. However, such a situation is studied here in section 4.3, where all oscillators are in resonance even for arbitrary small densities. A thorough analysis of the microscopic dynamics in this resonant situation gave the result $a = 1$, which was also perfectly verified in numerical simulations shown in Fig. 4.4. The reason for this difference between these results and the findings in [38] surely needs further investigation as well.

5.3. Outlook

In this work, it was tried to increase the understanding of chaotic Hamiltonian systems, especially in terms of its diffusive properties. For some cases, analytic predictions on the spreading properties could be obtained, which were also verified by extensive numerical simulations. Especially for the fully nonlinear case, more tests of the theory could be made to further support the analytic arguments, e.g. by studying different choices of nonlinear powers like 4–8 or 6–8. Furthermore, the slight deviations from the scaling prediction should be analyzed carefully, for example by testing the scaling for two dimensional numerical results in this case. Also, the properties and dependencies of the transient times before the subdiffusive spreading sets in have been completely neglected in this work. This might be interesting field of study as well.

However, the main puzzle that still remains is the understanding of the spreading mechanism in the case of harmonic oscillators with random frequencies. For such models, the energy scaling of the nonlinear diffusion equation was numerically verified, but an energy dependent spreading exponent was observed. Some arguments on the reason for this density dependence based on the complicated resonance structure for harmonic oscillators were given, but this is far from a full understanding of the microscopic dynamics. Also, the role of the nearest neighbor coupling on this density dependence should be further investigated to resolve the discrepancy with results for models with exponentially decaying coupling terms. Obviously, this case still requires more work, but hopefully the methods developed here will help to ultimately understand the diffusion process in this case as well.

Another open question is how these results should be generalized to situations with more than one conserved quantity. For example, one could study spreading in a strongly nonlinear Schrödinger lattice that also has only nearest neighbor coupling, but conserves norm and energy. First results on such models have been obtained in [110], but the relation to the nonlinear diffusion equation and its scaling properties is still to be made. Additionally, it might be appealing to apply the techniques and theories developed in this work to interacting spin chains, where also energy diffusion due to nonlinear interactions was found [111].

6. Acknowledgements

The work presented here was only possible with the outstanding support and guidance of my supervisor Arkady Pikovsky. During the whole time of my PhD it rather felt like working with him than working for him, which created an inspiring and pleasent atmosphere. His way of encouraging more than pressuring is outstanding and I highly appreciate doing my PhD with him.

I also thank my colleague and friend Karsten for the innumerous fruitful discussions and all the things I have learned from him. But I especially thank him for his commitment to our project ODEINT. I also thank my colleague Markus for the many discussions improving my physical understanding and for the good teamwork in our seminars on "Computational Physics".

Special thanks also to my dad for proof-reading this thesis in just a few days and providing very helpful feedback, especially on the mathematical clarity. Besides, I thank my friend David for the very fast proof-reading as well and for the very good feedback helping to increase the understandability of this work. In this regard, I also thank my brother Frank for his feedback as well as Mariana, Karsten and Arkady.

Many other people increased my understanding of the problems addressed here, most importantly I thank Dima Shepelyansky, Stefano Lepri and Vadim Oganesyan for lots of helpful discussions. Furthermore, I thank the Istituto dei Sistemi Complessi in Firenze for hospitality and the Institut Henri Poincaré in Paris for hospitality and support. Many of the numerical results have been obtained at the CINECA sp6 supercomputer under the Project HPC-EUROPA2 (Project number 228398), with the support of the European Community - under the FP7 "Research Infrastructure" Programme, which is highly appreciated. I also thank the DFG for financial support under the project PI 220/12-1.

Finally, I thank my family for their continuous support over all the years and for always providing a home I can return to. Last but certainly not least I thank Mariana who was the main motivation for eventually finishing this work. I thank her for her patience and sweet pressure.

A. Mathematical Calculations

A.1. Canonical Scaling

Here, it will be shown that the variable scalings introduced in section 2.2 are canonical transformations. The original Hamiltonian reads:

$$H = \sum_{k=1}^{N} \frac{p_k^2}{2} + U\frac{\omega_k^2}{\kappa} q_k^\kappa + \sum_{k=1}^{N-1} \frac{\tilde{\beta}}{\lambda}(q_{k+1} - q_k)^\lambda \,. \tag{A.1}$$

A.1.1. Nonhomogeneous Case

First the non-homogeneous case $\kappa \neq \lambda$ will be considered. There, a transformation to new variables Q_k, P_k, t' and H' was proposed in eq. (2.3):

$$\begin{aligned} q_k &= U^b \tilde{\beta}^{-b} Q_k \\ p_k &= U^{\lambda b/2} \tilde{\beta}^{-\kappa b/2} P_k \\ t &= U^{(2-\lambda)b/2} \tilde{\beta}^{(\kappa-2)b/2} t' \\ H &= U^{\lambda b} \tilde{\beta}^{-\kappa b} H', \\ &\text{with} \quad b = 1/(\lambda - \kappa). \end{aligned} \tag{A.2}$$

A simple substitution of variables into (A.2) immediately gives the Hamiltonian:

$$H' = \sum_{k=1}^{N} \frac{P_k^2}{2} + \frac{\omega_k^2}{\kappa} Q_k^\kappa + \frac{1}{\lambda} \sum_{k=1}^{N-1} (Q_{k+1} - Q_k)^\lambda \,, \tag{A.3}$$

where U and β disappeared and the only remaining parameter is the energy E. For the transformation to be canonical, however, also the equations of motions should be equivalent. This can be shown by a simple calculation, so first consider the equations for $\dot{q}_k$:

$$\dot{q}_k = \frac{\mathrm{d}q_k}{\mathrm{d}t} = \frac{\partial H}{\partial p_k} = p_k. \tag{A.4}$$

Now by substituting Q_k, P_k and t' one finds:

$$U^b \tilde{\beta}^{-b} \frac{\mathrm{d}t'}{\mathrm{d}t} \frac{\mathrm{d}Q_k}{\mathrm{d}t'} = U^{\lambda b/2} \tilde{\beta}^{-\kappa b/2} P_k \tag{A.5}$$

$$U^b \tilde{\beta}^{-b} W^{(\lambda-2)b/2} \tilde{\beta}^{(2-\kappa)b/2} \frac{\mathrm{d}Q_k}{\mathrm{d}t'} = U^{\lambda b/2} \tilde{\beta}^{-\kappa b/2} P_k \tag{A.6}$$

$$U^{\lambda b/2} \tilde{\beta}^{-\kappa b/2} \frac{\mathrm{d}Q_k}{\mathrm{d}t'} = U^{\lambda b/2} \tilde{\beta}^{-\kappa b/2} P_k \tag{A.7}$$

$$\frac{\mathrm{d}Q_k}{\mathrm{d}t'} = P_k \tag{A.8}$$

$$\dot{Q}_k = \frac{\partial H'}{\partial P_k}. \tag{A.9}$$

A similar calculation can be obtained for the momentum:

$$\dot{p}_k = -\partial H/\partial q_k = -U\omega_k^2 q_k^{\kappa-1} - \tilde{\beta}\left((q_k - q_{k+1})^{\lambda-1} + (q_k - q_{k-1})^{\lambda-1}\right). \tag{A.10}$$

Susbtituting P_k and t' for $\dot{p}_k$ one finds:

$$\dot{p}_k = U^{\lambda b/2} \tilde{\beta}^{-\kappa b/2} \frac{\mathrm{d}t'}{\mathrm{d}t} \frac{\mathrm{d}P_k}{\mathrm{d}t'} \tag{A.11}$$

$$= U^{\lambda b/2} \tilde{\beta}^{-\kappa b/2} U^{(\lambda-2)b/2} \tilde{\beta}^{(2-\kappa)b/2} \frac{\mathrm{d}P_k}{\mathrm{d}t'} \tag{A.12}$$

$$= U^{(\lambda-1)b} \tilde{\beta}^{(1-\kappa)b} \dot{P}_k. \tag{A.13}$$

While subsituting Q_k in the rhs gives:

$$\begin{aligned} \frac{\partial H}{\partial q_k} =& U\omega_k^2 U^{b(\kappa-1)} \tilde{\beta}^{-b(\kappa-1)} Q_k^{\kappa-1} \\ &+ \tilde{\beta} U^{b(\lambda-1)} \tilde{\beta}^{-b(\lambda-1)} \left((Q_{k+1} - Q_k)^{\lambda-1} + (Q_k - Q_{k-1})^{\lambda-1}\right). \end{aligned} \tag{A.14}$$

Using $b = 1/(\lambda - \kappa)$, hence $b(\kappa - 1) + 1 = b(\lambda - 1)$ and $-b(\lambda - 1) + 1 = -b(\kappa - 1)$, one obtains:

$$\frac{\partial H}{\partial q_k} = U^{b(\lambda-1)} \tilde{\beta}^{b(1-\kappa)} \left(\omega_k^2 Q_k^{\kappa-1} + (Q_{k+1} - Q_k)^{\lambda-1} + (Q_k - Q_{k-1})^{\lambda-1}\right). \tag{A.15}$$

Thus, $\dot{P}_k$ calculates as:

$$\dot{P}_k = -\omega_k^2 Q_k^{\kappa-1} - (Q_{k+1} - Q_k)^{\lambda-1} - (Q_k - Q_{k-1})^{\lambda-1} = -\frac{\partial H'}{\partial Q_k}. \tag{A.16}$$

Hence, the equations of motion are invariant under the scaling transformations (A.2) and thus they represent a canonical transformation to the new canonical variables Q_k, P_k, t' and H'.

A.1.2. Homogeneous Case

For the homogeneous case $\kappa = \lambda$, the proposed scaling transformation (2.5) is:

$$\begin{aligned} q_k &= E^{1/\kappa} U^{-1/\kappa} Q_k \\ p_k &= E^{1/2} P_k \\ t &= U^{-1/\kappa} E^{1/\kappa - 1/2} t' \\ H &= E H' \,. \end{aligned} \tag{A.17}$$

Again, a simple substitution in (A.1) gives:

$$1 = H' = \sum_{k=1}^{N} \frac{P_k^2}{2} + \frac{\omega_k^2}{\kappa} Q_k^\kappa + \frac{\beta}{\kappa} \sum_{k=1}^{N-1} (Q_{k+1} - Q_k)^\kappa \,, \tag{A.18}$$

with energy being scaled to $E' = 1$ and $\beta = \tilde{\beta}/W$ as the only parameter. As above, the transformation of the equations of motion will be checked starting with $\dot{q}_k = \partial H/\partial p_k = p_k$ and substituting Q_k, P_k and t':

$$E^{1/\kappa} U^{-1/\kappa} \frac{\mathrm{d}t'}{\mathrm{d}t} \frac{\mathrm{d}Q_k}{\mathrm{d}t'} = E^{1/2} P_k \tag{A.19}$$

$$E^{1/\kappa} U^{-1/\kappa} W^{1/\kappa} E^{1/2 - 1/\kappa} \frac{\mathrm{d}Q_k}{\mathrm{d}t'} = E^{1/2} P_k \tag{A.20}$$

$$E^{1/2} \frac{\mathrm{d}Q_k}{\mathrm{d}t'} = E^{1/2} P_k \tag{A.21}$$

$$\dot{Q}_k = P_k = \frac{\partial H'}{\partial P_k}. \tag{A.22}$$

For the momentum $\dot{p}_k = -\partial H/\partial q_k$ on finds:

$$\dot{p}_k = E^{1/2} \frac{\mathrm{d}t'}{\mathrm{d}t} \frac{\mathrm{d}P_k}{\mathrm{d}t'} = E^{1/2} U^{1/\kappa} E^{1/2 - 1/\kappa} \frac{\mathrm{d}P_k}{\mathrm{d}t'} = U^{1/\kappa} E^{1 - 1/\kappa} \, \dot{P}_k \,, \tag{A.23}$$

and $\partial H/\partial q_k$ calculates as:

$$\begin{aligned} \frac{\partial H}{\partial q_k} = E^{(\kappa-1)/\kappa} U^{(1-\kappa)/\kappa} \big(& U \omega_k^2 Q_k + \tilde{\beta} (Q_{k+1} - Q_k)^{\kappa - 1} \\ & + \tilde{\beta} (Q_k - Q_{k-1})^{\kappa - 1} \big). \end{aligned} \tag{A.24}$$

Hence one finds:

$$\dot{P}_k = -\omega_k^2 Q_k - \frac{\tilde{\beta}}{U} \left((Q_{k+1} - Q_k)^{\kappa - 1} + (Q_k - Q_{k-1})^{\kappa - 1} \right) = -\frac{\partial H'}{\partial Q_k}. \tag{A.25}$$

This shows that the scaling (A.17) also is a canonical transformation as it leaves the equations of motion invariant.

A.2. Derivation of the Self-Similar Solution

Here, the nonlinear diffusion equation is solved by using a self-similar ansatz suggested by the scaling properties of the NDE. This calculation can be found in many textbooks, e.g. [88], and is repeated here for completeness, adapting the choices of variables made in this work. The nonlinear diffusion equation with the nonlinear power $a > 0$ reads:

$$\frac{\partial \rho}{\partial t} = D_0 \frac{\partial}{\partial \vec{r}} \left(\rho^a \frac{\partial \rho}{\partial \vec{r}} \right) = \frac{D_0}{a+1} \triangle \rho^{a+1}, \qquad \text{with} \qquad \int \rho \, \mathrm{d}\vec{r} = E \, . \tag{A.26}$$

The self-similar ansatz is based on the scaling property shown in section 3.2.4 and is formulated in terms of some function $f(\vec{x})$:

$$\rho(\vec{r}, t) = t^{-\alpha} f(\vec{r} t^{-\beta}). \tag{A.27}$$

This gives the following derivatives:

$$\dot{\rho} = -\alpha t^{-\alpha-1} f - t^{-\alpha} \nabla f \cdot \beta \vec{r} / t^{\beta+1}, \tag{A.28}$$

$$\frac{D_0}{a+1} \triangle \rho^{a+1} = \frac{D_0}{a+1} t^{-\alpha(a+1)} \triangle f^{a+1} t^{-2\beta}, \tag{A.29}$$

where $\triangle f$ denotes the Laplace operater acting on $f(\vec{x})$ with respect to $\vec{x} = \vec{r} t^{-\beta}$. The NDE hence results in:

$$t^{2\beta+\alpha a-1} \left(-\alpha f - \beta \vec{x} \, \nabla f \right) = \frac{D_0}{a+1} \triangle f^{a+1}. \tag{A.30}$$

As the rhs of this equation is independent of t, the following relation must hold:

$$\alpha a + 2\beta = 1 \tag{A.31}$$

and the time dependence disappears in the scaled variable. Hence one is left with an ODE for f:

$$-\alpha f - \beta \vec{x} \, \nabla f = \frac{D_0}{a+1} \triangle f^{a+1} \tag{A.32}$$

A second relation between α, β and a can be found by substituting the scaling ansatz for ρ into the conservation law and assuming radial symmetry of $\rho = \rho(r, t)$ with $r = |\vec{r}|$ (and $x = |\vec{x}|$) and accounting for dimensionality $\vec{r} \in \mathbb{R}^d$:

$$\begin{aligned} E &= \int_{-\infty}^{\infty} \rho \, \mathrm{d}\vec{r} = 2\pi \int_0^{\infty} \rho(r, t) \, r^{d-1} \mathrm{d}r \\ &= 2\pi t^{-\alpha} \int_0^{\infty} f(x) t^{\beta} x^{d-1} t^{(d-1)\beta} \mathrm{d}x \\ &= 2\pi t^{d\beta-\alpha} \int_0^{\infty} x^{d-1} f(x) \mathrm{d}x. \end{aligned} \tag{A.33}$$

As E has to be independent of t, one finds:

$$\alpha = d\beta = \frac{d}{ad+2}, \tag{A.34}$$

and hence the following ordinary differential equation for $f(\vec{x})$:

$$-\frac{d}{ad+2}f - \frac{1}{ad+2}\vec{x}\,\nabla f = \frac{D_0}{a+1}\triangle f^{a+1}. \tag{A.35}$$

The whole problem is rotationally invariant and hence it is reasonable to seek for a symmetric solution $f = f(x)$ with $x = |\vec{x}|$. Then, denoting $f' = \mathrm{d}f/\mathrm{d}x$, one gets:

$$\frac{D_0}{a+1}\left(\frac{d-1}{x}(f^{a+1})' + (f^{a+1})''\right) + \beta x f' + d\beta f = 0. \tag{A.36}$$

After multiplying with x^{1-d}, this can be rewritten as:

$$\left(x^{d-1}\frac{D_0}{a+1}\left(f^{a+1}\right)' + \beta x^d f\right)' = 0, \tag{A.37}$$

which by integration yields:

$$x^{d-1}\frac{D_0}{a+1}\left(f^{a+1}\right)' + \beta x^d f = C. \tag{A.38}$$

As this solution should describe spreading states, the following boundary conditions can be claimed: $f(x \to \infty) \to 0$, hence $C = 0$ and thus:

$$D_0 f^{a-1} f' = -\beta x. \tag{A.39}$$

A simple integration then gives:

$$\frac{D_0}{a}f^a = -\frac{\beta}{2}x^2 + C, \tag{A.40}$$

which can be solved easily by the function:

$$f(x) = \left(B - \frac{a}{2(ad+2)D_0}x^2\right)^{1/a}, \tag{A.41}$$

where $\beta = 1/(ad+2)$ is substituted. From physical arguments, the density should be postive, hence one also demands $f(x) > 0$, which means this is only a solution in some region defined by the requirement:

$$x^2 < x_0^2 \qquad \text{with} \qquad x_0 = \sqrt{B\frac{2(ad+2)D_0}{a}}. \tag{A.42}$$

Outside this region, the solution $f = 0$, i.e. $\rho = 0$ is taken. At the boundary these solutions have to be connected and this represents severe mathematical difficulties that require the notion of weak solutions as mentioned earlier. However, here it is

just noted that this is possible and the above result indeed represents a reasonable solution of the NDE. The integration involves one parameter B that can be related to the energy E using (A.33):

$$E = 2\pi \int_0^\infty x^{d-1} f(x) \mathrm{d}x. \tag{A.43}$$

$$= 2\pi \int_0^{x_0} x^{d-1} \left(B - \frac{a}{2(ad+2)D_0} x^2 \right)^{1/a} \mathrm{d}x \tag{A.44}$$

$$\text{with} \quad y = \frac{a}{2(ad+2)D_0} x^2$$

$$= \pi \left(\frac{2(ad+2)}{a} D_0 \right)^{d/2} \int_0^B y^{d/2-1} (B-y)^{1/a} \mathrm{d}y \tag{A.45}$$

$$= \pi \left(\frac{2(ad+2)}{a} D_0 \right)^{d/2} \frac{\Gamma(1+1/a)\Gamma(d/2)}{\Gamma(d/2+1/a+1)} B^{(ad+2)/2a}, \tag{A.46}$$

where $\Gamma(x)$ is the usual gamma function. It is convenient to put all the constants into one parameter $\mu(a, d, D_0)$ and with $\alpha = d/(ad+2)$ one writes:

$$E = \frac{1}{\mu} B^{d/2\alpha a}. \tag{A.47}$$

Note that in two dimension, i.e. $d = 2$, μ takes a value independent of a:

$$\mu = (4\pi D_0)^{-1}. \tag{A.48}$$

Resubstituting into (A.27) with $\vec{x} = \vec{r}/t^\beta$ and adding a time offset t_0, the full self-similar solution is obtained:

$$\rho(\vec{r}, t) = \begin{cases} (t-t_0)^{-\alpha} \left((\mu E)^{2a\beta} - \frac{a}{2(ad+2)D_0} \frac{|\vec{r}|^2}{(t-t_0)^{2\beta}} \right)^{1/a} & \text{for} \quad |\vec{r}|^2 < R^2 \\ 0 & \text{for} \quad |\vec{r}|^2 > R^2 \end{cases} \tag{A.49}$$

$$\text{with} \quad \alpha = \frac{d}{ad+2} \quad \text{and} \quad \beta = \alpha/d = \frac{1}{ad+2},$$

$$\text{and} \quad R^2 = \frac{2(ad+2)D_0}{a} \left[(\mu E)^a (t-t_0) \right]^{2\beta} . \tag{A.50}$$

A.3. Spreading Properties of the Self-Similar Solution

To relate the spreading properties of the self-similar solution of the NDE to the observables of spreading states in Hamiltonian lattices, here some explicit calculations of the second moment, the participation number and the structural entropy for the self-similar solution will be given. In the following calculations, the time offset t_0 is neglected to avoid lengthy formulas, but it can be introduced simply by replacing t with $t - t_0$ everywhere.

A.3.1. Second Moment

To apply statistical methods to the self-similar solution, the normalized density $\rho(\vec{r},t)/E$ is interpreted as probability distribution. Using the radial symmetry and the fact that the center of the distribution is always at the origin, the following integral, already expressed in the radial coordinate $r = |\vec{r}|$, defines the second moment:

$$\Delta n^2 = \frac{2\pi}{E}\int_0^\infty r^2 \rho\, r^{d-1}\mathrm{d}r. \tag{A.51}$$

Substituting the self-similar ansatz (A.27) and introducing $x = rt^{-\beta}$, this gives:

$$\Delta n^2 = \frac{2\pi}{E}t^{-\alpha}\int_0^X f(x)x^{d+1}t^{\beta(d+1)}t^{\beta}\mathrm{d}x, \tag{A.52}$$

where $X = Rt^\beta = 2(ad+2)D_0(\mu E)^{2a\beta}/a$ does not depend on t. As $\alpha = d\beta$, one finds:

$$\Delta n^2 = \frac{2\pi}{E}t^{2\beta}\int_0^X f(x)x^{d+1}\mathrm{d}x. \tag{A.53}$$

Focusing only on the time dependence and with $R \sim t^\beta$, the following relation, claimed already in sections 3.4.1 and 3.4.2, is found:

$$\Delta n^2(t) \sim t^{2\beta} \sim R^2(t). \tag{A.54}$$

A.3.2. Participation Number

Here, the participation number for the self-similar solution of the NDE is calculated. Like the second moment, P is defined as an integral:

$$P^{-1} = \frac{2\pi}{E^2}\int_0^\infty \rho^2(r,t)r^{d-1}\mathrm{d}r. \tag{A.55}$$

Again substituting the self similar ansatz and using $x = rt^{-\beta}$ gives:

$$P^{-1} = \frac{2\pi}{E^2}t^{-2\alpha}\int_0^X f^2(x)x^{d-1}t^{\beta(d-1)}t^{\beta}\mathrm{d}r \tag{A.56}$$

$$= \frac{2\pi}{E^2}t^{-\alpha}\int_0^X f^2(x)x^{d-1}\,\mathrm{d}x. \tag{A.57}$$

where $\alpha = d\beta$ is used. The time dependence finally is obtained as:

$$P \sim t^\alpha \sim t^{d\beta} \sim R^d, \tag{A.58}$$

as claimed in sections 3.4.1 and 3.4.2.

A.3.3. Entropy

Here, the time dependence of the entropy of the self-similar solution of the NDE is calculated. The entropy is also defined straightforward interpreting ρ/E as probability density and using radial coordinates:

$$S = -\frac{2\pi}{E}\int_0^\infty \rho(r,t)\ln(\rho(r,t)/E)\, r^{d-1}\,\mathrm{d}r \tag{A.59}$$

Writing $\ln \rho/E = \ln\rho - \ln E$ and integrating the second term one arrives, after substituting the scaling ansatz $\rho = t^{-\alpha}f(rt^{-\beta})$ and $x = rt^{-\beta}$, at:

$$S - \ln E = -\frac{2\pi}{E}t^{-\alpha}\int_0^X f(x)\ln(t^{-\alpha}f(x))\, x^{d-1}t^{\beta(d-1)}t^{\beta}\,\mathrm{d}r \tag{A.60}$$

$$= \frac{2\pi}{E}t^{-\alpha+d\beta}\int_0^X f(x)[\ln t^{-\alpha} + \ln f(x)]x^{d-1}\mathrm{d}x \tag{A.61}$$

$$= \alpha\ln t - \frac{2\pi}{E}\int_0^X f(x)\ln f(x)\, x^{d-1}\mathrm{d}x, \tag{A.62}$$

where the last integral does not include any dependence on t. Hence the time dependence of the entropy is identified as:

$$S = \alpha\ln t + \text{const.} \tag{A.63}$$

For the structural entropy one then finds, using $P \sim t^\alpha$ from above:

$$S_{\text{str}} = S - \ln P = \text{const.} \tag{A.64}$$

A.4. Averaged Hamiltonian for a Resonant Perturbation

Here, the averaging method will be applied to obtain an effective perturbation Hamiltonian $\langle H_1\rangle$ describing the main resonance of two nonlinearly coupled, harmonic oscillators with equal frequencies studied in section 4.3.1. Starting point is the full perturbation H_1 given in eq. (4.13):

$$\begin{aligned} H_1 =& -(2I)^{3/2}\epsilon\cos^3\theta\cos(\Omega t) + 3I\epsilon^2\cos^2\theta\cos^2(\Omega t) \\ & -(2I)^{1/2}\epsilon^3\cos\theta\cos^3(\Omega t) \\ =& -(2I)^{3/2}\epsilon A_1 + 3I\epsilon^2 A_2 - (2I)^{1/2}\epsilon^3 A_3 \end{aligned} \tag{A.65}$$

This perturbation arises from the quartic coupling $\lambda = 4$ and $A_n(\theta,\Omega t)$ denote the angular parts that will be averaged. Starting with the first term A_1, naming $\varphi = \Omega t$ and making heavy use of trigonometric identities, one finds:

$$A_1 = \cos^3\theta\cos\varphi = \frac{1}{4}(3\cos\theta + \cos 3\theta)\cos\varphi \tag{A.66}$$

$$= \frac{1}{8}\left(3\cos(\theta-\varphi) + 3\cos(\theta+\varphi) + 3\cos(3\theta-\varphi) + \cos(3\theta+\varphi)\right). \tag{A.67}$$

Now from the fact that the main resonance is analyzed, one assumes $\omega \approx \Omega$, where $\theta = \omega t$ and hence $\theta \approx \varphi$. Introducing the slowly varying resonance variable $\psi = \theta - \varphi$, the first perturbation term A_1 gives:

$$A_1 = \frac{1}{8}\left(3\cos\psi + 3\cos(\psi + 2\varphi) + 3\cos(3\psi + 2\varphi) + \cos(3\psi + 4\varphi)\right) \tag{A.68}$$

$$\begin{aligned} = \frac{1}{8}(&3\cos\psi + 3\cos\psi\cos 2\varphi - 3\sin\psi\sin 2\varphi \\ &+ \cos 3\psi\cos 2\varphi - \sin 3\psi\sin 2\varphi + \cos 3\psi\cos 4\varphi - \sin 3\psi\sin 4\varphi). \end{aligned} \tag{A.69}$$

Now the averaging over one period of the fast oscillation φ is performed where the slowly varying resonance variable ψ is assumed to remain constant. Performing the integration over one period $\varphi = 0 \ldots 2\pi$, all but one terms evaluate to zero, hence:

$$\langle A_1 \rangle = \frac{1}{2\pi}\int_0^{2\pi} A_1(\psi, \varphi)\mathrm{d}\varphi = \frac{3}{8}\cos\psi. \tag{A.70}$$

Treating the second term A_2 in a similar way results in:

$$A_2 = \cos^2\theta\cos^2\varphi = \frac{1}{4}(1 - \cos 2\theta)(1 - \cos 2\varphi) \tag{A.71}$$

$$= \frac{1}{4}(1 - \cos 2\theta - \cos 2\varphi + \frac{1}{2}\cos 2(\theta - \varphi) - \frac{1}{2}\cos 2(\theta + \varphi)). \tag{A.72}$$

By introducing the resonance angle $\psi = \theta - \varphi$ one obtains:

$$\begin{aligned} A_2 = \frac{1}{4}(&1 - \cos 2\psi\cos 2\varphi + \sin 2\psi\sin 2\varphi - \cos 2\varphi \\ &+ \frac{1}{2}\cos 2\psi - \frac{1}{2}\cos 2\psi\cos 4\varphi + \frac{1}{2}\sin 2\psi\cos 4\varphi). \end{aligned} \tag{A.73}$$

The averaging then gives:

$$\langle A_2 \rangle = \frac{1}{2\pi}\int_0^{2\pi} A_1(\psi, \varphi)\mathrm{d}\varphi = \frac{1}{4} + \frac{1}{8}\cos 2\psi. \tag{A.74}$$

A similar calculation for A_3 can be done and reveals the same result as for A_1 because of the symmetry of the two terms:

$$\langle A_3 \rangle = \langle A_1 \rangle = \frac{3}{8}\cos\psi. \tag{A.75}$$

For the averaged perturbation one thus gets:

$$\langle H_1 \rangle = -(2I)^{3/2}\epsilon\langle A_1 \rangle + 3I\epsilon^2\langle A_2 \rangle - (2I)^{1/2}\epsilon^3\langle A_3 \rangle \tag{A.76}$$

$$= -\frac{3}{2\sqrt{2}}I^{3/2}\epsilon\cos\psi + \frac{3}{4}I\epsilon^2\left(1 + \frac{1}{2}\cos 2\psi\right) - \frac{3}{4\sqrt{2}}I^{1/2}\epsilon^3\cos\psi. \tag{A.77}$$

This is, after going back to $\theta - \Omega t = \psi$, the result used in section 4.3.1.

Bibliography

[1] A. Einstein, "Über die von der molekularkinetischen Theorie der Wärme geforderte Bewegung von in ruhenden Flüssigkeiten suspendierten Teilchen," *Annalen der Physik*, vol. 322, no. 8, pp. 549–560, 1905.

[2] E. Ott, *Chaos in Dynamical Systems*. Cambridge University Press, 2002.

[3] C. Beck and F. Schögl, *Thermodynamics of Chaotic Systems: An Introduction*. Cambridge Nonlinear Science Series, Cambridge University Press, 1995.

[4] B. V. Chirikov, "Research concerning the theory of nonlinear resonance and stochasticity," *Preprint (Russian)*, vol. N 267, 1969.

[5] R. S. Mackay, J. D. Meiss, and I. C. Percival, "Transport in hamiltonian systems," *Physica D: Nonlinear Phenomena*, vol. 13, no. 1–2, pp. 55 – 81, 1984.

[6] J. R. Dorfman, *An Introduction to Chaos in Nonequilibrium Statistical Mechanics*. Cambridge Lecture Notes in Physics, Cambridge University Press, 1999.

[7] L. Vlahos, H. Isliker, Y. Kominis, and K. Hizanidis, "Normal and anomalous diffusion: A tutorial," *Arxiv preprint arXiv:0805.0419*, 2008.

[8] A. Fick, "Über Diffusion," *Annalen der Physik*, vol. 170, no. 1, pp. 59–86, 1855.

[9] J. R. Pasta, S. M. Ulam, and E. Fermi, "Studies on nonlinear problems," in *Collected works of Enrico Fermi*, vol. 2, p. 978, Chicago: Univ. of Chicago Press, 1965.

[10] G. Gallavotti, ed., *The Fermi-Pasta-Ulam problem*. Springer Lecture Notes in Physics vol. 728, 2008.

[11] D. K. Campbell, P. Rosenau, and G. Zaslavsky, eds., *A focus issue on "The Fermi-Pasta-Ulam problem – the first 50 years"*, vol. 15. 2005.

[12] K. Kaneko, "Overview of coupled map lattices," *Chaos*, vol. 2, pp. 279–282, 1992.

[13] J. R. Chazottes and B. Fernandez, *Dynamics of Coupled Map Lattices and of Related Spatially Extended Systems*. Lecture Notes in Physics, Springer, 2005.

[14] A. N. Kolmogorov, "Preservation of conditionally periodic movements with small change in the Hamiltonian function," *Dokl. Akad. Nauk. SSSR*, vol. 98, p. 527, 1954.

[15] J. Moser, "On invariant curves of area-preserving mappings of an annulus," *Nach. Akad. Wiss. Göttingen, Math. Phys. Kl.*, vol. II 1, pp. 1–20, 1962.

[16] V. I. Arnol'd, "Proof of a theorem of A. N. Kolmogorov on the invariance of quasi-periodic motions under small perturbations of the hamiltonian," *Russian Mathematical Surveys*, vol. 18, no. 5, p. 9, 1963.

[17] A. Lichtenberg and M. Lieberman, *Regular and chaotic dynamics*. Applied mathematical sciences, Springer-Verlag, 1992.

[18] G. Gallavotti, *The Fermi-Pasta-Ulam Problem: A Status Report*. Lecture Notes in Physics, Springer, 2007.

[19] N. J. Zabusky and M. D. Kruskal, "Interaction of "solitons" in a collisionless plasma and the recurrence of initial states," *Phys. Rev. Lett.*, vol. 15, p. 240, 1965.

[20] T. Cretegny, T. Dauxois, S. Ruffo, and A. Torcini, "Localization and equipartition of energy in the β-fpu chain: Chaotic breathers," *Physica D: Nonlinear Phenomena*, vol. 121, no. 1–2, pp. 109 – 126, 1998.

[21] S. Aubry, "Breathers in nonlinear lattices: Existence, linear stability and quantization," *Physica D*, vol. 103, pp. 201–250, 1997.

[22] K. Ahnert, *Compactons in strongly nonlinear lattices*. PhD thesis, 2010.

[23] K. Ahnert and A. Pikovsky, "Compactons and chaos in strongly nonlinear lattices," *Phys. Rev. E*, vol. 79, p. 026209, 2009.

[24] B. V. Chirikov, "Resonance processes in magnetic traps," *Journal of Nuclear Energy. Part C, Plasma Physics, Accelerators, Thermonuclear Research*, vol. 1, no. 4, p. 253, 1960.

[25] B. V. Chirikov, "A universal instability of many-dimensional oscillator systems," *Phys. Rep.*, vol. 52, p. 265, 1979.

[26] S. Ruffo and T. Dauxois, "Fermi-Pasta-Ulam nonlinear lattice oscillations," *Scholarpedia*, vol. 3, no. 8, p. 5538, 2008.

[27] F. M. Izrailev, A. I. Khisamutdinov, and B. V. Chirikov, "Numerical experiments with a chain of coupled anharmonic oscillators," 1970.

[28] D. L. Shepelyansky, "Low-energy chaos in the Fermi - Pasta - Ulam problem," *Nonlinearity*, vol. 10, no. 5, p. 1331, 1997.

[29] A. Ponno, H. Christodoulidi, C. Skokos, and S. Flach, "The two-stage dynamics in the Fermi-Pasta-Ulam problem: From regular to diffusive behavior," *Chaos: An Interdisciplinary Journal of Nonlinear Science*, vol. 21, no. 4, p. 043127, 2011.

[30] A. S. Pikovsky and D. L. Shepelyansky, "Destruction of Anderson localization by a weak nonlinearity," *Phys. Rev. Lett.*, vol. 100, no. 9, p. 094101, 2008.

[31] P. W. Anderson, "Absence of diffusion in certain random lattices," *Phys. Rev.*, vol. 109, p. 1492, 1958.

[32] A. Lagendijk, B. v. Tiggelen, and D. S. Wiersma, "Fifty years of Anderson localization," *Physics Today*, vol. 62, no. 8, pp. 24–29, 2009.

[33] E. Abrahams, *50 Years of Anderson Localization*. International Journal of Modern Physics B, World Scientific, 2010.

[34] D. Shepelyansky, "Delocalization of quantum chaos by weak nonlinearity," *Phys. Rev. Lett.*, vol. 70, pp. 1787–1790, 1993.

[35] M. I. Molina, "Transport of localized and extended excitations in a nonlinear Anderson model," *Phys. Rev. B*, vol. 58, no. 19, pp. 12547–12550, 1998.

[36] S. Fishman, Y. Krivolapov, and A. Soffer, "On the problem of dynamical localization in the nonlinear Schrödinger equation with a random potential," *J. Stat. Phys.*, vol. 131, no. 5, pp. 843–865, 2008.

[37] I. Garcia-Mata and D. L. Shepelyansky, "Delocalization induced by nonlinearity in systems with disorder," *Phys. Rev. E*, vol. 79, p. 026205, 2009.

[38] S. Flach, D. O. Krimer, and C. Skokos, "Universal spreading of wave packets in disordered nonlinear systems," *Phys. Rev. Lett.*, vol. 102, no. 2, p. 024101, 2009.

[39] C. Skokos, D. O. Krimer, S. Komineas, and S. Flach, "Delocalization of wave packets in disordered nonlinear chains," *Phys. Rev. E*, vol. 79, no. 5, Part 2, p. 056211, 2009.

[40] M. Mulansky, K. Ahnert, A. Pikovsky, and D. L. Shepelyansky, "Dynamical thermalization of disordered nonlinear lattices," *Phys. Rev. E*, vol. 80, p. 056212, 2009.

[41] C. Skokos and S. Flach, "Spreading of wave packets in disordered systems with tunable nonlinearity," *Phys. Rev. E*, vol. 82, no. 1, p. 016208, 2010.

[42] S. Flach, "Spreading of waves in nonlinear disordered media," *Chem. Physics*, vol. 375, pp. 548–556, OCT 5 2010.

[43] T. V. Laptyeva, J. D. Bodyfelt, D. O. Krimer, C. Skokos, and S. Flach, "The crossover from strong to weak chaos for nonlinear waves in disordered systems," *Europhys. Lett.*, vol. 91, no. 3, p. 30001, 2010.

[44] M. Mulansky and A. Pikovsky, "Spreading in disordered lattices with different nonlinearities," *Europhys. Lett.*, vol. 90, p. 10015, 2010.

[45] M. Johansson, G. Kopidakis, and S. Aubry, "KAM tori in 1D random discrete nonlinear Schrödinger model?," *Europhys. Lett.*, vol. 91, no. 5, p. 50001, 2010.

[46] M. Mulansky, K. Ahnert, and A. Pikovsky, "Scaling of energy spreading in strongly nonlinear disordered lattices," *Phys. Rev. E*, vol. 83, p. 026205, 2011.

[47] M. V. Ivanchenko, T. V. Laptyeva, and S. Flach, "Anderson localization or nonlinear wave? A matter of probability," *Phys. Rev. Lett.*, vol. 107, p. 240602, 2011.

[48] E. Michaely and S. Fishman, "Effective noise theory for the nonlinear Schrödinger equation with disorder," *Phys. Rev. E*, vol. 85, p. 046218, Apr 2012.

[49] H. Veksler, Y. Krivolapov, and S. Fishman, "Double-humped states in the nonlinear Schrödinger equation with a random potential," *Phys. Rev. E*, vol. 81, no. 1, p. 017201, 2010.

[50] H. Veksler, Y. Krivolapov, and S. Fishman, "Spreading for the generalized nonlinear Schrödinger equation with disorder," *Phys. Rev. E*, vol. 80, no. 3, p. 037201, 2009.

[51] M. Larcher, F. Dalfovo, and M. Modugno, "Effects of interaction on the diffusion of atomic matter waves in one-dimensional quasiperiodic potentials," *Phys. Rev. A*, vol. 80, p. 053606, Nov 2009.

[52] S. Fishman, Y. Krivolapov, and A. Soffer, "Perturbation theory for the nonlinear Schrodinger equation with a random potential," *Nonlinearity*, vol. 22, no. 12, pp. 2861–2887, 2009.

[53] A. Rivkind, Y. Krivolapov, S. Fishman, and A. Soffer, "Eigenvalue repulsion estimates and some applications for the one-dimensional Anderson model," *Journal of Physics A: Mathematical and Theoretical*, vol. 44, no. 30, p. 305206, 2011.

[54] D. M. Basko, "Weak chaos in the disordered nonlinear Schroedinger chain: destruction of Anderson localization by Arnold diffusion," *Ann. Phys.*, vol. 326, no. 7, pp. 1577–1655, 2011.

[55] W.-M. Wang and Z. Zhang, "Long time Anderson localization for the nonlinear random Schrödinger equation," *J. Stat. Phys.*, vol. 134, no. 5-6, pp. 953–968, 2009.

[56] J. Bourgain and W.-M. Wang, "Diffusion bound for a nonlinear Schrödinger equation," in *Mathematical aspects of nonlinear dispersive equations* (J. Bourgain, C. E. Kenig, and S. Klainerman, eds.), pp. 21–42, Princeton: Princeton UP, 2007.

[57] J. Billy, V. Josse, Z. Zuo, A. Bernard, B. Hambrecht, P. Lugan, D. Clement, L. Sanchez-Palencia, P. Bouyer, and A. Aspectet, "Direct observation of Anderson localization of matter waves in a controlled disorder," *Nature*, vol. 453, no. 7197, pp. 891–894, 2008.

[58] G. Roati, C. D'Errico, L. Fallani, M. Fattori, C. Fort, M. Zaccanti, G. Modugno, M. Modugno, and M. Inguscio, "Anderson localization of a noninteracting Bose-Einstein condensate," *Nature*, vol. 453, pp. 895–898, 2008.

[59] R. Dalichaouch, J. P. Armstrong, S. Schultz, P. M. Platzman, and S. L. McCall, "Microwave localization by two-dimensional random scattering," *Nature*, vol. 354, pp. 53–55, Nov 1991.

[60] J. E. Lye, L. Fallani, M. Modugno, D. S. Wiersma, C. Fort, and M. Inguscio, "Bose-Einstein condensate in a random potential," *Phys. Rev. Lett.*, vol. 95, no. 7, p. 070401, 2005.

[61] C. Fort, L. Fallani, V. Guarrera, J. E. Lye, M. Modugno, D. S. Wiersma, and M. Inguscio, "Effect of optical disorder and single defects on the expansion of a Bose-Einstein condensate in a one-dimensional waveguide," *Phys. Rev. Lett.*, vol. 95, no. 17, p. 170410, 2005.

[62] T. Schwartz, G. Bartal, S. Fishman, and M. Segev, "Transport and Anderson localization in disordered two-dimensional photonic lattices," *Nature*, vol. 446, p. 52, 2007.

[63] Y. Lahini, A. Avidan, F. Pozzi, M. Sorel, R. Morandotti, D. N. Christodoulides, and Y. Silberberg, "Anderson localization and nonlinearity in one-dimensional disordered photonic lattices," *Phys. Rev. Lett.*, vol. 100, no. 1, p. 013906, 2008.

[64] E. Lucioni, B. Deissler, L. Tanzi, G. Roati, M. Zaccanti, M. Modugno, M. Larcher, F. Dalfovo, M. Inguscio, and G. G. Modugno, "Observation of subdiffusion in a disordered interacting system," *Phys. Rev. Lett.*, vol. 106, p. 230403, Jun 2011.

[65] B. Deissler, M. Zaccanti, G. Roati, C. D'Errico, M. Fattori, M. Modugno, G. Modugno, and M. Inguscio, "Delocalization of a disordered bosonic system by repulsive interactions," *Nat Phys*, vol. 6, pp. 354–358, May 2010.

[66] S. Fishman, Y. Krivolapov, and A. Soffer, "The nonlinear Schrödinger equation with a random potential: results and puzzles," *Nonlinearity*, vol. 25, no. 4, pp. R53–R72, 2012.

[67] R. Brown, "A brief account of microscopical observations made in the months of june, july and august, 1827, on the particles contained in the pollen of plants; and on the general existence of active molecules in organic and inorganic bodies.," *Phil. Mag.*, vol. 4, pp. 161—-173, 1828.

[68] G. Boffetta, G. Lacorata, and A. Vulpiani, "Introduction to chaos and diffusion," *arxiv:nlin*, vol. 0411023v1, 2004.

[69] R. Klages, *Deterministic diffusion in one-dimensional chaotic dynamical systems*. PhD thesis, 1996.

[70] D. L. Shepelyansky and B. V. Chirikov, "Chirikov standard map," *Scholarpedia*, vol. 3, no. 3, p. 3550, 2008.

[71] K. Kaneko and T. Konishi, "Diffusion in Hamiltonian dynamical systems with many degrees of freedom," *Phys. Rev. A*, vol. 40, no. 10, p. 40, 1989.

[72] P. A. Lee and T. V. Ramakrishnan, "Disordered electronic systems," *Reviews of Modern Physics*, vol. 57, no. 2, p. 287, 1985.

[73] M. Mulansky, "Localization properties of nonlinear disordered lattices (Diplomarbeit)," 2009.

[74] E. Michaely and S. Fishman, "Statistical properties of the one dimensional anderson model relevant for the nonlinear Schrödinger equation in a random potential," 2012.

[75] E. Michaely, "Effective noise theory for the nonlinear Schrödinger equation (Masterthesis)," 2012.

[76] J. Fröhlich, T. Spencer, and C. E. Wayne, "Localization in disordered, nonlinear dynamical systems," *Journal of Statistical Physics*, vol. 42, pp. 247–274, 1986. 10.1007/BF01127712.

[77] A. Ablowitz and P. A. Clarkson, *Solitons, Nonlinear Evolution Equations and Inverse Scattering*. London Mathematical Society Lecture Note Series, Cambridge University Press, 1991.

[78] P. G. Drazin and R. S. Johnson, *Solitons: An Introduction*. Cambridge Texts in Applied Mathematics, Cambridge University Press, 1989.

[79] P. Rosenau and S. Schochet, "Almost compact breathers in anharmonic lattices near the continuum limit," *Phys. Rev. Lett.*, vol. 94, no. 4, p. 045503, 2005.

[80] M. Mulansky, K. Ahnert, A. Pikovsky, and D. L. Shepelyansky, "Strong and weak chaos in weakly nonintegrable many-body Hamiltonian systems," *Journal of Statistical Physics*, pp. 1–19, 2011.

[81] A. Pikovsky and S. Fishman, "Scaling properties of weak chaos in nonlinear disordered lattices," *Phys. Rev. E*, vol. 83, p. 025201(R), 2011.

[82] D. M. Basko, "On the local nature and scaling of chaos in weakly nonlinear disordered chains," 2012.

[83] V. I. Arnol'd, "Instability of dynamical systems with several degrees of freedom(instability of motions of dynamic system with five-dimensional phase space)," *Soviet Mathematics*, vol. 5, pp. 581–585, 1964.

[84] B. V. Chirikov and V. V. Vecheslavov, "Theory of fast Arnold diffusion in many-frequency systems," *J. Stat. Phys.*, vol. 71, no. 1-2, pp. 243–258, 1993.

[85] A. Rényi, "On measures of entropy and information," in *Proc. Fourth Berkeley Symp. on Math. Statist. and Prob.*, pp. 547–561, Univ. of Calif. Press, 1961.

[86] J. Pipek and I. Varga, "Universal classification scheme for the spatial-localization properties of one-particle states in finite, d-dimensional systems," *Physical Review A*, vol. 46, pp. 3148–3163, Sep 1992.

[87] M. Muskat and R. D. Wyckoff, *The flow of homogeneous fluids through porous media*. International series in physics, J.W. Edwards, 1946.

[88] J. L. Vázquez, *The Porous Medium Equation: Mathematical Theory*. Clarendon Press Oxford Mathematical Monographs, 2006.

[89] Y. B. Zel'dovich and Y. P. Raizer, *Physics of Shock Waves and High-Temperature Hydrodynamic Phenomena*. Dover Books on Physics, Dover Publications, 2002.

[90] J. Crank, *The mathematics of diffusion*, vol. 1. Clarendon press Oxford, 1979.

[91] Z. Wu, J. Yin, H. Li, and J. Zhao, *Nonlinear Diffusion Equations*. World Scientific Publisher, Singapore, 2002.

[92] G. Schwiete and A. M. Finkel'stein, "Nonlinear wave-packet dynamics in a disordered medium," *Phys. Rev. Lett.*, vol. 104, p. 103904, Mar 2010.

[93] N. Cherroret and T. Wellens, "Fokker-planck equation for transport of wave packets in nonlinear disordered media," *Phys. Rev. E*, vol. 84, p. 021114, Aug 2011.

[94] O. A. Oleinik, A. S. Kalashnikov, and C. Y.-L., "The cauchy problem and boundary problems for equations of the typeof nonstationary filtration," *Akad. Nauk. SSSR Ser. Izv. Mat.*, vol. 22, pp. 667–704, 1958.

[95] Y. B. Zel'dovich and A. S. Kompaneetz, "Towards a theory of heat conduction with thermal conductivity depending on the temperature," *Collection of papers dedicated to 70th birthday of Academician AF Ioffe, Izd. Akad. Nauk SSSR, Moscow*, pp. 61–71, 1950.

[96] G. I. Barenblatt, "On self-similar motions of a compressible fluid in a porous medium," *Akad. Nauk SSSR. Prikl. Mat. Meh*, vol. 16, no. 6, pp. 79–6, 1952.

[97] L. A. Peletier, "Asymptotic behavior of solutions of the porous media equation," *SIAM Journal on Applied Mathematics*, vol. 21, no. 4, pp. pp. 542–551, 1971.

[98] G. I. Barenblatt and Y. B. Zel'dovich, "Self-similar solutions as intermediate asymptotics," *Annual Review of Fluid Mechanics*, vol. 4, no. 1, pp. 285–312, 1972.

[99] T. P. Witelski and A. J. Bernoff, "Self-similar asymptotics for linear and nonlinear diffusion equations," *Studies in Applied Mathematics*, vol. 100, no. 2, pp. 153–193, 1998.

[100] E. Hairer, S. P. Nørsett, and G. Wanner, *Solving Ordinary Differential Equations I: Nonstiff Problems*. Springer Series in Computational Mathematics, Springer, 2011.

[101] E. Hairer and G. Wanner, *Solving Ordinary Differential Equations II*. Springer Berlin Heidelberg, 2010.

[102] W. H. Press, S. A. Teukolsky, W. T. Vetterling, and B. P. Flannery, *Numerical Recipes in C++*. Cambridge University Press, 2002.

[103] B. Leimkuhler and S. Reich, *Simulating Hamiltonian Dynamics*. Cambridge Monographs on Applied and Computational Mathematics, Cambridge University Press, 2005.

[104] R. I. McLachlan, "On the numerical integration of ordinary differential equations by symmetric composition methods," *SIAM Journal on Scientific Computing*, vol. 16, no. 1, pp. 151–168, 1995.

[105] K. Ahnert and M. Mulansky, "odeint." `http://www.odeint.com`, 2009–2012.

[106] K. Ahnert and M. Mulansky, "odeint - Solving ordinary differential equations in C++," in *Symposium on the "Numerical Solution of Differential Equations and their Applications*, AIP Conference Proceedings, 2011.

[107] P. B. Kahn and Y. Zarmi, "Weakly nonlinear oscillations: A perturbative approach," *American Journal of Physics*, vol. 72, no. 4, pp. 538–552, 2004.

[108] J. D. Bodyfelt, T. V. Laptyeva, C. Skokos, D. O. Krimer, and S. Flach, "Nonlinear waves in disordered chains: Probing the limits of chaos and spreading," *Physical Review E*, vol. 84, no. 1, p. 016205, 2011.

[109] T. V. Laptyeva, J. D. Bodyfelt, and S. Flach, "Subdiffusion of nonlinear waves in two-dimensional disordered lattices," *EPL (Europhysics Letters)*, vol. 98, no. 6, p. 60002, 2012.

[110] F. A. B. F. de Moura, R. A. Caetano, and B. Santos, "Dynamics of one electron in a nonlinear disordered chain," *Journal of Physics: Condensed Matter*, vol. 24, no. 24, p. 245401, 2012.

[111] V. Oganesyan, A. Pal, and D. A. Huse, "Energy transport in disordered classical spin chains," *Phys. Rev. B*, vol. 80, p. 115104, Sep 2009.